



User's Manual for BECAS

A cross section analysis tool for anisotropic and inhomogeneous beam sections of arbitrary geometry

Blasques, José Pedro Albergaria Amaral

Publication date:
2012

Document Version
Publisher's PDF, also known as Version of record

[Link back to DTU Orbit](#)

Citation (APA):

Blasques, J. P. A. A. (2012). User's Manual for BECAS: A cross section analysis tool for anisotropic and inhomogeneous beam sections of arbitrary geometry. Risø DTU – National Laboratory for Sustainable Energy. Denmark. Forskningscenter Risø. Risø-R No. 1785(EN)

General rights

Copyright and moral rights for the publications made accessible in the public portal are retained by the authors and/or other copyright owners and it is a condition of accessing publications that users recognise and abide by the legal requirements associated with these rights.

- Users may download and print one copy of any publication from the public portal for the purpose of private study or research.
- You may not further distribute the material or use it for any profit-making activity or commercial gain
- You may freely distribute the URL identifying the publication in the public portal

If you believe that this document breaches copyright please contact us providing details, and we will remove access to the work immediately and investigate your claim.

User's Manual for

BECAS

A cross section analysis tool for anisotropic and inhomogeneous
beam sections of arbitrary geometry

José Pedro Blasques

Risø DTU – National Laboratory for Sustainable Energy
Technical University of Denmark
Frederiksborgvej 399, P.O. Box 49, Building 114,
DK-4000 Roskilde, Denmark
✉ jpbl@risoe.dtu.dk

RISØ-R 1785

February 23, 2012

Title of report:

User's Manual for BECAS v2.0 - a cross section analysis tool for anisotropic and inhomogeneous beam sections of arbitrary geometry

Author:

José Pedro Blasques

Address: Risø – National Laboratory for Sustainable Energy

Technical University of Denmark

Frederiksborgvej 399, P.O. Box 49, Building 114,

DK-4000 Roskilde, Denmark

E-mail: jpbl@risoe.dtu.dk

Copyright and ownership:

All rights to this User's Manual belong exclusively to Risø DTU. This User's Manual may only be accessed when the reader has a valid license from Risø DTU to use the BECAS software. A license can be obtained from José Pedro Blasques at jpbl@risoe.dtu.dk.

Disclaimer:

Risø DTU disclaims all responsibility for any kind of damage, including loss of profit, loss of capital or any caused damage or loss, which might appear by use or erroneous use of the BECAS software or Documentation, even though Risø DTU should have been informed of the possibilities of such damage.

Preface

The BEam Cross section Analysis Software - BECAS - is a group of Matlab functions used for the analysis of the stiffness and mass properties of beam cross sections. BECAS was originally developed under the EFP 2007 Project 33033-0075 - Anisotropic beam model for analysis and design of passive controlled wind turbine blades. BECAS was later updated, extended, and completely rewritten throughout part of the author's Ph.D. project (Optimal Design of Laminated Composite Beams, Ph.D. Thesis, Technical University of Denmark).

BECAS' code and user's guide is mostly developed and maintained by José Pedro Blasques (Risø DTU, National Laboratory for Sustainable Energy, Technical University of Denmark). Nonetheless, the author is indebted to the following people which at one point or another have given or currently give invaluable support throughout the development of BECAS:

- Boyan Lazarov (Department of Mechanical Engineering, Technical University of Denmark) Participated very actively in the development of the original BECAS v1.0. Among much other invaluable work, Boyan was the first to suggest the constraint equations which are used in the solution of the cross section equilibrium equations.
- Robert Bitsche (Risø DTU, National Laboratory for Sustainable Energy, Technical University of Denmark) An active member of the current BECAS development group. Robert is the main bug finder, and an invaluable source of good ideas and suggestions. Robert is also responsible for the interface between BECAS, commercial finite element packages, and HAWC2, Risø DTU's own code for the aeroelastic analysis of wind turbines.

Their contributions are gratefully acknowledged.

All feedback and suggestions for further improvements and extensions is most welcome.

José Pedro Blasques

Roskilde, November 2011

Contents

Preface	v
1 Introduction	1
1.1 Version history	3
2 Theory manual	5
2.1 Assumptions	5
2.2 Equilibrium equations	6
2.2.1 Basic definitions	6
2.2.2 Kinematics	7
2.2.3 Strain-displacement relation	8
2.2.4 Virtual work principle	9
2.3 Solutions to equilibrium equations	13
2.3.1 Extremity solutions	13
2.3.2 Central solutions	14
2.3.3 Constraint equations	16
2.4 On the properties of the solutions	16
2.4.1 Rigid motions	17
2.4.2 Warping displacements	19
2.5 Cross section properties	22
2.5.1 Cross section stiffness matrix	22
2.5.2 Shear center and elastic center positions	24
2.6 Cross section mass matrix	25
2.7 An alternative formulation based on solid finite elements	26
2.7.1 Evaluation of cross section stiffness matrix	26
3 Implementation manual	29
3.1 Two dimensional finite element analysis	29
3.1.1 Q4 and Q8 elements	29
3.1.2 Local and global finite element matrices	32
3.2 Material constitutive matrix	33
3.2.1 Definition	33
3.2.2 Rotation	34
3.3 Rotation and translation of constitutive matrices	36

4	Validation	37
4.1	Setup	37
4.2	Numerical examples	40
4.2.1	Square	41
4.2.2	Cylinder	50
4.2.3	Three cells	60
5	User's Manual	65
5.1	Input	66
5.1.1	Example	67
5.2	List of functions and output	67
5.2.1	BECAS_Utils	67
5.2.2	BECAS_Constitutive_Ks	67
5.2.3	BECAS_Constitutive_Ms	67
5.2.4	BECAS_CrossSectionProps	68
5.2.5	BECAS_RecoverStrains	69
5.2.6	BECAS_RecoverStresses	69
5.2.7	BECAS_Becas2Hawc2	70
5.2.8	BECAS_TransformMat	70
5.2.9	Examples	71
5.3	The BECAS 3D implementation	71
5.3.1	Input	71
5.3.2	List of functions and output	71
5.3.3	BECAS_3D_Utils	71
5.3.4	BECAS_3D_Constitutive_Ks	72
5.3.5	BECAS_3D_CrossSectionProps	72

List of Symbols

x, y, z	Coordinates of a point in the cross section	6
A	Cross section area	6
ϵ	Strain vector	6
σ	Stress vector	6
\mathbf{Q}	Material tensor	6
\mathbf{p}	Tractions on cross section	6
\mathbf{T}	Section forces - shear and axial forces	6
\mathbf{M}	Section forces - bending moments and torque	6
θ	Vector of section forces	6
\mathbf{n}	Two dimensional cross product matrix	6
\mathbf{Z}	Auxiliary matrix for evaluation of cross section forces	7
\mathbf{s}	Total displacement of a point in the cross section	7
\mathbf{v}	Rigid body displacement of a point in the cross section	7
\mathbf{g}	Warping displacement of a point in the cross section	7
\mathbf{r}	Cross section translation and rotation	7
χ	Translation of a reference point in the cross section	7
φ	Cross section rotation angles	7
\mathbf{B}	Two dimensional strain-displacement matrix	8
\mathbf{S}	One dimensional strain-displacement matrix	8
\mathbf{T}_r	Sixth order auxiliary matrix for definition of the section strains	8
ψ	Section strain parameters	8
\mathbf{N}	Matrix of finite element interpolation functions	9
\mathbf{u}	Nodal degrees of freedom in cross section finite element mesh	9
W_e	External work per unit length	9
W_i	Internal work or elastic energy per unit length	10
W_t	Total virtual work per unit length	12
n_n	Number of nodes in the cross section finite element mesh	16
\mathbf{F}_s	Cross section compliance matrix	23
\mathbf{K}_s	Cross section stiffness matrix	23
x_t, y_t	Coordinates of elastic center	24
x_s, y_s	Coordinates of shear center	24
\mathbf{M}_s	Cross section mass matrix	25
m	Mass per unit length	25
I_x, I_y, I_{xy}	Mass moments of inertia	25
x_m, y_m	Cross section mass center	25
n_q	Number of nodes in the cross section finite element mesh	31
n_e	Number of elements in the cross section finite element mesh	32

n_d	Number of d.o.f. in the cross section finite element equations	67
-------	--	----

Chapter 1

Introduction

This report describes the development and implementation of the **BEam Cross section Analysis Software – BECAS**.

Cross section analysis tools are commonly employed in the development of beam models for the analysis of long slender structures. These type of models can be very versatile when compared against its equivalent counterparts as they generally offer a very good compromise between accuracy and computational efficiency. When suited, beam models can be advantageously used in an optimal design context (see, e.g., Ganguli and Chopra [1], Li et al. [2], Blasques and Stolpe [3]) or in the development of complex multiphysics codes. Wind turbine aeroelastic codes, for example, commonly rely on these types of models for the representation of most parts of the wind turbine, from the tower to the blades (see, e.g., Hansen et al. [4], Chaviaropoulos et al. [5]). In specific, the development of beam models which correctly describe the behaviour of the wind turbine blades have been the focus of many investigations. The estimation of the properties of these types of structures becomes more complex as the use of different combinations of advanced materials becomes a standard. It is therefore paramount to develop cross section analysis tools which can correctly account for all geometrical and material effects. BECAS is a general purpose cross section analysis tool specifically developed for these types of applications. BECAS is able to handle a large range of arbitrary section geometries and correctly predict the effects of inhomogeneous material distribution and anisotropy. Based on a definition of the cross section geometry and material distribution, BECAS is able to determine the cross section stiffness properties while accounting for all the geometrical and material induced couplings. These properties can be consequently utilized in the development of beam models to accurately predict the response of wind turbine blades with complex geometries and made of advanced materials.

BECAS is based on the theory originally presented by Giavotto et al. [6] for the analysis of inhomogeneous anisotropic beams. The theory leads to the definition of two types of solutions of which, and in accordance to Saint-Venant's principle, the non-decaying solutions are the basis for the evaluation of the cross section stiffness properties. A slight modification to the theory was introduced later by Borri and Merlini [7] where the concept of *intrinsic warping* is introduced in the derivation of the cross section stiffness matrix. Despite the modifications, no difference in the results was reported. The theory was subsequently extended by Borri et al [8] to account for large displacements, curvature and twist. Ghiringhelli and Mantegazza

in [9] presented an implementation of the theory for commercial finite element codes. Finally Ghiringhelli in [10, 11] and Ghiringhelli et al. [12] presented a formulation incorporating thermoelastic and piezo-electric effects, respectively. The validation results presented throughout each of the previously mentioned publications highlight the robustness of the method in the analysis of the stiffness and strength properties of anisotropic and inhomogeneous beam cross sections. According to Yu et al. [13] implementations of this theory have been in fact used as a benchmark for the validation of any new tool emerging since the early 1980's (see, e.g., Yu et al. [13, 14] and Chen et al. [15]).

Many other cross section analysis tools have been described in the literature. The reader is referred to Jung et al. [16] and Volovoi et al. [17] for an assessment of different cross section analysis tools. Nonetheless, at this stage the Variational Asymptotic Beam Section analysis commercial package VABS by Yu et al. [13] is perhaps the state of the art for these type of tools. VABS has been extensively validated (see Yu et al. [13, 14], Chen et al. [15]) and is therefore used in this report as the benchmark for the validation of BECAS. As shall be seen the cross section properties estimated by both tools are in very good agreement.

The theory presented in this report concerns only the determination of the cross section stiffness properties for inhomogeneous and anisotropic beam cross sections of arbitrary geometry, i.e., the theory implemented in BECAS. Most of the relevant information which is spread across the different publications (namely [6]-[12]) and which concerns the estimation of the cross section stiffness properties is compiled here. The aim was to produce a self-contained document which can serve as a developer's manual for the readers wishing to use, understand and further develop BECAS.

This report is organized as follows:

Chapter 2 Theory Manual All the theory leading to the evaluation of the cross section stiffness properties is presented in this chapter. The assumptions underlying the presented theory are stated first in Section 2.1. The equilibrium equations are established next in Section 2.2 and consequently resolved in Section 2.3. Some of the mathematical properties invoked in the resolution of the equilibrium equations are described in detail in Section 2.4. Finally, the expressions for the cross section stiffness matrix, and positions of shear and elastic centers, are determined in Section 2.5.

Chapter 3 Implementation Manual The details concerning the numerical implementation of the theory are presented in this chapter. A two dimensional implementation based on four node plane finite elements is presented in Section 3.1. Furthermore, an implementation of the method for commercial finite element codes is described next in Section 2.7. Finally, in Section 3.2, the constitutive matrix is defined and some important conventions utilized in its transformation are stated.

Chapter 4 Validation All numerical experiments performed for the validation of VABS are presented in this Chapter. The general setup for the numerical experiments is described first in Section 4.1. The validation results obtained for the different cross sections are finally presented in Section 4.2.

Chapter 5 User's Manual The user's manual for the MATLAB implementation of BECAS is presented here. This chapter covers the practical use of BECAS as a cross section analysis tool.

1.1 Version history

- **Version 2.0:** **Authors:** JPBL, ROBI; **Date:** 09.02.2012; **Change:** First stable version.
- **Version 2.1:** **Authors:** JPBL, ROBI; **Date:** 23.02.2012; **Change:** The sign of the fiber and fiber plane orientation angles have been switched such that the results (beam displacements and cross section stresses) now match the ABAQUS results. The calculation of the shear center position now neglects the bend-twist coupling terms ($z=0$ in the calculations).

Chapter 2

Theory manual

This chapter describes the theory underlying the implementation of the cross section analysis tool BECAS. The chapter is organized as follows. In the first section, Section 2.2, some general definitions are introduced. The beam kinematics are subsequently described. The displacement of a point in the cross section is described as the sum of a rigid body motion and a warping displacement accounting for the cross section deformation. A two dimensional discretization of the warping following the typical finite element approach is introduced. The principle of virtual work is then invoked in the derivation of the expressions for the external and internal virtual work per unit length. The equilibrium equations for the cross section are consequently established.

The solution to the equilibrium equations, a set of second order linear differential equations, is discussed in Section 2.3. As shall be seen, the solution is defined by a particular integral which depends on the boundary conditions – or internal force resultants in this case – and a general integral which resolves into an eigenvalue problem. The particular integral corresponds to solutions far from the ends of the beam where the end effects are negligible– the *central* solutions – while the general integrals corresponds to the solutions at the extremities of the beam are applied – *extremity* solutions (nomenclature according to Giavotto et al. [6]). At this point some mathematical properties of the solutions are invoked which are only detailed later in Section 2.4. The reader may wish to avoid this section if only a general overview of the method is required.

The equations for the cross section stiffness matrix are presented in Section 2.5. Based on the cross section stiffness properties it is possible to compute the positions of the shear and elastic center.

2.1 Assumptions

The theory presented in the next sections is valid for long slender structures which present a certain level of geometric and structural continuity. Thus, there should not be abrupt variations of the cross section geometry and material properties along the beam length. Moreover, the same should be valid for the loads applied. Consequently, the gradients of the resulting strains and displacement along the beam axis should also be small. All the assumptions mentioned before are not imposed along the cross section coordinates in the cross section plane. Finally, the theory is based on the assumptions of small displacements and rotations.

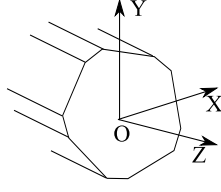


Figure 2.1: Cross section coordinate system.

2.2 Equilibrium equations

The derivation of the equilibrium equations for the beam cross section are presented in this section.

2.2.1 Basic definitions

The reference coordinate system for a generic cross section with area A is presented in Figure 2.1. The displacement of a point in the section $\mathbf{s} = [s_x \ s_y \ s_z]^T$ is defined with respect to the cross section coordinate system x, y, z . The strain and stress, $\boldsymbol{\epsilon}$ and $\boldsymbol{\sigma}$, are given as

$$\begin{aligned}\boldsymbol{\epsilon}^T &= [\epsilon_{xx} \ \epsilon_{yy} \ 2\epsilon_{xy} \ 2\epsilon_{xz} \ 2\epsilon_{yz} \ \epsilon_{zz}] \\ \boldsymbol{\sigma}^T &= [\sigma_{xx} \ \sigma_{yy} \ \sigma_{xy} \ \sigma_{xz} \ \sigma_{yz} \ \sigma_{zz}]\end{aligned}$$

The stress and strain relate through Hooke's law

$$\boldsymbol{\sigma} = \mathbf{Q}\boldsymbol{\epsilon} \quad (2.1)$$

where \mathbf{Q} is the typical material constitutive matrix. It is assumed that the material is linear elastic, otherwise there are no restrictions regarding the level of anisotropy (see Section 3.2). The ordering of the entries in $\boldsymbol{\epsilon}$ and $\boldsymbol{\sigma}$ is such that the tractions or the components of stress acting on the cross section face, can be easily isolated in

$$\mathbf{p}^T = [\sigma_{xz} \ \sigma_{yz} \ \sigma_{zz}]$$

The tractions \mathbf{p} acting upon the cross section face are statically equivalent to a force \mathbf{T} and moment \mathbf{M} (cf. Figure 2.2)

$$\begin{aligned}\mathbf{T} &= \int_A \mathbf{p} \, dA \\ \mathbf{M} &= \int_A \mathbf{n}^T \mathbf{p} \, dA\end{aligned} \quad (2.2)$$

where the two dimensional cross product matrix \mathbf{n} is

$$\mathbf{n} = \begin{bmatrix} 0 & 0 & y \\ 0 & 0 & -x \\ -y & x & 0 \end{bmatrix}$$

and thus $\tilde{\mathbf{n}} \times \mathbf{p} = \mathbf{n}^T \mathbf{p}$ where $\tilde{\mathbf{n}} = [x \ y \ z]^T$ is the vector position of a point in the cross section. The vector of section forces $\boldsymbol{\theta} = [\mathbf{T}^T \ \mathbf{M}^T]^T$ can then be written as

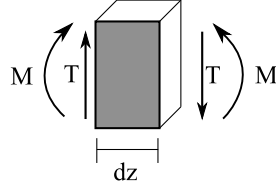
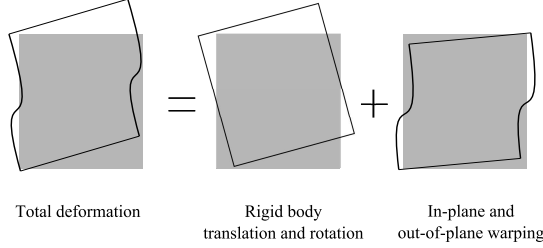
Figure 2.2: Cross section resultant forces for a slice dx of the beam.

Figure 2.3: Schematic description of the different contributions for the deformation of the cross section.

$$\boldsymbol{\theta} = \int_A \mathbf{Z}^T \mathbf{p} \, dA \quad (2.3)$$

where the matrix $\mathbf{Z} = [\mathbf{I}_3 | \mathbf{n}^T]$, and \mathbf{I}_i is the i^{th} order identity matrix,

$$\mathbf{Z} = \begin{bmatrix} 1 & 0 & 0 & 0 & 0 & -y \\ 0 & 1 & 0 & 0 & 0 & x \\ 0 & 0 & 1 & y & -x & 0 \end{bmatrix}$$

2.2.2 Kinematics

The displacement $\mathbf{s} = [s_x, s_y, s_z]^T$ at a point of the cross section is defined as

$$\mathbf{s} = \mathbf{v} + \mathbf{g}$$

where $\mathbf{v} = [v_x, v_y, v_z]^T$ is the vector of displacements associated with the rigid body translation and rotation of the cross section. The vector $\mathbf{g} = [g_x, g_y, g_z]^T$ is the vector of warping displacements associated with the cross section deformation (see Figure 2.3). Assuming small displacements and rotations, the rigid displacements \mathbf{v} can be obtained as

$$\mathbf{v} = \mathbf{Z}\mathbf{r}$$

a linear combination of the the components of $\mathbf{r} = [\boldsymbol{\chi}^T \boldsymbol{\varphi}^T]^T$. The components of $\boldsymbol{\chi}(z) = [\chi_x, \chi_y, \chi_z]^T$ represent the translations of the cross section reference point, while $\boldsymbol{\varphi}(z) = [\varphi_x, \varphi_y, \varphi_z]^T$ are the cross section rotations. The total displacement can be rewritten as

$$\mathbf{s} = \mathbf{Z}\mathbf{r} + \mathbf{g} \quad (2.4)$$

2.2.3 Strain-displacement relation

The strain-displacement relation can be written as

$$\epsilon = \mathbf{B}\mathbf{s} + \mathbf{S}\frac{\partial \mathbf{s}}{\partial z} \quad (2.5)$$

where \mathbf{B} and \mathbf{S} are defined next. The strain displacement relation can then be cast as

$$\begin{bmatrix} \epsilon_{xx} \\ \epsilon_{yy} \\ 2\epsilon_{xy} \\ 2\epsilon_{xz} \\ 2\epsilon_{yz} \\ \epsilon_{zz} \end{bmatrix} = \underbrace{\begin{bmatrix} \partial/\partial x & 0 & 0 \\ 0 & \partial/\partial y & 0 \\ \partial/\partial y & \partial/\partial x & 0 \\ 0 & 0 & \partial/\partial x \\ 0 & 0 & \partial/\partial y \\ 0 & 0 & 0 \end{bmatrix}}_{\mathbf{B}} \begin{bmatrix} s_x \\ s_y \\ s_z \end{bmatrix} + \underbrace{\begin{bmatrix} 0 & 0 & 0 \\ 0 & 0 & 0 \\ 0 & 0 & 0 \\ 1 & 0 & 0 \\ 0 & 1 & 0 \\ 0 & 0 & 1 \end{bmatrix}}_{\mathbf{S}} \begin{bmatrix} \partial s_x / \partial z \\ \partial s_y / \partial z \\ \partial s_z / \partial z \end{bmatrix} \quad (2.6)$$

Note that this is the common linear three dimensional strain-displacement relation where the terms $\partial/\partial z$ have been set apart. Inserting (2.4) into (2.5) yields

$$\epsilon = \mathbf{BZ}\mathbf{r} + \mathbf{SZ}\frac{\partial \mathbf{r}}{\partial z} + \mathbf{Bg} + \mathbf{S}\frac{\partial \mathbf{g}}{\partial z} \quad (2.7)$$

It can be shown that

$$\mathbf{BZ} = \mathbf{SZT}_r$$

where

$$\mathbf{T}_r = \begin{bmatrix} 0 & 0 & 0 & 0 & -1 & 0 \\ 0 & 0 & 0 & 1 & 0 & 0 \\ 0 & 0 & 0 & 0 & 0 & 0 \\ 0 & 0 & 0 & 0 & 0 & 0 \\ 0 & 0 & 0 & 0 & 0 & 0 \\ 0 & 0 & 0 & 0 & 0 & 0 \end{bmatrix}$$

Utilizing the relation above, Equation (2.7) can be written as

$$\epsilon = \mathbf{SZ} \left(\mathbf{T}_r \mathbf{r} + \frac{\partial \mathbf{r}}{\partial z} \right) + \mathbf{Bg} + \mathbf{S}\frac{\partial \mathbf{g}}{\partial z}$$

It is possible at this point to define the strain parameters

$$\boxed{\psi = \mathbf{T}_r \mathbf{r} + \frac{\partial \mathbf{r}}{\partial z}} \quad (2.8)$$

and thus rewrite the strain displacement relation in its final form

$$\epsilon = \mathbf{SZ}\psi + \mathbf{Bg} + \mathbf{S}\frac{\partial \mathbf{g}}{\partial z} \quad (2.9)$$

The section strain parameters $\psi = [\tau_x, \tau_y, \tau_z, \kappa_x, \kappa_y, \kappa_z]^T$ are representative of the strain due to the rigid displacement of two adjacent cross sections that remain undeformed. The components $\tau_x = \frac{\partial \chi_x}{\partial z} - \varphi_y$ and $\tau_y = \frac{\partial \chi_y}{\partial z} + \varphi_x$ represent shear strains of the cross section in the x and y directions, respectively. The component $\tau_z = \frac{\partial \chi_z}{\partial z}$ is the axial elongation. Furthermore, $\kappa_x = \frac{\partial \varphi_x}{\partial z}$ and $\kappa_y = \frac{\partial \varphi_y}{\partial z}$ are the curvatures around x and y , respectively, and $\kappa_z = \frac{\partial \varphi_z}{\partial z}$ is the torsion term.

Finite element discretization

The warping displacements \mathbf{g} are discretized as

$$\mathbf{g}(x, y, z) = \mathbf{N}_i(x, y) \mathbf{u}(x_i, y_i, z) \quad (2.10)$$

where \mathbf{N} are the typical finite element shape functions and \mathbf{u} the nodal warping displacements. Note that the latter depend on the position along the beam axis although the shape functions are only defined in the plane of the section. The displacement of a point in the cross section is then given as

$$\mathbf{s} = \mathbf{Z}\mathbf{r} + \mathbf{N}\mathbf{u} \quad (2.11)$$

and finally introducing (2.10) in (2.9) yields

$$\boxed{\boldsymbol{\epsilon} = \mathbf{S}\mathbf{Z}\boldsymbol{\psi} + \mathbf{B}\mathbf{N}\mathbf{u} + \mathbf{S}\mathbf{N}\frac{\partial \mathbf{u}}{\partial z}} \quad (2.12)$$

2.2.4 Virtual work principle

The total virtual work per unit length W is given as

$$W = W_e + W_i$$

The first variation of the total virtual work per unit length can be written as

$$\delta \frac{\partial W}{\partial z} = \delta \frac{\partial W_e}{\partial z} + \delta \frac{\partial W_i}{\partial z} \quad (2.13)$$

where W_i is the work done by the internal elastic forces, and W_e the work done by the external forces acting on the cross section.

External virtual work

Assuming that the surface and the body forces are zero, the axial derivative of the work produced by the section stresses is the only contribution to the external work W_e . Thus(cf. Figure 2.2)

$$\delta \frac{\partial W_e}{\partial z} = \int_A \frac{\partial (\delta \mathbf{s}^T \mathbf{p})}{\partial z} dA$$

The external virtual work expression can be obtained by replacing the displacement \mathbf{s} as defined in (2.4) into the equation above

$$\begin{aligned} \delta \frac{\partial W_e}{\partial z} &= \int_A \frac{\partial (\delta \mathbf{v}^T \mathbf{p})}{\partial z} dA + \int_A \frac{(\delta \mathbf{g}^T \mathbf{p})}{\partial z} dA \\ &= \underbrace{\delta \frac{\partial \mathbf{r}^T}{\partial z} \int_A \mathbf{Z}^T \mathbf{p} dA + \delta \mathbf{r}^T \int_A \mathbf{Z}^T \frac{\partial \mathbf{p}}{\partial z} dA}_{\text{Work from rigid displacement}} \\ &\quad + \underbrace{\delta \frac{\partial \mathbf{u}^T}{\partial z} \int_A \mathbf{N}^T \mathbf{p} dA + \delta \mathbf{u}^T \int_A \mathbf{N}^T \frac{\partial \mathbf{p}}{\partial z} dA}_{\text{Work from warping displacements}} \end{aligned}$$

Using Equation (2.3) it is possible to further simplify the previous equation

$$\begin{aligned}\delta \frac{\partial W_e}{\partial z} &= \delta \frac{\partial \mathbf{r}^T}{\partial z} \boldsymbol{\theta} + \delta \mathbf{r}^T \frac{\partial \boldsymbol{\theta}}{\partial z} \\ &+ \delta \frac{\partial \mathbf{u}^T}{\partial z} \int_A \mathbf{N}^T \mathbf{P} \, dA + \delta \mathbf{u}^T \int_A \mathbf{N}^T \frac{\partial \mathbf{P}^T}{\partial z} \, dA\end{aligned}$$

Note that it is possible to introduce the strain parameters in the following manner

$$\begin{aligned}\delta \frac{\partial \mathbf{r}^T}{\partial z} \boldsymbol{\theta} + \delta \mathbf{r}^T \frac{\partial \boldsymbol{\theta}}{\partial z} &= \delta \frac{\partial \mathbf{r}^T}{\partial z} \boldsymbol{\theta} + \delta \mathbf{r}^T \frac{\partial \boldsymbol{\theta}}{\partial z} + \delta \mathbf{r}^T \mathbf{T}_r^t \boldsymbol{\theta} - \delta \mathbf{r}^T \mathbf{T}_r^T \boldsymbol{\theta} \\ &= \delta \mathbf{r}^T \frac{\partial \boldsymbol{\theta}}{\partial z} - \delta \mathbf{r}^T \mathbf{T}_r^T \boldsymbol{\theta} + \delta \underbrace{\left(\mathbf{r}^T \mathbf{T}_r^t + \frac{\partial \mathbf{r}^T}{\partial z} \right)}_{\boldsymbol{\psi}^T} \boldsymbol{\theta} \\ &= \delta \mathbf{r}^T \frac{\partial \boldsymbol{\theta}}{\partial z} - \delta \mathbf{r}^T \mathbf{T}_r^T \boldsymbol{\theta} + \delta \boldsymbol{\psi}^T \boldsymbol{\theta}\end{aligned}$$

The expression for the external virtual work is then given as

$$\begin{aligned}\delta \frac{\partial W_e}{\partial z} &= \delta \mathbf{r}^T \frac{\partial \boldsymbol{\theta}}{\partial z} - \delta \mathbf{r}^T \mathbf{T}_r^T \boldsymbol{\theta} + \delta \boldsymbol{\psi}^T \boldsymbol{\theta} \\ &+ \delta \frac{\partial \mathbf{u}^T}{\partial z} \int_A \mathbf{N}^T \mathbf{P} \, dA + \delta \mathbf{u}^T \int_A \mathbf{N}^T \frac{\partial \mathbf{P}^T}{\partial z} \, dA\end{aligned}$$

which in matrix form read as

$$\delta \frac{\partial W_e}{\partial z} = \begin{bmatrix} \delta \frac{\partial \mathbf{u}^T}{\partial z} \\ \delta \mathbf{u} \\ \delta \boldsymbol{\psi} \end{bmatrix}^T \begin{bmatrix} \mathbf{P} \\ \frac{\partial \mathbf{P}}{\partial z} \\ \boldsymbol{\theta} \end{bmatrix} + \delta \mathbf{r}^T \left(\frac{\partial \boldsymbol{\theta}}{\partial z} - \mathbf{T}_r^T \boldsymbol{\theta} \right) \quad (2.14)$$

where

$$\begin{aligned}\mathbf{P} &= \int_A \mathbf{N}^T \mathbf{p} \, dA \\ \frac{\partial \mathbf{P}}{\partial z} &= \int_A \mathbf{N}^T \frac{\partial \mathbf{p}^T}{\partial z} \, dA\end{aligned}$$

The vector \mathbf{P} can be seen as the nodal stresses in the cross section finite element discretization as it represents the discretized stresses acting on the cross section face.

Internal virtual work

The internal work or the work done by the elastic strain energy per unit length can be written as

$$\delta \frac{\partial W_i}{\partial z} = \int_A \delta \boldsymbol{\epsilon}^T \boldsymbol{\sigma} \, dA \quad (2.15)$$

Observing the stress-strain relation in Equation (2.1), the internal work expression in (2.15) can be restated as

$$\delta \frac{\partial W_i}{\partial z} = \int_A \delta \boldsymbol{\epsilon}^T \mathbf{Q} \boldsymbol{\epsilon} \, dA$$

Inserting the expression for the strain-displacement relation in (2.12) in the equation above yields

$$\begin{aligned}
\delta \frac{\partial W_i}{\partial z} &= \int_A \left(\delta \boldsymbol{\psi}^T \mathbf{Z}^T \mathbf{S}^T + \delta \mathbf{u}^T \mathbf{N}^T \mathbf{B}^T + \delta \frac{\partial \mathbf{u}^T}{\partial z} \mathbf{N}^T \mathbf{S}^T \right) \mathbf{Q} \\
&\quad \left(\mathbf{S} \mathbf{Z} \boldsymbol{\psi} + \mathbf{B} \mathbf{N} \mathbf{u} + \mathbf{S} \mathbf{N} \frac{\partial \mathbf{u}}{\partial z} \right) dA \\
&= \int_A \delta \boldsymbol{\psi}^T \mathbf{Z}^T \mathbf{S}^T \mathbf{Q} \mathbf{S} \mathbf{Z} \boldsymbol{\psi} dA \\
&\quad + \int_A \delta \boldsymbol{\psi}^T \mathbf{Z}^T \mathbf{S}^T \mathbf{Q} \mathbf{B} \mathbf{N} \mathbf{u} dA \\
&\quad + \int_A \delta \boldsymbol{\psi}^T \mathbf{Z}^T \mathbf{S}^T \mathbf{Q} \mathbf{S} \mathbf{N} \frac{\partial \mathbf{u}}{\partial z} dA \\
&\quad + \int_A \delta \mathbf{u}^T \mathbf{N}^T \mathbf{B}^T \mathbf{Q} \mathbf{S} \mathbf{Z} \boldsymbol{\psi} dA \\
&\quad + \int_A \delta \mathbf{u}^T \mathbf{N}^T \mathbf{B}^T \mathbf{Q} \mathbf{B} \mathbf{N} \mathbf{u} dA \\
&\quad + \int_A \delta \mathbf{u}^T \mathbf{N}^T \mathbf{B}^T \mathbf{Q} \mathbf{S} \mathbf{N} \frac{\partial \mathbf{u}}{\partial z} dA \\
&\quad + \int_A \delta \frac{\partial \mathbf{u}^T}{\partial z} \mathbf{N}^T \mathbf{S}^T \mathbf{Q} \mathbf{S} \mathbf{Z} \boldsymbol{\psi} dA \\
&\quad + \int_A \delta \frac{\partial \mathbf{u}^T}{\partial z} \mathbf{N}^T \mathbf{S}^T \mathbf{Q} \mathbf{B} \mathbf{N} \mathbf{u} dA \\
&\quad + \int_A \delta \frac{\partial \mathbf{u}^T}{\partial z} \mathbf{N}^T \mathbf{S}^T \mathbf{Q} \mathbf{S} \mathbf{N} \frac{\partial \mathbf{u}}{\partial z} dA
\end{aligned}$$

where the following matrices can be identified

$$\begin{aligned}
\mathbf{A} &= \int_A \mathbf{Z}^T \mathbf{S}^T \mathbf{Q} \mathbf{S} \mathbf{Z} dA \\
\mathbf{R} &= \int_A \mathbf{N}^T \mathbf{B}^T \mathbf{Q} \mathbf{S} \mathbf{Z} dA \\
\mathbf{E} &= \int_A \mathbf{N}^T \mathbf{B}^T \mathbf{Q} \mathbf{B} \mathbf{N} dA \\
\mathbf{C} &= \int_A \mathbf{N}^T \mathbf{S}^T \mathbf{Q} \mathbf{B} \mathbf{N} dA \\
\mathbf{L} &= \int_A \mathbf{N}^T \mathbf{S}^T \mathbf{Q} \mathbf{S} \mathbf{Z} dA \\
\mathbf{M} &= \int_A \mathbf{N}^T \mathbf{S}^T \mathbf{Q} \mathbf{S} \mathbf{N} dA
\end{aligned} \tag{2.16}$$

Hence, rearranging the state variables it is possible to write the internal virtual work in matrix form as

$$\delta \frac{\partial W_i}{\partial z} = \begin{bmatrix} \delta \frac{\partial \mathbf{u}}{\partial z} \\ \delta \mathbf{u} \\ \delta \boldsymbol{\psi} \end{bmatrix}^T \begin{bmatrix} \mathbf{M} & \mathbf{C} & \mathbf{L} \\ \mathbf{C}^T & \mathbf{E} & \mathbf{R} \\ \mathbf{L}^T & \mathbf{R}^T & \mathbf{A} \end{bmatrix} \begin{bmatrix} \frac{\partial \mathbf{u}}{\partial z} \\ \mathbf{u} \\ \boldsymbol{\psi} \end{bmatrix} \tag{2.17}$$

Total virtual work

According to Equation (2.13) the total virtual work per unit length can be written as

$$\delta \frac{\partial W}{\partial z} = \delta \frac{\partial W_e}{\partial z} - \delta \frac{\partial W_i}{\partial z} = \int_A \frac{\partial (\delta \mathbf{s}^T \mathbf{p})}{\partial z} dA - \int_A \delta \boldsymbol{\epsilon}^T \boldsymbol{\sigma} dA \quad (2.18)$$

For a general virtual displacement $\delta \mathbf{s}$ and virtual strain $\delta \boldsymbol{\epsilon}$, a necessary and sufficient equilibrium condition is

$$\delta \frac{\partial W}{\partial z} = 0$$

Thus, inserting Equation (2.14) and (2.17) into (2.18) the following relation is obtained

$$\begin{aligned} & \underbrace{\begin{bmatrix} \delta \frac{\partial \mathbf{u}}{\partial z} \\ \delta \mathbf{u} \\ \delta \psi \end{bmatrix}^T \begin{bmatrix} \mathbf{M} & \mathbf{C} & \mathbf{L} \\ \mathbf{C}^T & \mathbf{E} & \mathbf{R} \\ \mathbf{L}^T & \mathbf{R}^T & \mathbf{A} \end{bmatrix} \begin{bmatrix} \frac{\partial \mathbf{u}}{\partial z} \\ \mathbf{u} \\ \psi \end{bmatrix}}_{\text{Internal virtual work of the beam slice}} = \\ & = \underbrace{\begin{bmatrix} \delta \frac{\partial \mathbf{u}}{\partial z} \\ \delta \mathbf{u} \\ \delta \psi \end{bmatrix}^T \begin{bmatrix} \mathbf{P} \\ \frac{\partial \mathbf{P}}{\partial z} \\ \boldsymbol{\theta} \end{bmatrix}}_{\text{External virtual work of the beam slice}} \\ & + \underbrace{\delta \mathbf{r}^T \left(\frac{\partial \boldsymbol{\theta}}{\partial z} - \mathbf{T}_r^T \boldsymbol{\theta} \right)}_{\text{Equilibrium of the beam slice}} \end{aligned}$$

The previous equation must be true for any admissible virtual displacement $\delta \psi$, $\delta \mathbf{u}$, $\delta \frac{\partial \mathbf{u}^T}{\partial z}$ and $\delta \mathbf{r}$, thus leading to the following set of equations

$$\begin{aligned} \mathbf{M} \frac{\partial \mathbf{u}}{\partial z} + \mathbf{C}^T \mathbf{u} + \mathbf{L} \psi &= \mathbf{P} \\ \mathbf{C} \frac{\partial \mathbf{u}}{\partial z} + \mathbf{E} \mathbf{u} + \mathbf{R} \psi &= \frac{\partial \mathbf{P}}{\partial z} \\ \mathbf{L}^T \frac{\partial \mathbf{u}}{\partial z} + \mathbf{R}^T \mathbf{u} + \mathbf{A} \psi &= \boldsymbol{\theta} \\ \frac{\partial \boldsymbol{\theta}}{\partial z} &= \mathbf{T}_r^T \boldsymbol{\theta} \end{aligned}$$

It is possible to further simplify the former by differentiating the first equation with respect to z

$$\begin{aligned} \mathbf{M} \frac{\partial^2 \mathbf{u}}{\partial z^2} + \mathbf{C}^T \frac{\partial \mathbf{u}}{\partial z} + \mathbf{L} \frac{\partial \psi}{\partial z} &= \frac{\partial \mathbf{P}}{\partial z} \\ \mathbf{C} \frac{\partial \mathbf{u}}{\partial z} + \mathbf{E} \mathbf{u} + \mathbf{R} \psi &= \frac{\partial \mathbf{P}}{\partial z} \\ \mathbf{L}^T \frac{\partial \mathbf{u}}{\partial z} + \mathbf{R}^T \mathbf{u} + \mathbf{A} \psi &= \boldsymbol{\theta} \\ \frac{\partial \boldsymbol{\theta}}{\partial z} &= \mathbf{T}_r^T \boldsymbol{\theta} \end{aligned}$$

and obtain the equilibrium equations for the cross section

$$\begin{aligned} \mathbf{M} \frac{\partial^2 \mathbf{u}}{\partial z^2} + (\mathbf{C} - \mathbf{C}^T) \frac{\partial \mathbf{u}}{\partial z} + \mathbf{L} \frac{\partial \psi}{\partial z} - \mathbf{E} \mathbf{u} - \mathbf{R} \psi &= \mathbf{0} \\ \mathbf{L}^T \frac{\partial \mathbf{u}}{\partial z} + \mathbf{R}^T \mathbf{u} + \mathbf{A} \psi &= \boldsymbol{\theta} \\ \frac{\partial \boldsymbol{\theta}}{\partial z} &= \mathbf{T}_r^T \boldsymbol{\theta} \end{aligned} \quad (2.19)$$

This concludes the derivation of the equilibrium equations of the cross section.

2.3 Solutions to equilibrium equations

The set of equations in (2.19) admits two types of solutions – a particular integral which depends on the boundary conditions, or the internal force resultants $\boldsymbol{\theta}$ in this case, and a homogeneous integral which corresponds to the eigensolutions when $\boldsymbol{\theta} = \mathbf{0}$. The homogeneous and particular solutions will be henceforth referred to as the *extremity* and the *central* solutions (cf. Giavotto et al. [6]), respectively. A more detailed discussion on this topic is presented in Section 2.4.

2.3.1 Extremity solutions

The extremity solutions owe their name to the fact that they correspond to the solutions at the extremities of the beam where the loads are applied. These are the self-balanced, $\boldsymbol{\theta} = \mathbf{0}$, eigensolutions of (2.19), that is, the solutions to the following set

$$\begin{aligned} \mathbf{M} \frac{\partial^2 \mathbf{u}}{\partial z^2} + (\mathbf{C} - \mathbf{C}^T) \frac{\partial \mathbf{u}}{\partial z} + \mathbf{L} \frac{\partial \psi}{\partial z} - \mathbf{E} \mathbf{u} - \mathbf{R} \psi &= \mathbf{0} \\ \mathbf{L}^T \frac{\partial \mathbf{u}}{\partial z} + \mathbf{R}^T \mathbf{u} + \mathbf{A} \psi &= \mathbf{0} \end{aligned}$$

or in matrix form

$$\begin{bmatrix} \mathbf{M} & \mathbf{0} \\ \mathbf{0} & \mathbf{0} \end{bmatrix} \begin{bmatrix} \frac{\partial^2 \mathbf{u}}{\partial z^2} \\ \frac{\partial^2 \psi}{\partial z^2} \end{bmatrix} + \begin{bmatrix} (\mathbf{C} - \mathbf{C}^T) & \mathbf{L} \\ -\mathbf{L}^T & \mathbf{0} \end{bmatrix} \begin{bmatrix} \frac{\partial \mathbf{u}}{\partial z} \\ \frac{\partial \psi}{\partial z} \end{bmatrix} - \begin{bmatrix} \mathbf{E} & \mathbf{R} \\ \mathbf{R}^T & \mathbf{A} \end{bmatrix} \begin{bmatrix} \mathbf{u} \\ \psi \end{bmatrix} = \begin{bmatrix} \mathbf{0} \\ \mathbf{0} \end{bmatrix} \quad (2.20)$$

Assuming solutions of the type

$$\begin{aligned} \mathbf{u} &= \tilde{\mathbf{u}} e^{\lambda z} \\ \psi &= \tilde{\psi} e^{\lambda z} \end{aligned}$$

and introducing the previous equation in (2.20) yields

$$\left(\lambda^2 \begin{bmatrix} \mathbf{M} & \mathbf{0} \\ \mathbf{0} & \mathbf{0} \end{bmatrix} + \lambda \begin{bmatrix} (\mathbf{C} - \mathbf{C}^T) & \mathbf{L} \\ -\mathbf{L}^T & \mathbf{0} \end{bmatrix} - \begin{bmatrix} \mathbf{E} & \mathbf{R} \\ \mathbf{R}^T & \mathbf{A} \end{bmatrix} \right) \begin{bmatrix} \tilde{\mathbf{u}} \\ \tilde{\psi} \end{bmatrix} = \mathbf{0}$$

The solution to (2.20) can be stated in terms of a linear combination of the solutions to the eigenvalue problem

$$\lambda^2 \begin{bmatrix} \mathbf{M} & \mathbf{0} \\ \mathbf{0} & \mathbf{0} \end{bmatrix} + \lambda \begin{bmatrix} (\mathbf{C} - \mathbf{C}^T) & \mathbf{L} \\ -\mathbf{L}^T & \mathbf{0} \end{bmatrix} - \begin{bmatrix} \mathbf{E} & \mathbf{R} \\ \mathbf{R}^T & \mathbf{A} \end{bmatrix} = \mathbf{0}$$

where λ are the eigenvalues and $\tilde{\mathbf{u}}$ and $\tilde{\psi}$ the corresponding eigenvectors. The eigenvectors represent the extremity modes and the corresponding eigenvalues define a diffusion length. The lowest eigenvalues are the most interesting as they propagate farther into the beam. Choosing the eigenvectors corresponding to the lowest eigenvalues it should be possible to study the effect of the loads at the extremities of the beam. Nonetheless, the solution to this eigenvalue problem may be cumbersome as the size of the matrices becomes larger.

2.3.2 Central solutions

The central solution refer to the solutions obtained at the central part of the beam corresponding to non-zero stress resultants ($\boldsymbol{\theta} \neq 0$). For convenience, let us rewrite the equilibrium equations in (2.19) so that all the terms with derivatives of the same order are grouped

$$\begin{cases} \mathbf{E}\mathbf{u} + \mathbf{R}\psi = (\mathbf{C} - \mathbf{C}^T) \frac{\partial \mathbf{u}}{\partial z} + \mathbf{L} \frac{\partial \psi}{\partial z} + \mathbf{M} \frac{\partial^2 \mathbf{u}}{\partial z^2} \\ \mathbf{R}^T \mathbf{u} + \mathbf{A}\psi = -\mathbf{L}^T \frac{\partial \mathbf{u}}{\partial z} + \boldsymbol{\theta} \end{cases} \quad (2.21)$$

At this point the reader may opt to read Section 2.4 first to get an insight into the mathematical properties of the central solutions. Otherwise the necessary results to retain are that the central solutions \mathbf{u}_c and ψ_c are linear combinations of polynomial functions in z with n being the highest degree of such polynomials (see Equation (2.32) in Section 2.4.2). Thus

$$\frac{\partial^n \mathbf{u}_c}{\partial z^n} = 0 \text{ and } \frac{\partial^n \psi_c}{\partial z^n} = 0$$

Furthermore, from the equilibrium equations for a rigid cross section (see Equation (2.28) in Section 2.4.1) the following must hold

$$\frac{\partial^2 \boldsymbol{\theta}}{\partial z^2} = 0 \quad (2.22)$$

and, recall from the equilibrium equations in (2.19) that

$$\frac{\partial \boldsymbol{\theta}}{\partial z} = \mathbf{T}_r^T \boldsymbol{\theta} \quad (2.23)$$

We shall now utilize each of the results above to find an expression for the central solutions based on the set (2.21).

Let us consider the following sets which are obtained from the evaluation of the n^{th} order derivative of set (2.21)

$$\begin{aligned} (0) \quad & \begin{cases} \mathbf{E}\mathbf{u} + \mathbf{R}\psi = (\mathbf{C} - \mathbf{C}^T) \frac{\partial \mathbf{u}}{\partial z} + \mathbf{L} \frac{\partial \psi}{\partial z} + \underbrace{\mathbf{M} \frac{\partial^2 \mathbf{u}}{\partial z^2}}_{=0} \\ \mathbf{R}^T \mathbf{u} + \mathbf{A}\psi = -\mathbf{L}^T \frac{\partial \mathbf{u}}{\partial z} + \boldsymbol{\theta} \end{cases} \\ & \quad \uparrow \quad \partial \mathbf{u} / \partial z \neq 0 \text{ and } \partial \psi / \partial z \neq 0 \\ (1) \quad & \begin{cases} \mathbf{E} \frac{\partial \mathbf{u}}{\partial z} + \mathbf{R} \frac{\partial \psi}{\partial z} = (\mathbf{C} - \mathbf{C}^T) \underbrace{\frac{\partial^2 \mathbf{u}}{\partial z^2}}_{=0} + \mathbf{L} \underbrace{\frac{\partial^2 \psi}{\partial z^2}}_{=0} + \mathbf{M} \underbrace{\frac{\partial^3 \mathbf{u}}{\partial z^3}}_{=0} \\ \mathbf{R}^T \frac{\partial \mathbf{u}}{\partial z} + \mathbf{A} \frac{\partial \psi}{\partial z} = -\mathbf{L}^T \underbrace{\frac{\partial^2 \mathbf{u}}{\partial z^2}}_{=0} + \underbrace{\frac{\partial \boldsymbol{\theta}}{\partial z}}_{\neq 0 \text{ from (2.23)}} \end{cases} \end{aligned}$$

$$\begin{aligned}
& \uparrow \quad \partial^2 \mathbf{u} / \partial z^2 = 0 \text{ and } \partial^2 \boldsymbol{\psi} / \partial z^2 = 0 \\
(2) \quad & \left\{ \begin{aligned} \mathbf{E} \frac{\partial^2 \mathbf{u}}{\partial z^2} + \mathbf{R} \frac{\partial^2 \boldsymbol{\psi}}{\partial z^2} &= (\mathbf{C} - \mathbf{C}^T) \underbrace{\frac{\partial^3 \mathbf{u}}{\partial z^3}}_{=0} + \mathbf{L} \underbrace{\frac{\partial^3 \boldsymbol{\psi}}{\partial z^3}}_{=0} + \mathbf{M} \underbrace{\frac{\partial^4 \mathbf{u}}{\partial z^4}}_0 \\ \mathbf{R}^T \frac{\partial^2 \mathbf{u}}{\partial z^2} + \mathbf{A} \frac{\partial^2 \boldsymbol{\psi}}{\partial z^2} &= -\mathbf{L}^T \underbrace{\frac{\partial^3 \mathbf{u}}{\partial z^3}}_{=0} + \underbrace{\frac{\partial^2 \boldsymbol{\theta}}{\partial z^2}}_{=0 \text{ from (2.22)}} \end{aligned} \right. \\
& \uparrow \quad \partial^3 \mathbf{u} / \partial z^3 = 0 \text{ and } \partial^3 \boldsymbol{\psi} / \partial z^3 = 0 \\
& \cdot \\
& \cdot \\
& \uparrow \quad \partial^{(n-1)} \mathbf{u} / \partial z^{(n-1)} = 0 \text{ and } \partial^{(n-1)} \boldsymbol{\psi} / \partial z^{(n-1)} = 0 \\
(n-1) \quad & \left\{ \begin{aligned} \mathbf{E} \frac{\partial^{(n-1)} \mathbf{u}}{\partial z^{(n-1)}} + \mathbf{R} \frac{\partial^{(n-1)} \boldsymbol{\psi}}{\partial z^{(n-1)}} &= (\mathbf{C} - \mathbf{C}^T) \underbrace{\frac{\partial^{(n)} \mathbf{u}}{\partial z^{(n)}}}_{=0} + \mathbf{L} \underbrace{\frac{\partial^{(n)} \boldsymbol{\psi}}{\partial z^{(n)}}}_{=0} \\ \mathbf{R}^T \frac{\partial^{(n-1)} \mathbf{u}}{\partial z^{(n-1)}} + \mathbf{A} \frac{\partial^{(n-1)} \boldsymbol{\psi}}{\partial z^{(n-1)}} &= -\mathbf{L}^T \underbrace{\frac{\partial^{(n)} \mathbf{u}}{\partial z^{(n)}}}_{=0} \end{aligned} \right. \\
& \uparrow \quad \partial^{(n)} \mathbf{u} / \partial z^{(n)} = 0 \text{ and } \partial^{(n)} \boldsymbol{\psi} / \partial z^{(n)} = 0 \\
(n) \quad & \left\{ \begin{aligned} \mathbf{E} \frac{\partial^{(n)} \mathbf{u}}{\partial z^{(n)}} + \mathbf{R} \frac{\partial^{(n)} \boldsymbol{\psi}}{\partial z^{(n)}} &= 0 \\ \mathbf{R}^T \frac{\partial^{(n)} \mathbf{u}}{\partial z^{(n)}} + \mathbf{A} \frac{\partial^{(n)} \boldsymbol{\psi}}{\partial z^{(n)}} &= 0 \end{aligned} \right.
\end{aligned}$$

The analysis of the former sets will be done from bottom to top. The last set, set (n), corresponds to the n^{th} order derivative of the equilibrium equations in set (2.21). It is a linear homogeneous system of equations with unknowns $\partial^{(n)} \mathbf{u} / \partial z^{(n)}$ and $\partial^{(n)} \boldsymbol{\psi} / \partial z^{(n)}$ whose solutions are $\partial^{(n)} \mathbf{u} / \partial z^{(n)} = 0$ and $\partial^{(n)} \boldsymbol{\psi} / \partial z^{(n)} = 0$. These result can now be replaced in set (n-1). Hence, for set (n-1), it is possible to see that $\partial^{(n-1)} \mathbf{u} / \partial z^{(n-1)} = 0$ and $\partial^{(n-1)} \boldsymbol{\psi} / \partial z^{(n-1)} = 0$ also and so on up to set (1). In set (1) the derivative of the surface stresses $\partial \boldsymbol{\theta} / \partial z \neq 0$ and thus $\partial \mathbf{u} / \partial z \neq 0$ and $\partial \boldsymbol{\psi} / \partial z \neq 0$ as well. It is therefore demonstrated that the displacements \mathbf{u} and strain parameters $\boldsymbol{\psi}$ are at most linear functions of z . The displacements are obtained from the solution to the following sets

$$\boxed{
\begin{cases} \mathbf{E} \frac{\partial \mathbf{u}}{\partial z} + \mathbf{R} \frac{\partial \boldsymbol{\psi}}{\partial z} = 0 \\ \mathbf{R}^T \frac{\partial \mathbf{u}}{\partial z} + \mathbf{A} \frac{\partial \boldsymbol{\psi}}{\partial z} = \frac{\partial \boldsymbol{\theta}}{\partial z} \end{cases}
\begin{cases} \mathbf{E} \mathbf{u} + \mathbf{R} \boldsymbol{\psi} = (\mathbf{C} - \mathbf{C}^T) \frac{\partial \mathbf{u}}{\partial z} + \mathbf{L} \frac{\partial \boldsymbol{\psi}}{\partial z} \\ \mathbf{R}^T \mathbf{u} + \mathbf{A} \boldsymbol{\psi} = -\mathbf{L}^T \frac{\partial \mathbf{u}}{\partial z} + \boldsymbol{\theta} \end{cases}
\quad (2.24)$$

where, from Equation (2.19),

$$\frac{\partial \boldsymbol{\theta}}{\partial z} = \mathbf{T}_r^T \boldsymbol{\theta}$$

The set first set in equation (2.24) is solved first to obtain $\partial \mathbf{u} / \partial z$ and $\partial \boldsymbol{\psi} / \partial z$ for a given $\boldsymbol{\theta}$. It is then possible to evaluate the right hand side of the second set and thus obtain \mathbf{u} and $\boldsymbol{\psi}$. Note that the same coefficient matrix is used twice in the solution and it is therefore possible to decrease the solution time using a proper matrix factorization.

2.3.3 Constraint equations

The displacement formulation as described in (2.11) is six times redundant. Each of the redundancies corresponds to a description of each of the rigid body motions and translations by the warping displacements \mathbf{u} . It is therefore necessary to ensure that the warping displacement \mathbf{u} is uncoupled from the rigid displacements \mathbf{r} . The following set of constraints are therefore incorporated into the solution of the sets (2.24)

$$\begin{aligned} \sum_{n=1}^{n_n} u_{x,n} &= 0, \quad \sum_{n=1}^{n_n} u_{y,n} = 0, \quad \sum_{n=1}^{n_n} u_{z,n} = 0, \\ \sum_{n=1}^{n_n} -z_n u_{y,n} + y_n u_{z,n} &= 0, \quad \sum_{n=1}^{n_n} z_n u_{x,n} - x_n u_{z,n} = 0, \quad \sum_{n=1}^{n_n} -y_n u_{x,n} + x_n u_{y,n} = 0. \end{aligned}$$

where n_n is the number of nodes in the cross section finite element mesh, and (x_n, y_n, z_n) and $(u_{x,n}, u_{y,n}, u_{z,n})$ are the position and displacement of node n , respectively. The constraints are imposed on both the displacements \mathbf{u} and corresponding derivatives $\partial \mathbf{u} / \partial z$ and can be written in matrix form as

$$\begin{bmatrix} \mathbf{D}^T & \mathbf{0} \\ \mathbf{0} & \mathbf{D}^T \end{bmatrix} \begin{bmatrix} \mathbf{u} \\ \frac{\partial \mathbf{u}}{\partial z} \end{bmatrix} = \begin{bmatrix} \mathbf{0} \\ \mathbf{0} \end{bmatrix}, \text{ where } \mathbf{D} = \begin{bmatrix} \mathbf{I}_3 & \dots & \mathbf{I}_3 \\ \mathbf{n}_1 & \dots & \mathbf{n}_{n_n} \end{bmatrix}^T$$

where \mathbf{I}_3 is the 3×3 identity matrix, and \mathbf{n}_n is obtained from replacing the nodal coordinates (x_n, y_n, z_n) of node n in (2.2.1).

2.4 On the properties of the solutions

Some results used earlier in this manuscript to justify some of the steps in the derivation of the cross section stiffness matrix of beams are described in this section. In particular, (2.28) and (2.32) are an important result in establishing the equilibrium equations for the central solutions in Section 2.3.2. The reader may skip this section altogether if only a general overview of the method is necessary.

The section is divided in two parts. In the first part it is assumed that only the rigid body translations and rotations contribute to the displacement vector of a point in the cross section, i.e., the cross section deformation is not accounted for. The equilibrium equations are derived and it is possible to show that the force and moment resultants $\boldsymbol{\theta}$ vary linearly with respect to z or along the beam length.

In the second part the displacement of a point in the cross section is obtained through a finite element discretization of the warping displacements. The equilibrium equations are derived once again. The result is a second order homogeneous linear differential equation. The different types of solutions are identified according to Saint Venant's principle. The solutions for which the eigenvalues are different from zero will decay as z either increases or decreases. These are self-balanced ($\boldsymbol{\theta} = 0$) solutions corresponding to the modes at the extremities of the beam where the loads are applied – the *extremity* solutions. On the other hand, the solutions for which the eigenvalues are zero will not present any decay and, most importantly, it is possible to show that these will be polynomials in z . These correspond to non-zero stress resultants and account for the displacements at a section of the beam

sufficiently far from the extremities so that the influence of the external forces in the stress field is negligible – the so-called *central* solutions.

2.4.1 Rigid motions

In this section we look only at the displacements \mathbf{v} which do not strain the section, that is, we do not include the warping displacements. Thus

$$\mathbf{s} = \mathbf{v} = \mathbf{Z}\mathbf{r} = \boldsymbol{\chi} + \mathbf{n}\boldsymbol{\varphi} = \begin{bmatrix} \chi_x - y\varphi_z \\ \chi_y + x\varphi_z \\ \chi_z + y\varphi_x - x\varphi_y \end{bmatrix} \quad (2.25)$$

recalling that $\boldsymbol{\chi} = \boldsymbol{\chi}(z)$ and $\boldsymbol{\varphi} = \boldsymbol{\varphi}(z)$ correspond to the translation of the cross section reference point and rotations, respectively. The three dimensional strain components in this case are given by

$$\begin{aligned} \epsilon_{xx} &= \frac{1}{2} \left(\frac{\partial v_x}{x} + \frac{\partial v_x}{x} \right) = 0 \\ \epsilon_{yy} &= \frac{1}{2} \left(\frac{\partial v_y}{y} + \frac{\partial v_y}{y} \right) = 0 \\ 2\epsilon_{xy} &= \frac{1}{2} \left(\frac{\partial v_y}{x} + \frac{\partial v_x}{y} \right) = 0 \\ 2\epsilon_{xz} &= \left(\frac{\partial v_z}{x} + \frac{\partial v_x}{z} \right) = -\varphi_y + \frac{\partial \chi_x}{\partial z} - y \frac{\partial \varphi_z}{\partial z} \\ 2\epsilon_{yz} &= \left(\frac{\partial v_z}{y} + \frac{\partial v_y}{z} \right) = \frac{\partial \chi_y}{\partial z} + x \frac{\partial \varphi_z}{\partial z} + \varphi_x \\ \epsilon_{zz} &= \frac{1}{2} \left(\frac{\partial v_z}{z} + \frac{\partial v_z}{z} \right) = \frac{\partial \chi_z}{\partial z} + y \frac{\partial \varphi_x}{\partial z} - x \frac{\partial \varphi_y}{\partial z} \end{aligned}$$

In matrix form the previous equations can be reduced to

$$\mathbf{p} = \mathbf{t}\boldsymbol{\varphi} + \frac{\partial \boldsymbol{\chi}}{\partial z} + \mathbf{n} \frac{\partial \boldsymbol{\varphi}}{\partial z}$$

where

$$\mathbf{t} = \begin{bmatrix} 0 & -1 & 0 \\ 1 & 0 & 0 \\ 0 & 0 & 0 \end{bmatrix}$$

It is convenient at this point to introduce the vector of strain parameters $\boldsymbol{\psi} = [\tau_x, \tau_y, \tau_z, \kappa_x, \kappa_y, \kappa_z]^T$ defined in (2.8) and restated here as

$$\boldsymbol{\psi} = \begin{bmatrix} \frac{\partial \boldsymbol{\chi}}{\partial z} + \mathbf{t}\boldsymbol{\varphi} \\ \frac{\partial \boldsymbol{\varphi}}{\partial z} \end{bmatrix}$$

The three dimensional strain are hence

$$\boldsymbol{\epsilon} = \mathbf{S}\mathbf{Z}\boldsymbol{\psi} \quad (2.26)$$

Recalling the expression for the total work has been defined as

$$\delta \frac{\partial W}{\partial z} = \int_A \frac{\partial (\mathbf{p}^T \delta \mathbf{v})}{\partial z} dA - \int_A \boldsymbol{\sigma}^T \delta \boldsymbol{\epsilon} dA = 0 \quad (2.27)$$

where the displacement \mathbf{s} in (2.18) has been simply replaced here by \mathbf{v} . Replacing (2.25) and (2.26) in (2.27) yields

$$\begin{aligned}
\delta \frac{\partial W}{\partial z} &= \int_A \frac{\partial (\mathbf{p}^T \delta \chi + \mathbf{p}^T \mathbf{n} \delta \varphi)}{\partial z} dA - \int_A \boldsymbol{\sigma}^T \mathbf{S} \mathbf{Z} \delta \psi dA \\
&= \int_A \frac{\partial \mathbf{p}^T}{\partial z} \delta \chi dA + \int_A \mathbf{p}^T \frac{\partial \mathbf{n}}{\partial z} \delta \varphi dA - \int_A \boldsymbol{\sigma}^T \mathbf{S} \mathbf{Z} \delta \psi dA \\
&= \int_A \frac{\partial \mathbf{p}^T}{\partial z} \delta \chi dA + \int_A \mathbf{p}^T \frac{\partial \delta \chi}{\partial z} dA + \int_A \frac{\mathbf{p}^T}{\partial z} \mathbf{n} \delta \varphi dA + \int_A \mathbf{p}^T \mathbf{n} \frac{\delta \varphi}{\partial z} dA \\
&\quad - \int_A \boldsymbol{\sigma}^T \mathbf{S} \mathbf{Z} \delta \psi dA \\
&= \underbrace{\int_A \frac{\partial \mathbf{p}^T}{\partial z} dA}_{\partial \mathbf{T} / \partial z} \delta \chi + \underbrace{\int_A \mathbf{p}^T dA}_{\mathbf{T}} \frac{\partial \delta \chi}{\partial z} + \underbrace{\int_A \frac{\mathbf{p}^T}{\partial z} \mathbf{n} dA}_{\partial \mathbf{M} / \partial z} \delta \varphi + \underbrace{\int_A \mathbf{p}^T \mathbf{n} dA}_{\mathbf{M}} \frac{\delta \varphi}{\partial z} \\
&\quad - \int_A \boldsymbol{\sigma}^T \mathbf{S} \mathbf{Z} \delta \psi dA \\
&= \frac{\partial \mathbf{T}^T}{\partial z} \delta \chi + \mathbf{T}^T \frac{\partial \delta \chi}{\partial z} + \frac{\partial \mathbf{M}^T}{\partial z} \delta \varphi + \mathbf{M}^T \frac{\delta \varphi}{\partial z} - \int_A \boldsymbol{\sigma}^T \mathbf{S} \mathbf{Z} \delta \psi dA
\end{aligned}$$

Noting that

$$\boldsymbol{\theta}^T \psi = \mathbf{T}^T \frac{\partial \chi}{\partial z} - \mathbf{T}^T \mathbf{t} \varphi + \mathbf{M}^T \frac{\partial \varphi}{\partial z}$$

it is possible to further simplify in the following manner

$$\begin{aligned}
\delta \frac{\partial W}{\partial z} &= \frac{\partial \mathbf{T}^T}{\partial z} \delta \chi + \mathbf{T}^T \frac{\partial \delta \chi}{\partial z} + \frac{\partial \mathbf{M}^T}{\partial z} \delta \varphi + \mathbf{M}^T \frac{\delta \varphi}{\partial z} - \int_A \boldsymbol{\sigma}^T \mathbf{S} \mathbf{Z} \delta \psi dA \\
&= \frac{\partial \mathbf{T}^T}{\partial z} \delta \chi + \mathbf{T}^T \frac{\partial \delta \chi}{\partial z} + \frac{\partial \mathbf{M}^T}{\partial z} \delta \varphi + \mathbf{M}^T \frac{\delta \varphi}{\partial z} \underbrace{- \mathbf{T}^T \mathbf{t} \delta \varphi + \mathbf{T}^T \mathbf{t} \delta \varphi}_{\text{for convenience}} - \int_A \boldsymbol{\sigma}^T \mathbf{S} \mathbf{Z} \delta \psi dA \\
&= \frac{\partial \mathbf{T}^T}{\partial z} \delta \chi + \frac{\partial \mathbf{M}^T}{\partial z} \delta \varphi + \mathbf{T}^T \mathbf{t} \delta \varphi + \underbrace{\mathbf{T}^T \frac{\partial \delta \chi}{\partial z} + \mathbf{M}^T \frac{\delta \varphi}{\partial z} - \mathbf{T}^T \mathbf{t} \delta \varphi}_{\boldsymbol{\theta}^T \delta \psi} - \int_A \boldsymbol{\sigma}^T \mathbf{S} \mathbf{Z} \delta \psi dA \\
&= \frac{\partial \mathbf{T}^T}{\partial z} \delta \chi + \left(\frac{\partial \mathbf{M}^T}{\partial z} + \mathbf{T}^T \mathbf{t} \right) \delta \varphi + \left(\boldsymbol{\theta}^T - \int_A \boldsymbol{\sigma}^T \mathbf{S} \mathbf{Z} dA \right) \delta \psi
\end{aligned}$$

and isolate each of the variation terms in the equation. Thus, for the arbitrary variation of $\delta \psi$ we get

$$\boldsymbol{\theta} = \int_A \mathbf{Z} \mathbf{S} \boldsymbol{\sigma} dA$$

where $\mathbf{p} = \mathbf{S} \boldsymbol{\sigma}$. The equation above is the definition of the resultant forces acting on the cross section as stated in (2.2). Subsequently, for the arbitrary variation of $\delta \varphi$ and $\delta \chi$ we obtain, respectively

$$\frac{\partial \mathbf{M}^T}{\partial z} = -\mathbf{T}^T \mathbf{t} \quad , \quad \frac{\partial \mathbf{T}^T}{\partial z} = 0$$

The two expressions above are the equilibrium equations or the one dimensional beam equations when only the cross section rigid displacements are considered. These equations are typically obtained from simple statics and so this result shows the consistency between the one and three dimensional approaches. Furthermore, based on the results above it is possible to conclude that

$$\frac{\partial^2 \mathbf{M}^T}{\partial z^2} = 0$$

and so

$$\frac{\partial^2 \boldsymbol{\theta}}{\partial z^2} = 0 \quad (2.28)$$

The equation above states that the resulting forces acting on the section vary linearly along the beam.

2.4.2 Warping displacements

In this section we assume that

$$\mathbf{s} = \mathbf{g}$$

The displacement of a point in the cross section is given here as a function of the cross section deformation only. Note however that this definition of the displacements entails also the representation of the rigid translation $\boldsymbol{\chi}$ and rotation $\boldsymbol{\varphi}$. This is in fact the underlying motivation for the use of constraint equations as described in Section 2.3.3 to uncouple the rigid body motions and cross section deformation.

The stress-strain relation in this case is given as

$$\boldsymbol{\epsilon} = \mathbf{B}\mathbf{g} + \mathbf{S}\frac{\partial \mathbf{g}}{\partial z}$$

and the expression for the variation of the total energy is

$$\delta \frac{\partial W}{\partial z} = \int_A \frac{\partial (\mathbf{p}^T \delta \mathbf{s})}{\partial z} dA - \int_A \boldsymbol{\sigma}^T \delta \boldsymbol{\epsilon} dA$$

Recalling the generalized Hooke's law $\boldsymbol{\sigma} = \mathbf{Q}\boldsymbol{\epsilon}$ and noting that $\mathbf{p} = \mathbf{S}\boldsymbol{\sigma}$, the expression for the total virtual work of the beam cross section considering only the

warping displacements is given by

$$\begin{aligned}
\delta \frac{\partial W}{\partial z} &= \int_A \frac{\partial (\boldsymbol{\sigma}^T \mathbf{S} \delta \mathbf{g})}{\partial z} dA - \int_A \boldsymbol{\sigma}^T \left(\mathbf{B} \delta \mathbf{g} + \mathbf{S} \frac{\partial \delta \mathbf{g}}{\partial z} \right) dA \\
&= \int_A \frac{\partial \boldsymbol{\sigma}^T}{\partial z} \mathbf{S} \delta \mathbf{g} dA + \int_A \boldsymbol{\sigma}^T \mathbf{S} \frac{\partial \delta \mathbf{g}}{\partial z} dA \\
&\quad - \int_A \boldsymbol{\sigma}^T \mathbf{B} \delta \mathbf{g} dA - \int_A \boldsymbol{\sigma}^T \mathbf{S} \frac{\partial \delta \mathbf{g}}{\partial z} dA \\
&= \int_A \frac{\partial \boldsymbol{\sigma}^T}{\partial z} \mathbf{S} \delta \mathbf{g} dA - \int_A \boldsymbol{\sigma}^T \mathbf{B} \delta \mathbf{g} dA \\
&= \int_A \frac{\partial \boldsymbol{\epsilon}^T}{\partial z} \mathbf{Q} \mathbf{S} \delta \mathbf{g} dA - \int_A \boldsymbol{\epsilon}^T \mathbf{Q} \mathbf{B} \delta \mathbf{g} dA \\
&= \int_A \frac{\partial \mathbf{g}^T}{\partial z} \mathbf{B}^T \mathbf{Q} \mathbf{S} \delta \mathbf{g} dA + \int_A \frac{\partial^2 \mathbf{g}^T}{\partial z^2} \mathbf{S}^T \mathbf{Q} \mathbf{S} \delta \mathbf{g} dA \\
&\quad - \int_A \mathbf{g}^T \mathbf{B}^T \mathbf{Q} \mathbf{B} \delta \mathbf{g} dA - \int_A \frac{\partial \mathbf{g}^T}{\partial z} \mathbf{S}^T \mathbf{Q} \mathbf{B} \delta \mathbf{g} dA
\end{aligned} \tag{2.29}$$

Expanding \mathbf{g} using the typical finite element approach (cf. Equation (2.10))

$$\mathbf{g}(x, y, z) = \mathbf{N}_i(x, y) \mathbf{u}(x_i, y_i, z) \tag{2.30}$$

and replacing (2.30) in (2.29) yields

$$\begin{aligned}
\delta \frac{\partial W}{\partial z} &= \int_A \frac{\partial \mathbf{u}^T}{\partial z} \mathbf{N}^T \mathbf{B}^T \mathbf{Q} \mathbf{S} \mathbf{N} \delta \mathbf{u} dA + \int_A \frac{\partial^2 \mathbf{u}^T}{\partial z^2} \mathbf{N}^T \mathbf{S}^T \mathbf{Q} \mathbf{S} \mathbf{N} \delta \mathbf{u} dA \\
&\quad - \int_A \mathbf{u}^T \mathbf{N}^T \mathbf{B}^T \mathbf{Q} \mathbf{B} \mathbf{N} \delta \mathbf{u} dA - \int_A \frac{\partial \mathbf{u}^T}{\partial z} \mathbf{N}^T \mathbf{S}^T \mathbf{Q} \mathbf{B} \mathbf{N} \delta \mathbf{u} dA
\end{aligned}$$

From the equation above it is possible then to identify the matrices

$$\begin{aligned}
\mathbf{M} &= \int_A \mathbf{N}^T \mathbf{S}^T \mathbf{Q} \mathbf{S} \mathbf{N} dA \\
\mathbf{C} &= \int_A \mathbf{N}^T \mathbf{B}^T \mathbf{Q} \mathbf{S} \mathbf{N} dA \\
\mathbf{E} &= \int_A \mathbf{N}^T \mathbf{B}^T \mathbf{Q} \mathbf{B} \mathbf{N} dA
\end{aligned}$$

where \mathbf{M} and \mathbf{E} are symmetrical while $\mathbf{H} = \mathbf{C} - \mathbf{C}^T$ is skew-symmetrical. Rewriting the total virtual work expression

$$\delta \frac{\partial W}{\partial z} = \delta u \left(\mathbf{M} \frac{\partial^2 \mathbf{u}}{\partial z^2} - \mathbf{H} \frac{\partial \mathbf{u}}{\partial z} - \mathbf{E} \mathbf{u} \right)$$

The following must hold for an arbitrary variation of δu

$$\mathbf{M} \frac{\partial^2 \mathbf{u}}{\partial z^2} - \mathbf{H} \frac{\partial \mathbf{u}}{\partial z} - \mathbf{E} \mathbf{u} = 0 \tag{2.31}$$

This concludes the derivation of the equilibrium equations for the cross section considering only the warping displacements. The aim now is not to solve the equation

above but rather discuss the properties of the solutions for this second order linear homogeneous differential equation.

The general solution is sought as a linear combination of

$$\mathbf{u}(z) = \mathbf{h}e^{\lambda z}$$

Inserting the above into (2.31) yields

$$(\lambda^2 \mathbf{M} - \lambda \mathbf{H} - \mathbf{E}) \mathbf{h} = 0$$

where \mathbf{h} are the eigenvectors associated with the eigenvalues λ resulting from the solution to

$$\lambda^2 \mathbf{M} - \lambda \mathbf{H} - \mathbf{E} = 0$$

According to physical considerations and Saint-Venant's principle, we expect to have a self-balanced ($\boldsymbol{\theta} = 0$) solution associated with the exponentially decaying modes ($\lambda \neq 0$) – *extremity solutions* – and a solution presenting no decay ($\lambda = 0$) for which the stress resultants are non-zero ($\boldsymbol{\theta} \neq 0$) – *central solutions* (see [6]).

Owing to the structure of matrices \mathbf{M} , \mathbf{E} and \mathbf{H} (and mostly due to the fact that \mathbf{H} is skew-symmetric), for the extremity solutions the eigenvalues will be complex and come in pairs. That is, to each eigenvalue $\lambda_j = a + ib$ corresponds a second $\lambda_j = a - ib$. The solution corresponding to the first eigenvalue decays while z increases (moving away from the first end of the beam), whereas the solution associated with the second eigenvalue in the pair is identical but decays as z decreases (moving away from the second end of the beam). These solutions can be used to study end effects and determining the diffusion length or the distance at which the effects from the external loads become negligible (e.g., see Horgan [18] and Choi and Horgan [19] for a discussion on the diffusion length in anisotropic elasticity).

The central solutions for which $\boldsymbol{\theta} \neq 0$, on the other hand, do not have any exponential decay as they correspond to eigenvalues $\lambda_j = 0$ with multiplicity p_j . These are the solutions at the central part of the beam sufficiently away from the extremities so that the effect from the external loads is negligible on the stress field. The solutions for problems where $\lambda_j = 0$ and its multiplicity $p_j \geq 2$, are given as (see [21] for a comprehensive presentation of this topic)¹

$$\begin{aligned} \mathbf{u}_{1j}(z) &= \mathbf{h}_{11}e^{\lambda_j z} \\ \mathbf{u}_{2j}(z) &= \mathbf{h}_{21}e^{\lambda_j z} + \mathbf{h}_{22}ze^{\lambda_j z} \\ &\vdots \\ \mathbf{u}_{p_j j}(z) &= \mathbf{h}_{p_j 1}e^{\lambda_j z} + \mathbf{h}_{p_j 2}ze^{\lambda_j z} + \dots + z^{p_j-1}\mathbf{h}_{p_j p_j}e^{\lambda_j z} \end{aligned}$$

where the corresponding solution in this case is

$$\begin{aligned} \mathbf{u}_j(z) &= c_1 \mathbf{h}_{11}e^{\lambda_j z} + c_2 (\mathbf{h}_{21} + z\mathbf{h}_{22})e^{\lambda_j z} + \dots \\ &\quad + c_{p_j} (\mathbf{h}_{21} + z\mathbf{h}_{22} + \dots + z^{p_j-1}\mathbf{h}_{p_j p_j})e^{\lambda_j z} \end{aligned}$$

¹The authors would like to express its gratitude to Assoc. Prof. Mads Peter Sørensen (DTU-MAT) for all the help unravelling this step of the derivation.

In our specific case where $\lambda_j = 0$ the solutions in this case are of the polynomial type

$$\mathbf{u}_j(z) = c_1 \mathbf{h}_{11} + c_2 (\mathbf{h}_{21} + z \mathbf{h}_{22}) + \dots + c_p (\mathbf{h}_{21} + z \mathbf{h}_{22} + \dots + z^{p_j-1} \mathbf{h}_{p_j p_j})$$

A central solution \mathbf{u}_c will be any linear combination of the solutions \mathbf{u}_j for which $\lambda_j = 0$. If n is the maximum of all p_j then

$$\frac{\partial^n \mathbf{u}_c}{\partial z^n} = 0 \quad (2.32)$$

Thus the central solutions are polynomial functions in z of at most degree n .

2.5 Cross section properties

We look first for the compliance matrix of a cross section of the beam. That is we are interested in finding an expression for the strain energy as function of the stress resultants and moments. These are in fact the central solutions derived above – a particular solution depending on the applied section forces at a given cross section subject to particular boundary conditions which guarantee that the effects of the extremity solutions are negligible. A procedure is presented in this section for the practical determination of the cross section stiffness matrix based on the result of the central solutions. Finally expressions for the determination of the shear and elastic center are derived.

2.5.1 Cross section stiffness matrix

From Equation (2.24) it is important to note that the central solutions are linear and homogeneous² functions of the force resultants. Thus it is possible to write

$$\begin{aligned} \mathbf{u} &= \mathbf{X}\boldsymbol{\theta}, & \frac{\partial \mathbf{u}}{\partial z} &= \frac{\partial \mathbf{X}}{\partial z} \boldsymbol{\theta} \\ \boldsymbol{\psi} &= \mathbf{Y}\boldsymbol{\theta}, & \frac{\partial \boldsymbol{\psi}}{\partial z} &= \frac{\partial \mathbf{Y}}{\partial z} \boldsymbol{\theta} \end{aligned} \quad (2.33)$$

Inserting the expressions above in (2.24) yields

$$\boxed{\begin{cases} \mathbf{E}\mathbf{X} + \mathbf{R}\mathbf{Y} = (\mathbf{C} - \mathbf{C}^T) \frac{\partial \mathbf{X}}{\partial z} + \mathbf{L} \frac{\partial \mathbf{Y}}{\partial z} \\ \mathbf{R}^T \mathbf{X} + \mathbf{A}\mathbf{Y} = -\mathbf{L}^T \frac{\partial \mathbf{X}}{\partial z} + \mathbf{I}_6 \\ \mathbf{E} \frac{\partial \mathbf{X}}{\partial z} + \mathbf{R} \frac{\partial \mathbf{Y}}{\partial z} = 0 \\ \mathbf{R}^T \frac{\partial \mathbf{X}}{\partial z} + \mathbf{A} \frac{\partial \mathbf{Y}}{\partial z} = \mathbf{T}_r^T \end{cases}} \quad (2.34)$$

Note that the set of equations above can be obtained by replacing $\boldsymbol{\theta} = \mathbf{I}_6$ in (2.24). This corresponds to determining the central solutions for six different choices of the stress resultant $\boldsymbol{\theta}$ in an orderly way, i.e., setting one of the entries to unity and the remaining to zero. In fact, each of the six columns of \mathbf{X} , \mathbf{Y} , $\frac{\partial \mathbf{X}}{\partial z}$ and $\frac{\partial \mathbf{Y}}{\partial z}$ hold the corresponding displacement solution for each of the different stress resultants.

²An homogeneous function is such that $f(\alpha x) = \alpha f(x)$. In this specific case, one important inference is that homogeneous functions do not have an independent term.

Restating the expression for the variation of the total energy obtained from the virtual work principle

$$\delta \frac{\partial W}{\partial z} = \int_A \frac{\partial (\mathbf{p}^T \delta \mathbf{v})}{\partial z} dA - \int_A \boldsymbol{\sigma}^T \delta \boldsymbol{\epsilon} dA = 0$$

The previous equation can be restated as

$$\delta \boldsymbol{\theta}^T \mathbf{F}_s \boldsymbol{\theta} = \int_A \boldsymbol{\sigma}^T \delta \boldsymbol{\epsilon} dA$$

where \mathbf{F}_s is the compliance matrix of the section. The strain is redefined by inserting (2.33) in (2.12)

$$\boldsymbol{\epsilon} = \mathbf{S}\mathbf{Z}\mathbf{Y}\boldsymbol{\theta} + \mathbf{B}\mathbf{N}\mathbf{X}\boldsymbol{\theta} + \mathbf{S}\mathbf{N}\frac{\partial \mathbf{X}}{\partial z}\boldsymbol{\theta}$$

which then yields for the internal energy

$$\delta \frac{\partial W_i}{\partial z} = \int_A \delta \boldsymbol{\theta} \left(\mathbf{Y}^T \mathbf{Z}^T \mathbf{S}^T + \mathbf{X}^T \mathbf{N}^T \mathbf{B}^T + \frac{\partial \mathbf{X}^T}{\partial z} \mathbf{N}^T \mathbf{S}^T \right) \mathbf{Q} \\ \left(\mathbf{S}\mathbf{Z}\mathbf{Y} + \mathbf{B}\mathbf{N}\mathbf{X} + \mathbf{S}\mathbf{N}\frac{\partial \mathbf{X}}{\partial z} \right) \boldsymbol{\theta} dA$$

The former can be stated in matrix form as

$$\delta \frac{\partial W_i}{\partial z} = \begin{bmatrix} \delta \boldsymbol{\theta} \mathbf{X} \\ \delta \boldsymbol{\theta} \frac{\partial \mathbf{X}}{\partial z} \\ \delta \boldsymbol{\theta} \mathbf{Y} \end{bmatrix}^T \begin{bmatrix} \mathbf{E} & \mathbf{C} & \mathbf{R} \\ \mathbf{C}^T & \mathbf{M} & \mathbf{L} \\ \mathbf{R}^T & \mathbf{L}^T & \mathbf{A} \end{bmatrix} \begin{bmatrix} \mathbf{X} \boldsymbol{\theta} \\ \frac{\partial \mathbf{X}}{\partial z} \boldsymbol{\theta} \\ \mathbf{Y} \boldsymbol{\theta} \end{bmatrix}$$

The total virtual work expression becomes

$$\delta \boldsymbol{\theta}^T \mathbf{F}_s \boldsymbol{\theta} = \begin{bmatrix} \delta \boldsymbol{\theta} \mathbf{X} \\ \delta \boldsymbol{\theta} \frac{\partial \mathbf{X}}{\partial z} \\ \delta \boldsymbol{\theta} \mathbf{Y} \end{bmatrix}^T \begin{bmatrix} \mathbf{E} & \mathbf{C} & \mathbf{R} \\ \mathbf{C}^T & \mathbf{M} & \mathbf{L} \\ \mathbf{R}^T & \mathbf{L}^T & \mathbf{A} \end{bmatrix} \begin{bmatrix} \mathbf{X} \boldsymbol{\theta} \\ \frac{\partial \mathbf{X}}{\partial z} \boldsymbol{\theta} \\ \mathbf{Y} \boldsymbol{\theta} \end{bmatrix}$$

For any admissible virtual displacement $\delta \boldsymbol{\theta} \mathbf{X}$, $\delta \boldsymbol{\theta} \frac{\partial \mathbf{X}}{\partial z}$ and $\delta \boldsymbol{\theta} \mathbf{Y}$ it is possible to obtain an expression for the cross section compliance matrix defined as

$$\mathbf{F}_s = \begin{bmatrix} \mathbf{X} \\ \frac{\partial \mathbf{X}}{\partial z} \\ \mathbf{Y} \end{bmatrix}^T \begin{bmatrix} \mathbf{E} & \mathbf{C} & \mathbf{R} \\ \mathbf{C}^T & \mathbf{M} & \mathbf{L} \\ \mathbf{R}^T & \mathbf{L}^T & \mathbf{A} \end{bmatrix} \begin{bmatrix} \mathbf{X} \\ \frac{\partial \mathbf{X}}{\partial z} \\ \mathbf{Y} \end{bmatrix}$$

The corresponding stiffness matrix \mathbf{K}_s can be computed as

$$\mathbf{K}_s = \mathbf{F}_s^{-1} \quad (2.35)$$

This result can be used to generate beam finite element models for which the strains can be exactly described by the six strain parameters in $\boldsymbol{\psi}$. The material may be anisotropic, inhomogeneously distributed, and the reference coordinate system may be arbitrarily located. The stiffness matrix \mathbf{K}_s will correctly account for any geometrical or material couplings.

2.5.2 Shear center and elastic center positions

The expressions for the positions of the shear and elastic center are presented next.

The shear center is defined as the point at which a load applied parallel to the plane of the section will produce no torsion (i.e., $\kappa_z = 0$). Hence, assume that two transverse forces, T_x and T_y are applied at a point (x_s, y_s) at a given cross section. The moments induced by the two forces are

$$M_x = -T_y(L - z) \quad , \quad M_y = T_x(L - z) \quad , \quad M_z = -T_x y_s + T_y x_s \quad (2.36)$$

The aim is to find the position (x_s, y_s) for which the curvature associated with the twist $\kappa_z = 0$. Thus, taking into account the cross section constitutive relation $\psi = \mathbf{F}_s \boldsymbol{\theta}$, the following holds

$$\kappa_z = F_{s,61}T_x + F_{s,62}T_y + F_{s,64}M_x + F_{s,65}M_y + F_{s,66}M_z = 0$$

Inserting (2.36) into the previous equation yields

$$[F_{s,61} + F_{s,62}(L - z) - F_{s,66}y_s]T_x + [F_{s,62} - F_{s,64}(L - z) + F_{s,66}x_s]T_y = 0$$

Since the above has to be valid for any T_x and T_y ,

$$\begin{aligned} x_s &= -\frac{F_{s,62} + F_{s,64}(L - z)}{F_{s,66}} \\ y_s &= \frac{F_{s,61} + F_{s,65}(L - z)}{F_{s,66}} \end{aligned}$$

From the previous equation it can be seen that the shear center is not a property of the cross section. Instead, in the case where the entries $F_{s,64}$ and $F_{s,65}$ associated with the bending-twist coupling are not zero, the position of the shear center varies linearly along the beam length .

The expressions for the position of the elastic center can be determined in the same manner. The elastic center is defined as the point where a force applied normal to the cross section will produce no bending curvatures (i.e., $\kappa_x = \kappa_y = 0$). Thus, assume that a load T_z is applied at the point (x_t, y_t) in the cross section. The moments induced by this force are

$$M_x = T_z y_t \quad , \quad M_y = -T_z x_t \quad (2.37)$$

We look for the positions (x_t, y_t) for which $\kappa_x = \kappa_y = 0$. From the cross section constitutive relation,

$$\begin{aligned} \kappa_x &= F_{s,43}T_z + F_{s,44}M_x + F_{s,45}M_y = 0 \\ \kappa_y &= F_{s,53}T_z + F_{s,54}M_x + F_{s,55}M_y = 0 \end{aligned}$$

Since the previous must be valid for any force T_z , inserting (2.37) into the previous equation will result in the following set of linear equations

$$\begin{cases} F_{s,43} + F_{s,44}y_t - F_{s,45}x_t = 0 \\ F_{s,53} + F_{s,54}y_t - F_{s,55}x_t = 0 \end{cases}$$

and so

$$x_t = -\frac{-F_{s,44}F_{s,53} + F_{s,45}F_{s,43}}{F_{s,44}F_{s,55} - F_{s,45}^2}$$

$$y_t = -\frac{F_{s,43}F_{s,55} - F_{s,45}F_{s,53}}{F_{s,44}F_{s,55} - F_{s,45}^2}$$

which are the expressions for the position of the elastic center.

2.6 Cross section mass matrix

The analysis of the cross section mass properties is significantly simpler than the analysis of the cross section stiffness parameters. The 6×6 cross section mass matrix \mathbf{M}_s relates the linear and angular velocities in ϕ to the inertial linear and angular momentum in γ through $\phi = \mathbf{M}_s \gamma$. The cross section mass matrix is given with respect to the cross section reference point as (cf. Hodges [22])

$$\mathbf{M}_s = \begin{bmatrix} m & 0 & 0 & 0 & 0 & -my_m \\ 0 & m & 0 & 0 & 0 & mx_m \\ 0 & 0 & m & my_m & -mx_m & 0 \\ 0 & 0 & my_m & I_{xx} & -I_{xy} & 0 \\ 0 & 0 & -mx_m & -I_{xy} & I_{yy} & 0 \\ -my_m & mx_m & 0 & 0 & 0 & I_{xx} + I_{yy} \end{bmatrix}$$

where m is the mass per unit length of the cross section. The cross section moments of inertia with respect to x and y are given by I_{xx} and I_{yy} , respectively, while I_{xy} is the cross section product of inertia. The term $I_{xx} + I_{yy}$ is the polar moment of inertia associated with the torsion of the cross section. The mass and moments of inertia are obtained through integration of the mass properties on the cross section finite element mesh and defined as

$$\begin{bmatrix} m & 0 & 0 \\ 0 & I_{xx} & I_{xy} \\ 0 & 0 & I_{yy} \end{bmatrix} = \int_A \begin{bmatrix} 1 & 0 & 0 \\ 0 & y^2 & xy \\ 0 & 0 & x^2 \end{bmatrix} \varrho \, dA$$

The off-diagonal terms are associated with the offset between the mass center position $\mathbf{m}_c = (x_m, y_m)$ and the cross section reference point. The position of the mass center \mathbf{m}_c is given as

$$x_m = \left(\sum_{e=1}^{n_e} x_{c_e} v_e \varrho_e \right) / \left(\sum_{e=1}^{n_e} v_e \varrho_e \right)$$

$$y_m = \left(\sum_{e=1}^{n_e} y_{c_e} v_e \varrho_e \right) / \left(\sum_{e=1}^{n_e} v_e \varrho_e \right)$$

where (x_{m_e}, y_{m_e}) , v_e and ϱ_e are the coordinates of the centroid, the volume and the density of element e , respectively, and n_e is the number of elements in the cross section mesh.

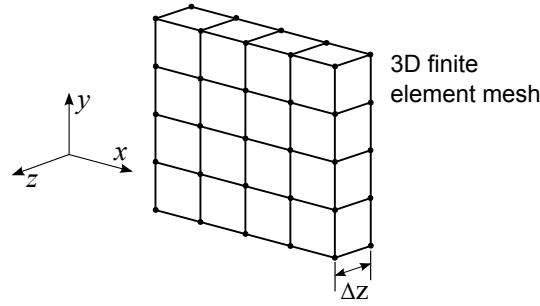


Figure 2.4: Three dimensional finite element mesh created inside commercial finite element package. Coordinate system convention and definition of the element width Δz .

2.7 An alternative formulation based on solid finite elements

An alternative formulation for commercial finite element codes of the theory presented before is briefly described here. In this case the matrices necessary to solve the sets in (2.34) and (2.35) are evaluated based on the global stiffness matrix of a three dimensional mesh of the cross section using solid finite elements. The most important advantage of this approach concerns the possibility of using layered solid elements in the cross section mesh. As a result it is possible to decrease the number of elements in the cross section and simplify significantly the generation of the cross section finite element model. The theory presented here has been originally described by Ghiringhelli and Mantegazza [9].

2.7.1 Evaluation of cross section stiffness matrix

This formulation assumes that the cross section is generated in a finite element package. The cross section is represented by a three-dimensional slice meshed using solid finite elements. The number of nodes in the faces of the elements facing the cross section plane is not restricted. However, along the length it is required that exactly two Gauss points only are used in the length direction. The choice of the slice thickness Δz should be such that the resulting solid finite elements are not too distorted as to affect the quality of the results (see Figure 2.4). Thus, a length of the order of the average side length of the two-dimensional finite elements is recommended. Finally, the preferred commercial finite element package should necessarily allow the user to access and manipulate the global finite element stiffness matrix.

The finite element equilibrium equations for the three-dimensional model are

$$\mathbf{S}\mathbf{w} = \mathbf{f}$$

where \mathbf{S} is the finite element stiffness matrix, \mathbf{w} the displacement vector and \mathbf{f} the external load vector. The following decomposition of the finite element stiffness matrix \mathbf{S} and corresponding displacement and load vector is allowed

$$\begin{bmatrix} \mathbf{S}_{11} & \mathbf{S}_{12} \\ \mathbf{S}_{21} & \mathbf{S}_{22} \end{bmatrix} \begin{bmatrix} \mathbf{w}_1 \\ \mathbf{w}_2 \end{bmatrix} = \begin{bmatrix} \mathbf{f}_1 \\ \mathbf{f}_2 \end{bmatrix}$$

where the index 1 and 2 refer to the contributions from the nodes at $z = 0$ and $z = \Delta z$, respectively,. Based on the above submatrices Ghiringhelli and Mantegazza [9] have derived the expressions for the matrices necessary for the computation of the cross section stiffness matrix. Hence, after proper derivation the following are defined

$$\begin{aligned}\mathbf{M} &= ((\mathbf{S}_{11} + \mathbf{S}_{22}) - 2(\mathbf{S}_{12} + \mathbf{S}_{21})) \frac{\Delta z}{6} \\ \mathbf{C} &= \frac{1}{2} ((\mathbf{S}_{11} - \mathbf{S}_{22}) - (\mathbf{S}_{12} - \mathbf{S}_{21})) \\ \mathbf{E} &= (\mathbf{S}_{11} + \mathbf{S}_{22} + \mathbf{S}_{12} + \mathbf{S}_{21}) \frac{1}{\Delta z}\end{aligned}$$

Note that deriving the original equations in Ghiringhelli and Mantegazza [9] yields the $1/2$ factor in matrix \mathbf{C} . This factor is not present in the derivation by Ghiringhelli and Mantegazza [9]. The remaining matrices can be determined as

$$\mathbf{R} = \mathbf{C}\mathbf{Z}_G, \quad \mathbf{L} = \mathbf{M}\mathbf{Z}_G, \quad \mathbf{A} = \mathbf{Z}_G^T \mathbf{M}\mathbf{Z}_G$$

where \mathbf{Z}_G is defined as

$$\mathbf{Z}_G = \begin{bmatrix} 1 & 0 & 0 & 0 & 0 & -y_1 \\ 0 & 1 & 0 & 0 & 0 & x_1 \\ 0 & 0 & 1 & y_1 & -x_1 & 0 \\ & & \vdots & & & \\ 1 & 0 & 0 & 0 & 0 & -y_{n_n} \\ 0 & 1 & 0 & 0 & 0 & x_{n_n} \\ 0 & 0 & 1 & y_{n_n} & -x_{n_n} & 0 \end{bmatrix}$$

where n_n is the number of nodes in the reference cross section face (i.e., half the nodes in the whole three dimensional model). Having defined all the matrices it is possible now to solve the sets (2.34) while remembering to account for the matrix of constraint equations \mathbf{D} presented in 2.3.3. Replacing the solutions of (2.34) into (2.35) it is straight forward to evaluate the cross section stiffness matrix \mathbf{K}_s .

The formulation presented here has been implemented in the class of Matlab functions BECAS_3D.

Chapter 3

Implementation manual

The theory presented in the previous sections up to the determination of the cross section stiffness matrix and, shear and elastic centers, is implemented in the BEam Cross section Analysis Software – BECAS. This section addresses the practical implementation of the theory. The MATLAB implementation of BECAS described in Appendix 5 is according to the expressions described in this section.

Two different approaches have been implemented. The first approach is based on a two dimensional finite element mesh and is mostly attractive for readers which work on their own finite element code. The second approach is based on a three dimensional mesh of the cross section using eight node solid finite elements. The approach is described in detail in Ghiringhelli and Mantegazza [9] and only the most important results are presented here. The approach is implemented in BECAS for illustrative purposes only.

Although these are standard procedures, the transformation of the material constitutive matrix is a topic where, in the authors' opinion, there is often some ambiguity concerning specific definitions for specific implementations. Hence, the final section of this chapter has been dedicated to the presentation of the material constitutive matrix for orthotropic materials and the corresponding necessary transformations.

3.1 Two dimensional finite element analysis

3.1.1 Q4 and Q8 elements

The first step in the evaluation of the cross section properties is the generation of a two dimensional finite element mesh of the cross section. An example of a discretized profile section using Q4 elements is presented in Figure 3.1. The material properties, fiber plane orientation and fiber directions are defined at each element of the finite element mesh. Thus, a layer of a certain material is defined using a layer of elements. Having defined the cross section mesh and material properties, the subsequent step concerns the derivation of each of the matrices in Equation (2.16).

The implementation is based on four or eight node isoparametric elements. The node numbering and isoparametric coordinate system are presented in Figure 3.2. The shape functions employed in the derivation of the four node isoparametric finite

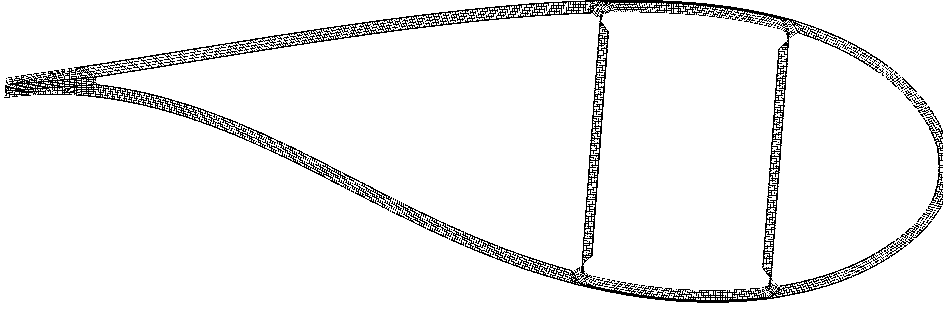


Figure 3.1: Example of the two dimensional finite element mesh of a generic wind turbine section using four node isoparametric finite elements.

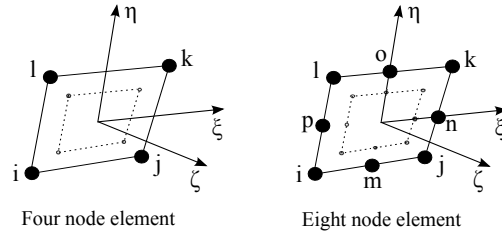


Figure 3.2: Isoparametric coordinate system, nodal positions and position of Gauss points for the four node isoparametric plane finite element.

element are

$$\begin{aligned} N_1(\xi, \eta) &= \frac{1}{4}(1 - \xi)(1 - \eta) & N_2(\xi, \eta) &= \frac{1}{4}(1 + \xi)(1 - \eta) \\ N_3(\xi, \eta) &= \frac{1}{4}(1 + \xi)(1 + \eta) & N_4(\xi, \eta) &= \frac{1}{4}(1 - \xi)(1 + \eta) \end{aligned}$$

In the case of the eight node isoparametric finite element, the shape functions are

$$\begin{aligned} N_1(\xi, \eta) &= \frac{1}{4}(1 - \xi)(1 - \eta) - \frac{1}{2}(N_8 + N_5) \\ N_2(\xi, \eta) &= \frac{1}{4}(1 + \xi)(1 - \eta) - \frac{1}{2}(N_5 + N_6) \\ N_3(\xi, \eta) &= \frac{1}{4}(1 + \xi)(1 + \eta) - \frac{1}{2}(N_6 + N_7) \\ N_4(\xi, \eta) &= \frac{1}{4}(1 - \xi)(1 + \eta) - \frac{1}{2}(N_7 + N_8) \\ N_5(\xi, \eta) &= \frac{1}{2}(1 - \xi^2)(1 - \eta) & N_6(\xi, \eta) &= \frac{1}{2}(1 + \xi)(1 - \eta^2) \\ N_7(\xi, \eta) &= \frac{1}{2}(1 - \xi^2)(1 + \eta) & N_8(\xi, \eta) &= \frac{1}{2}(1 - \xi)(1 - \eta^2) \end{aligned}$$

The position of a point in the element is given by interpolation of the nodal positions as

$$x = \sum_{i=1}^{n_q} N_i(\xi, \eta) x_i \quad y = \sum_{i=1}^{n_q} N_i(\xi, \eta) y_i \quad z(\xi, \eta) = \sum_{i=1}^{n_q} N_i(\xi, \eta) z_i$$

where n_q is the number of nodes in the element, and (x_i, y_i, z_i) are the nodal positions. In matrix form for the four node element

$$\mathbf{N} = \begin{bmatrix} N_1 \mathbf{I}_3 & N_2 \mathbf{I}_3 & N_3 \mathbf{I}_3 & N_4 \mathbf{I}_3 \end{bmatrix}$$

and for the eight node element

$$\mathbf{N} = \begin{bmatrix} N_1 \mathbf{I}_3 & N_2 \mathbf{I}_3 & N_3 \mathbf{I}_3 & N_4 \mathbf{I}_3 & N_5 \mathbf{I}_3 & N_6 \mathbf{I}_3 & N_7 \mathbf{I}_3 & N_8 \mathbf{I}_3 \end{bmatrix}$$

The integration is performed with respect to the element coordinate system although the integrals in (2.16) are defined with respect to the cross section coordinate system. To account for the change of coordinates we employ the following transformation

$$\begin{bmatrix} \frac{\partial}{\partial \xi} \\ \frac{\partial}{\partial \eta} \\ \frac{\partial}{\partial \zeta} \end{bmatrix} = \mathbf{J} \begin{bmatrix} \frac{\partial}{\partial x} \\ \frac{\partial}{\partial y} \\ \frac{\partial}{\partial z} \end{bmatrix}$$

where

$$\mathbf{J} = \begin{bmatrix} \frac{\partial x}{\partial \xi} & \frac{\partial y}{\partial \xi} & \frac{\partial z}{\partial \xi} \\ \frac{\partial x}{\partial \eta} & \frac{\partial y}{\partial \eta} & \frac{\partial z}{\partial \eta} \\ \frac{\partial x}{\partial \zeta} & \frac{\partial y}{\partial \zeta} & \frac{\partial z}{\partial \zeta} \end{bmatrix}$$

is the Jacobian matrix. In this specific case

$$\mathbf{J} = \begin{bmatrix} \frac{\partial x}{\partial \xi} & \frac{\partial y}{\partial \xi} & 0 \\ \frac{\partial x}{\partial \eta} & \frac{\partial y}{\partial \eta} & 0 \\ 0 & 0 & 1 \end{bmatrix} \quad (3.1)$$

Using (2.6) and finding \mathbf{J}^{-1} from (3.1) it is possible to define the strain operator \mathbf{B} as

$$\mathbf{B}(\xi, \eta) = \mathbf{B}_\xi \frac{\partial}{\partial \xi} + \mathbf{B}_\eta \frac{\partial}{\partial \eta}$$

where

$$\mathbf{B}_\xi = \begin{bmatrix} J_{11}^{-1} & 0 & 0 \\ 0 & J_{21}^{-1} & 0 \\ J_{21}^{-1} & J_{11}^{-1} & 0 \\ 0 & 0 & J_{11}^{-1} \\ 0 & 0 & J_{21}^{-1} \\ 0 & 0 & 0 \end{bmatrix} \quad \mathbf{B}_\eta = \begin{bmatrix} J_{12}^{-1} & 0 & 0 \\ 0 & J_{22}^{-1} & 0 \\ J_{22}^{-1} & J_{12}^{-1} & 0 \\ 0 & 0 & J_{12}^{-1} \\ 0 & 0 & J_{22}^{-1} \\ 0 & 0 & 0 \end{bmatrix}$$

The strain operator is then applied in the derivation of the matrix product

$$\mathbf{BN} = \mathbf{B}_\xi \frac{\partial \mathbf{N}}{\partial \xi} + \mathbf{B}_\eta \frac{\partial \mathbf{N}}{\partial \eta}$$

where

$$\begin{aligned} \frac{\partial \mathbf{N}}{\partial \xi} &= \begin{bmatrix} \frac{\partial N_1}{\partial \xi} \mathbf{I}_3 & \frac{\partial N_2}{\partial \xi} \mathbf{I}_3 & \frac{\partial N_3}{\partial \xi} \mathbf{I}_3 & \frac{\partial N_4}{\partial \xi} \mathbf{I}_3 \end{bmatrix} \\ \frac{\partial \mathbf{N}}{\partial \eta} &= \begin{bmatrix} \frac{\partial N_1}{\partial \eta} \mathbf{I}_3 & \frac{\partial N_2}{\partial \eta} \mathbf{I}_3 & \frac{\partial N_3}{\partial \eta} \mathbf{I}_3 & \frac{\partial N_4}{\partial \eta} \mathbf{I}_3 \end{bmatrix} \end{aligned}$$

The remaining matrix products \mathbf{SZ} and \mathbf{SN} are obtained by simple matrix multiplication.

3.1.2 Local and global finite element matrices

The integration is performed at the element level and hence the element matrices are evaluated as

$$\begin{aligned}
\mathbf{A}_e &= \int_A \mathbf{Z}^T \mathbf{S}^T \mathbf{Q} \mathbf{S} \mathbf{Z} \, dx dy = \int_A \mathbf{Z}^T \mathbf{S}^T \mathbf{Q} \mathbf{S} \mathbf{Z} |J| \, d\xi \, d\eta \\
\mathbf{R}_e &= \int_A \mathbf{N}^T \mathbf{B}^T \mathbf{Q} \mathbf{S} \mathbf{Z} \, dx dy = \int_A \mathbf{N}^T \mathbf{B}^T \mathbf{Q} \mathbf{S} \mathbf{Z} |J| \, d\xi \, d\eta \\
\mathbf{E}_e &= \int_A \mathbf{N}^T \mathbf{B}^T \mathbf{Q} \mathbf{B} \mathbf{N} \, dx dy = \int_A \mathbf{N}^T \mathbf{B}^T \mathbf{Q} \mathbf{B} \mathbf{N} |J| \, d\xi \, d\eta \\
\mathbf{C}_e &= \int_A \mathbf{N}^T \mathbf{B}^T \mathbf{Q} \mathbf{S} \mathbf{N} \, dx dy = \int_A \mathbf{N}^T \mathbf{B}^T \mathbf{Q} \mathbf{S} \mathbf{N} |J| \, d\xi \, d\eta \\
\mathbf{L}_e &= \int_A \mathbf{N}^T \mathbf{S}^T \mathbf{Q} \mathbf{S} \mathbf{Z} \, dx dy = \int_A \mathbf{N}^T \mathbf{S}^T \mathbf{Q} \mathbf{S} \mathbf{Z} |J| \, d\xi \, d\eta \\
\mathbf{M}_e &= \int_A \mathbf{N}^T \mathbf{S}^T \mathbf{Q} \mathbf{S} \mathbf{N} \, dx dy = \int_A \mathbf{N}^T \mathbf{S}^T \mathbf{Q} \mathbf{S} \mathbf{N} |J| \, d\xi \, d\eta
\end{aligned}$$

where the integration is performed using a four point Gauss quadrature (cf. Figure 3.2). The global matrices are subsequently assembled following typical finite element procedures

$$\begin{aligned}
\mathbf{A} &= \sum_{i=1}^{n_e} \mathbf{A}_e \quad , \quad \mathbf{R} = \sum_{i=1}^{n_e} \mathbf{R}_e \quad , \quad \mathbf{E} = \sum_{i=1}^{n_e} \mathbf{E}_e \\
\mathbf{C} &= \sum_{i=1}^{n_e} \mathbf{C}_e \quad , \quad \mathbf{L} = \sum_{i=1}^{n_e} \mathbf{L}_e \quad , \quad \mathbf{M} = \sum_{i=1}^{n_e} \mathbf{M}_e
\end{aligned}$$

where n_e is the number of finite elements in the cross section mesh.

Having obtained each of the matrices it is possible to finally solve the cross section equilibrium equations

$$\begin{aligned}
\begin{bmatrix} \mathbf{E} & \mathbf{R} & \mathbf{D} \\ \mathbf{R}^T & \mathbf{A} & \mathbf{0} \\ \mathbf{D}^T & \mathbf{0} & \mathbf{0} \end{bmatrix} \begin{bmatrix} \mathbf{X} \\ \mathbf{Y} \\ \mathbf{\Lambda}_2 \end{bmatrix} &= \begin{bmatrix} (\mathbf{C} - \mathbf{C}^T) & \mathbf{L} \\ \mathbf{L}^T & \mathbf{0} \\ \mathbf{0} & \mathbf{0} \end{bmatrix} \begin{bmatrix} \frac{\partial \mathbf{X}}{\partial z} \\ \frac{\partial \mathbf{Y}}{\partial z} \end{bmatrix} + \begin{bmatrix} \mathbf{0} \\ \mathbf{I} \\ \mathbf{0} \end{bmatrix} \\
\begin{bmatrix} \mathbf{E} & \mathbf{R} & \mathbf{D} \\ \mathbf{R}^T & \mathbf{A} & \mathbf{0} \\ \mathbf{D}^T & \mathbf{0} & \mathbf{0} \end{bmatrix} \begin{bmatrix} \frac{\partial \mathbf{X}}{\partial z} \\ \frac{\partial \mathbf{Y}}{\partial z} \\ \mathbf{\Lambda}_1 \end{bmatrix} &= \begin{bmatrix} \mathbf{0} \\ \mathbf{T}_r^T \\ \mathbf{0} \end{bmatrix}
\end{aligned}$$

where \mathbf{D} is the matrix of constraint equations defined in 2.3.3, and $\mathbf{\Lambda}_1$ and $\mathbf{\Lambda}_2$ are the corresponding Lagrange multipliers. The two sets above make use of the same coefficient matrix and can be solved efficiently using a proper factorization (e.g., LU factorization). The solutions are then obtained doing a forward and backward substitution.

The cross section compliance matrix is then readily obtained by inserting the solutions of the previous set into

$$\mathbf{F}_s = \begin{bmatrix} \mathbf{X} \\ \frac{\partial \mathbf{X}}{\partial z} \\ \mathbf{Y} \end{bmatrix}^T \begin{bmatrix} \mathbf{E} & \mathbf{C} & \mathbf{R} \\ \mathbf{C}^T & \mathbf{M} & \mathbf{L} \\ \mathbf{R}^T & \mathbf{L}^T & \mathbf{A} \end{bmatrix} \begin{bmatrix} \mathbf{X} \\ \frac{\partial \mathbf{X}}{\partial z} \\ \mathbf{Y} \end{bmatrix}$$

A MATLAB implementation of BECAS according to the theory presented above is described in Chapter 5.

3.2 Material constitutive matrix

At each element of the cross section finite element mesh, the user of BECAS must specify

- Material properties
- Orientation of the laminate plane
- Orientation of the fibers laminate

Based on this input, the first step consists of assembling the material constitutive matrix in the material coordinate system based on a set of material properties.

3.2.1 Definition

In the case of orthotropic materials, the stress-strain relation or generalized Hookes' Law is stated as

$$\begin{bmatrix} \sigma_{22} \\ \sigma_{33} \\ \sigma_{23} \\ \sigma_{12} \\ \sigma_{13} \\ \sigma_{11} \end{bmatrix} = \underbrace{\begin{bmatrix} \frac{1}{E_{22}} & -\frac{\nu_{23}}{E_{22}} & 0 & 0 & 0 & -\frac{\nu_{21}}{E_{11}} \\ -\frac{\nu_{23}}{E_{22}} & \frac{1}{E_{33}} & 0 & 0 & 0 & -\frac{\nu_{31}}{E_{11}} \\ 0 & 0 & \frac{1}{G_{23}} & 0 & 0 & 0 \\ 0 & 0 & 0 & \frac{1}{G_{12}} & 0 & 0 \\ 0 & 0 & 0 & 0 & \frac{1}{G_{13}} & 0 \\ -\frac{\nu_{2z}}{E_{11}} & -\frac{\nu_{13}}{E_{11}} & 0 & 0 & 0 & \frac{1}{E_{11}} \end{bmatrix}}_{\mathbf{Q}}^{-1} \begin{bmatrix} \gamma_{22} \\ \gamma_{33} \\ \gamma_{23} \\ \gamma_{12} \\ \gamma_{13} \\ \gamma_{11} \end{bmatrix}$$

where the material properties are given in the material coordinate system (see Figure 3.3c) and defined as

- E_{11} the Young modulus of material the 1 direction.
- E_{22} the Young modulus of material the 2 direction.
- E_{33} the Young modulus of material the 3 direction.
- G_{12} the shear modulus in the 12 plane.
- G_{13} the shear modulus in the 13 plane.
- G_{23} the shear modulus in the 23 plane.
- ν_{12} the Poisson's ratio in the 12 plane.
- ν_{13} the Poisson's ratio in the 13 plane.
- ν_{23} the Poisson's ratio in the 23 plane.
- ρ the material density.

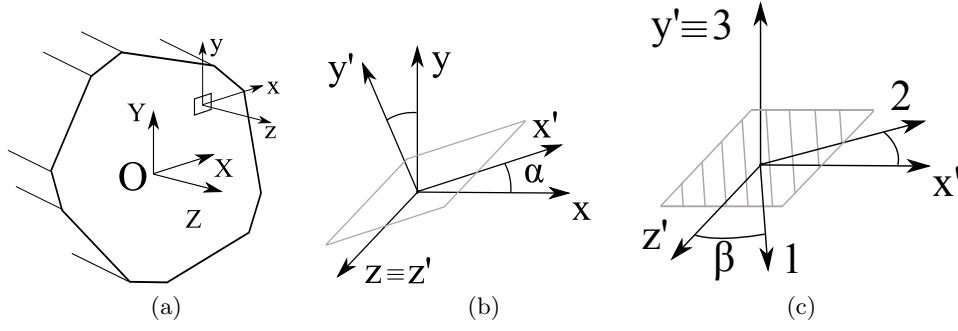


Figure 3.3: Determination of the material constitutive matrix at each finite element of the cross section mesh. (a) Definition of the cross section coordinate system XYZ and element coordinate system xyz . (b) Convention adopted for the rotation of the element coordinate system xyz into the fiber plane coordinate system $x'y'z'$. (c) Convention adopted for the rotation of the fiber plane coordinate system $x'y'z'$ into the material coordinate system 123.

Moreover, note that

$$\frac{\nu_{ij}}{E_{ii}} = \frac{\nu_{ji}}{E_{jj}}$$

where ν_{ij} is the Poisson's ration that characterizes the transverse strain in the j -direction when the material is stressed in the i direction. The natural strains ϵ_{ij} are related to the engineering strains γ_{ij} by

$$\begin{aligned} \gamma_{22} &= \epsilon_{22}, & \gamma_{33} &= \epsilon_{33}, & \gamma_{11} &= \epsilon_{11}, \\ \gamma_{13} &= 2\epsilon_{13}, & \gamma_{12} &= 2\epsilon_{12}, & \gamma_{23} &= 2\epsilon_{23} \end{aligned}$$

3.2.2 Rotation

The next two steps concern the two rotations of the material constitutive matrix necessary to determine the element material constitutive matrix in the fiber coordinate system. The three element coordinate systems – element, fiber plane, and fiber – and respective conventions for each of the rotations are defined in Figure 3.3. The material constitutive matrix is rotated first into the fiber plane coordinate system and subsequently into the fiber coordinate system. Each of the rotations is performed following the procedure described next.

The following approach for the rotation of the material constitutive matrix is based on Reddy [24]. We consider the relationship between the stress components in a material (m) and a problem (p) coordinate systems. In tensor format, the stress tensor is transformed as

$$(\sigma_{ij})_m = l_{im}l_{jn}(\sigma_{mn})_p, \quad (\sigma_{mn})_p = l_{mi}l_{nj}(\sigma_{ij})_m,$$

where l_{ij} are the direction cosines defined as

$$l_{ij} = (\mathbf{e}_i)_m \cdot (\mathbf{e}_j)_p$$

The vectors \mathbf{e} are unit vectors associated with the axis at each of the coordinate systems. The components of the stress in the material and problem coordinate systems are

$$\begin{aligned}\boldsymbol{\sigma}_m &= [\sigma_{xx_m} \quad \sigma_{yy_m} \quad \sigma_{xy_m} \quad \sigma_{xz_m} \quad \sigma_{yz_m} \quad \sigma_{zz_m}]^T \\ \boldsymbol{\sigma}_p &= [\sigma_{xx_p} \quad \sigma_{yy_p} \quad \sigma_{xy_p} \quad \sigma_{xz_p} \quad \sigma_{yz_p} \quad \sigma_{zz_p}]^T\end{aligned}$$

The 3×3 arrays with the stress components are given by

$$\hat{\boldsymbol{\sigma}}_m = \begin{bmatrix} \sigma_{xx_m} & \sigma_{xy_m} & \sigma_{xz_m} \\ \sigma_{yx_m} & \sigma_{yy_m} & \sigma_{yz_m} \\ \sigma_{zx_m} & \sigma_{zy_m} & \sigma_{zz_m} \end{bmatrix}, \quad \hat{\boldsymbol{\sigma}}_p = \begin{bmatrix} \sigma_{xx_p} & \sigma_{xy_p} & \sigma_{xz_p} \\ \sigma_{yx_p} & \sigma_{yy_p} & \sigma_{yz_p} \\ \sigma_{zx_p} & \sigma_{zy_p} & \sigma_{zz_p} \end{bmatrix}$$

where the $(\hat{})$ refers to the array notation. Then the rotations in Equation 3.2.2 can be expressed as

$$\hat{\boldsymbol{\sigma}}_m = \mathbf{L} \hat{\boldsymbol{\sigma}}_p \mathbf{L}^T, \quad \hat{\boldsymbol{\sigma}}_p = \mathbf{L}^T \hat{\boldsymbol{\sigma}}_m \mathbf{L}$$

The vector of engineering strains in the material and problem coordinate systems is

$$\begin{aligned}\boldsymbol{\gamma}_m &= [\gamma_{xx_m} \quad \gamma_{yy_m} \quad \gamma_{zz_m} \quad \gamma_{yz_m} \quad \gamma_{xz_m} \quad \gamma_{xy_m}]^T \\ \boldsymbol{\gamma}_p &= [\gamma_{xx_p} \quad \gamma_{yy_p} \quad \gamma_{zz_p} \quad \gamma_{yz_p} \quad \gamma_{xz_p} \quad \gamma_{xy_p}]^T\end{aligned}$$

The natural strain components may be defined in function of the engineering strains as

$$\hat{\boldsymbol{\epsilon}}_m = \begin{bmatrix} \gamma_{xx_m} & \frac{1}{2}\gamma_{xy_m} & \frac{1}{2}\gamma_{xz_m} \\ \frac{1}{2}\gamma_{yx_m} & \gamma_{yy_m} & \frac{1}{2}\gamma_{yz_m} \\ \frac{1}{2}\gamma_{zx_m} & \frac{1}{2}\gamma_{zy_m} & \gamma_{zz_m} \end{bmatrix}, \quad \hat{\boldsymbol{\epsilon}}_p = \begin{bmatrix} \gamma_{xx_p} & \frac{1}{2}\gamma_{xy_p} & \frac{1}{2}\gamma_{xz_p} \\ \frac{1}{2}\gamma_{yx_p} & \gamma_{yy_p} & \frac{1}{2}\gamma_{yz_p} \\ \frac{1}{2}\gamma_{zx_p} & \frac{1}{2}\gamma_{zy_p} & \gamma_{zz_p} \end{bmatrix}$$

where $\hat{\gamma}$ are the engineering strains. Since the strains are also second order tensors, the relations derived for the stresses are also valid for the strains

$$\hat{\boldsymbol{\epsilon}}_m = \mathbf{L} \hat{\boldsymbol{\epsilon}}_p \mathbf{L}^T, \quad \hat{\boldsymbol{\epsilon}}_p = \mathbf{L}^T \hat{\boldsymbol{\epsilon}}_m \mathbf{L}$$

Based on the expressions presented before it is possible to establish the equations for the transformation of the material constitutive matrix. The constitutive matrix in the problem coordinate system, \mathbf{Q}_p , is obtained by transformation of the material constitutive matrix in the material coordinate system, \mathbf{Q}_m . The following steps should be followed in the rotation of the material constitutive matrix:

1. The array $\hat{\boldsymbol{\epsilon}}_p$ is assembled based on the engineering strains $\boldsymbol{\gamma}_p$ remembering to observe the $1/2$ factor;
2. The strains are then rotated employing $\hat{\boldsymbol{\epsilon}}_m = \mathbf{L} \hat{\boldsymbol{\epsilon}}_p \mathbf{L}^T$;
3. Having $\hat{\boldsymbol{\epsilon}}_m$ it is possible to assemble the vector of engineering strains $\boldsymbol{\gamma}_m$ remembering to multiply by 2 the natural shear strain components;
4. The stress-strain relation $\boldsymbol{\sigma}_m = \mathbf{Q}_m \boldsymbol{\gamma}_m$ is invoked to determine $\boldsymbol{\sigma}_m$;

5. The array with the stress components $\hat{\sigma}_m$ is then assembled to evaluate the stresses in the problem coordinate system $\hat{\sigma}_p = \mathbf{L}^T \hat{\sigma}_m \mathbf{L}$;
6. Assemble the vector σ_p based on the components of $\hat{\sigma}_p$;
7. Finally, each of the stress components is a function of the strain components in γ_p , the direction cosines in \mathbf{L} and the entries of the constitutive matrix \mathbf{Q}_m . The coefficients multiplying each of the strain components in γ_p are the components of the constitutive matrix in the problem coordinate system \mathbf{Q}_p .

The procedure is used to orient the fibers in a laminate or to orient the laminate plane. When orienting the fiber plane, the rotation matrix \mathbf{L} will be

$$\mathbf{L}_\alpha = \begin{bmatrix} \cos \alpha & -\sin \alpha & 0 \\ \sin \alpha & \cos \alpha & 0 \\ 0 & 0 & 1 \end{bmatrix}$$

whereas for the fiber orientation

$$\mathbf{L}_\beta = \begin{bmatrix} \cos \beta & 0 & \sin \beta \\ 0 & 1 & 0 \\ -\sin \beta & 0 & \cos \beta \end{bmatrix}$$

which are the typical two dimensional rotational matrices.

3.3 Rotation and translation of constitutive matrices

The translation matrix \mathbf{T}_T is obtained from static considerations as follows.

$$\mathbf{T}_T = \begin{bmatrix} 1 & 0 & 0 & 0 & 0 & 0 \\ 0 & 1 & 0 & 0 & 0 & 0 \\ 0 & 0 & 1 & 0 & 0 & 0 \\ 0 & 0 & -y & 1 & 0 & 0 \\ 0 & 0 & x & 0 & 1 & 0 \\ y & -x & 0 & 0 & 0 & 1 \end{bmatrix}$$

$$M' = \mathbf{T}_T \mathbf{M} \mathbf{T}_T^T$$

$$\mathbf{T}_R = \begin{bmatrix} c & s & 0 & 0 & 0 & 0 \\ -s & c & 0 & 0 & 0 & 0 \\ 0 & 0 & 1 & 0 & 0 & 0 \\ 0 & 0 & 0 & c & s & 0 \\ 0 & 0 & 0 & -s & c & 0 \\ 0 & 0 & 0 & 0 & 0 & 1 \end{bmatrix}$$

Chapter 4

Validation

In this section numerical results obtained using BECAS – the BEam Cross Section analysis Software – are presented. BECAS is the current implementation of the method presented in the previous sections. At this point the output is the cross section compliance and stiffness matrix, and the positions of the shear and elastic centers. The resulting entries of the cross section stiffness matrix \mathbf{K}_s as well as the positions of the shear and elastic center are compared to the results from VABS – the Variational Asymptotic Beam Section analysis code (Yu et al. [13, 14]). VABS has been extensively validated against different cross section analysis tools and analytical results (see Yu et al. [13, 14], Chen et al. [15] and Volovoi et al. [17]) and it is therefore a benchmark for validation of new cross section analysis codes.

The numerical experiments presented for validation have been chosen so that different material and geometrical effects are analyzed. From a material properties standpoint, the aim is to analyze the effect of material anisotropy and its inhomogeneous distribution over the cross section. In terms of cross section geometry we look at solid, thin-walled, open and multi-cell cross sections.

This chapter is organized as follows. First, the setup for the numerical experiments is described. The material properties are defined, and the cross section coordinate systems as well as the cross section constitutive relation are restated. Moreover, the general organization of the numerical experiments and the aim of each is described. The results for the numerical experiments are presented next.

4.1 Setup

Three material types have been considered – two isotropic and one orthotropic material. Their stiffness properties are presented in Table 4.1. Furthermore, four different cross section geometries have been considered – solid square, cylinder, half cylinder and three cells. All the combinations of cross section geometry and material properties, are summarized in Table 4.2.

Recall from Section 2.2.1 the orientation of the coordinate system presented again here for convenience in Figure 4.1. The non-zero entries of the cross section stiffness matrix \mathbf{K}_s , the position of the shear and elastic center, and the warping displacements are calculated for each of the numerical experiments. The entries of \mathbf{K}_s and the position of the shear and elastic center are compared to the results from

Table 4.1: Material properties for isotropic material #1 and #2, and orthotropic material (scaled values for E-glass according to Handbook of Composites [25]). The factor $\alpha = E_1/E_2$ shall be used in the study of extremely inhomogeneous sections.

Material	Isotropic #1	Isotropic #2	Orthotropic
E_{zz}	100	$100/\alpha$	480
$E_{xx} = E_{yy}$	100	$100/\alpha$	120
G_{yz}	41.667	$41.667/\alpha$	50
$G_{xz} = G_{xy}$	41.667	$41.667/\alpha$	60
ν_{yz}	0.2	$0.2/\alpha$	0.26
$\nu_{xz} = \nu_{xy}$	0.2	$0.2/\alpha$	0.19

Table 4.2: Catalogue of cross section properties analysed for validation.

Ref.	Geometry	Material
S1	Solid square	Isotropic
S2	Solid square	Isotropic #1 + Isotropic #2
S3	Solid square	Orthotropic
C1	Cylinder	Isotropic #1
C2	Half-cylinder	Isotropic #1
C3	Cylinder	Isotropic #1 + Isotropic #2
C4	Cylinder (layered)	Isotropic #1 + Isotropic #2
T1	Three-cells	Isotropic #1
T2	Three-cells	Isotropic #1 + Orthotropic

VABS. Recall the relations between the strains and direction of forces and moments

$$\begin{bmatrix} T_x \\ T_y \\ T_z \\ M_x \\ M_y \\ M_z \end{bmatrix} = \begin{bmatrix} K_{s,11} & K_{s,12} & K_{s,13} & K_{s,14} & K_{s,15} & K_{s,16} \\ & K_{s,22} & K_{s,23} & K_{s,24} & K_{s,25} & K_{s,26} \\ & & K_{s,33} & K_{s,34} & K_{s,35} & K_{s,36} \\ & & & K_{s,44} & K_{s,45} & K_{s,46} \\ & & & & K_{s,55} & K_{s,56} \\ sym. & & & & & K_{s,66} \end{bmatrix} \begin{bmatrix} \tau_x \\ \tau_y \\ \tau_z \\ \kappa_x \\ \kappa_y \\ \kappa_z \end{bmatrix}$$

The warping displacements are presented only for a qualitative analysis of the solutions.

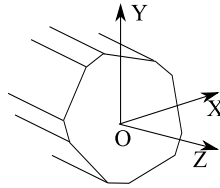


Figure 4.1: Cross section coordinate system.

The accuracy of \mathbf{K}_s depends on the size of the cross section finite element mesh. Just like in standard finite element analysis, a mesh convergence study should be performed in order to establish the minimum size of the cross section finite element mesh required to obtain realistic values of \mathbf{K}_s . Nonetheless, since BECAS is only being compared to VABS (which is also based on a finite element discretization of the cross section) a mesh convergence study has not been performed. Provided the same finite element mesh is used, both tools will give the same results as can be seen next.

4.2 Numerical examples

All numerical experiments conducted to validate the current implementation of BECAS are presented in this section. The first results are presented for cross section (S1). This first example illustrates the ability of BECAS to handle solid square cross section. In the second case the same solid square cross section geometry is analyzed although in this case it is made of two different materials (S2). The aim is to analyze the behaviour of BECAS when handling cross sections made of different materials with a high contrast between stiffnesses. In the third case the solid square cross section is made of orthotropic material (S3). The objective is to validate the effect of material anisotropy on the cross section stiffness properties estimated by BECAS. In particular we look at the estimated coupling terms arising from the material anisotropy. In the fourth case the cylinder cross section made of isotropic materials is analyzed (C1). The aim is to analyze the behaviour of BECAS when dealing with thin-walled cross sections. In the fifth example only half the cylinder is modelled (C2). This experiment serves to validate the behaviour of BECAS when handling open thin-walled cross sections. The cylinder cross section is then divided in two and made of two different isotropic materials in the sixth example (C3). Much like in the case of the solid square cross section S2, the aim here is to validate the results of BECAS when studying thin-walled cross sections with extreme material inhomogeneity. A similar procedure is adopted in the seventh example where a layered type of structure is assumed through the thickness of the cylinder (C4). In the eighth example, a three cell isotropic cross section is considered (T1). The aim is to validate BECAS for the analysis of multi-celled, thin-walled cross sections. The final example assumes that the three cell cross section is made of isotropic and orthotropic materials (T2). The aim in this case is to validate the results from BECAS for thin-walled, multi-celled, closed cross sections with anisotropic material properties.

4.2.1 Square

The dimensions of the solid square cross section are given in Table 4.3. The cross section is presented in Figure 4.2.

Table 4.3: Geometrical dimensions of solid square beam.

Width (W)	0.1 m
Height (H)	0.1 m

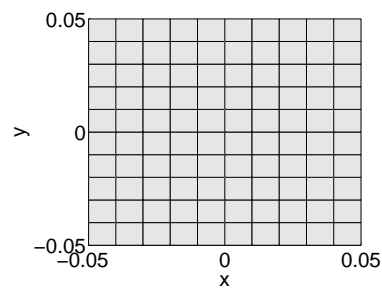


Figure 4.2: Geometry and finite element mesh of square cross section with one material.

Square cross section of isotropic material - S1

In this case the solid square cross section is made of isotropic material #1. The resulting non-zero entries of the cross section stiffness matrix are presented in Table 4.4 for both BECAS and VABS. As can be seen there is a very good agreement between the two approaches. The shear and elastic center calculated by both BECAS and VABS are exactly situated at the origo of the cross section coordinate system. Thus, $x_s = y_s = x_t = y_t = 0$ using both methods. The warping displacements are

Table 4.4: Non-zero entries of cross section stiffness matrix for square cross section (S1). Comparison between BECAS and VABS

	BECAS	VABS	Diff. (%)
$K_{s,11}$	3.4899E-01	3.4900E-01	7.1515E-04
$K_{s,22}$	3.4899E-01	3.4900E-01	7.1515E-04
$K_{s,33}$	1.0000E+00	1.0000E+00	0.00
$K_{s,44}$	8.3384E-04	8.3384E-04	0.00
$K_{s,55}$	8.3384E-04	8.3384E-04	0.00
$K_{s,66}$	5.9084E-04	5.9084E-04	0.00

presented in Figure 4.3 for each of the strain components. The shear strains, $\tau_x = 1$ and $\tau_y = 1$, induces a cross section deformation which matches the analytical results presented by Timoshenko and Goodier in [26]. The same holds for the warping displacements obtained when the torsional curvature $\kappa_z = 1$. The Poisson effect is visible in the results obtained for $\kappa_x = 1$ and $\kappa_y = 1$ with an in-plane expansion and contraction of the compression and tension sides, respectively.

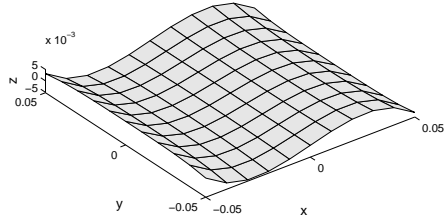
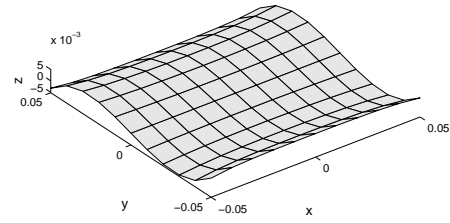
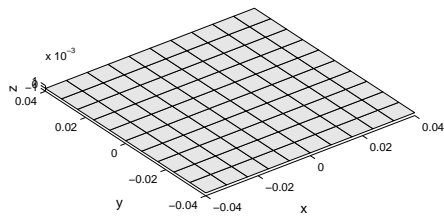
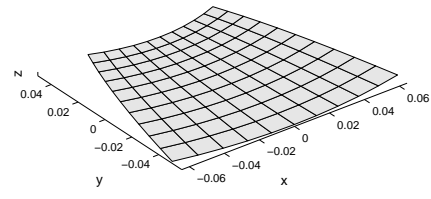
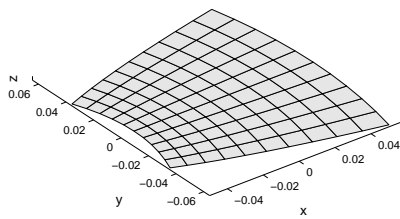
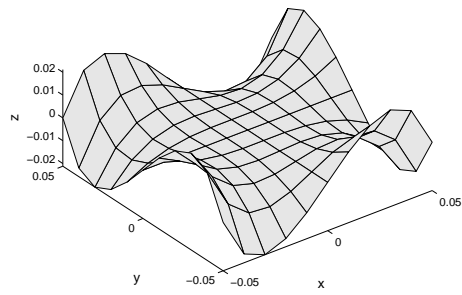
(a) $\tau_x = 1$ (b) $\tau_y = 1$ (c) $\tau_z = 1$ (d) $\kappa_x = 1$ (e) $\kappa_y = 1$ (f) $\kappa_z = 1$

Figure 4.3: Cross section warping displacements for square cross section (S1) (displacements not to scale).

Square cross section of two isotropic materials - S2

The solid square geometry is now divided in two. The section geometry and material distribution are presented in Figure 4.4. The mechanical properties of the

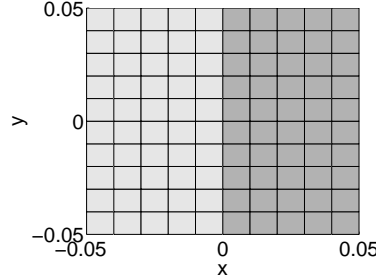


Figure 4.4: Geometry and finite element mesh of square cross section with two materials (S2) – isotropic material #1 (light) and #2 (dark).

isotropic material #2 are obtained by simply dividing the mechanicals properties of the isotropic material #1 (see Table 4.1) by a factor $\alpha = E_1/E_2$. The variation of the value of the non-zero entries of the cross section stiffness matrix with respect to the stiffness ration E_1/E_2 is presented in Table 4.5. The estimated positions of the shear and elastic centers are presented in Table 4.6. Once again there is a very good agreement between the results from BECAS and VABS. As the stiffness

Table 4.5: Non-zero entries of cross section stiffness matrix for square cross section (S2) with respect to E_1/E_2 ration. Comparison between BECAS and VABS.

BECAS							
E_1/E_2	$K_{s,11}$	$K_{s,22}$	$K_{s,33}$	$K_{s,44} = K_{s,55}$	$K_{s,66}$	$K_{s,26}$	$K_{s,35}$
1E+00	1.00E+00	3.49E-01	3.49E-01	5.91E-04	8.34E-04	0.00E+00	0.00E+00
1E+01	5.50E-01	1.28E-01	1.92E-01	2.77E-04	4.59E-04	-3.93E-03	1.13E-02
1E+02	5.05E-01	1.38E-01	1.77E-01	2.35E-04	4.21E-04	-4.33E-03	1.24E-02
1E+03	5.00E-01	1.68E-01	1.75E-01	2.31E-04	4.17E-04	-4.37E-03	1.25E-02
1E+04	5.00E-01	1.73E-01	1.75E-01	2.30E-04	4.17E-04	-4.38E-03	1.25E-02
1E+05	5.00E-01	1.73E-01	1.75E-01	2.30E-04	4.17E-04	-4.38E-03	1.25E-02
VABS							
E_1/E_2	$K_{s,11}$	$K_{s,22}$	$K_{s,33}$	$K_{s,44} = K_{s,55}$	$K_{s,66}$	$K_{s,26}$	$K_{s,35}$
1E+00	1.00E+00	3.49E-01	3.49E-01	5.91E-04	8.34E-04	0.00E+00	0.00E+00
1E+01	5.50E-01	1.28E-01	1.92E-01	2.77E-04	4.59E-04	-3.93E-03	1.13E-02
1E+02	5.05E-01	1.38E-01	1.77E-01	2.35E-04	4.21E-04	-4.33E-03	1.24E-02
1E+03	5.01E-01	1.68E-01	1.75E-01	2.31E-04	4.17E-04	-4.37E-03	1.25E-02
1E+04	5.00E-01	1.73E-01	1.75E-01	2.30E-04	4.17E-04	-4.38E-03	1.25E-02
1E+05	5.00E-01	1.73E-01	1.75E-01	2.30E-04	4.17E-04	-4.38E-03	1.25E-02
Diff. (%)							
E_1/E_2	$K_{s,11}$	$K_{s,22}$	$K_{s,33}$	$K_{s,44} = K_{s,55}$	$K_{s,66}$	$K_{s,26}$	$K_{s,35}$
1E+00	0.00E+00	-7.15E-04	-7.15E-04	-7.20E-04	-1.20E-07	0.00E+00	0.00E+00
1E+01	-5.45E-13	-7.10E-04	-7.17E-04	-7.19E-04	-1.19E-07	-7.17E-04	0.00E+00
1E+02	-3.96E-13	-6.89E-04	-7.19E-04	-7.20E-04	-1.19E-07	-7.19E-04	0.00E+00
1E+03	-3.99E-13	-6.75E-04	-7.19E-04	-7.20E-04	-1.19E-07	-7.19E-04	0.00E+00
1E+04	2.00E-13	-6.73E-04	-7.19E-04	-7.20E-04	-1.19E-07	-7.19E-04	0.00E+00
1E+05	-2.00E-13	-6.72E-04	-7.19E-04	-7.20E-04	-1.19E-07	-7.19E-04	-8.05E-13

of the material #2 vanishes, the stiffness values and positions of shear and elastic centers converge to those which would be obtained if only half the cross section was considered. Note however the variation of the entry $K_{s,11}$ with respect to the ration E_1/E_2 plotted in Figure 4.5. The shear stiffness as estimated by both BECAS and VABS decrease past the value obtained for half the section and have a local minima at $E_1/E_2 = 10$. Chen et al. in [15] present a similar result using a different cross

Table 4.6: Shear and elastic center positions $((x_s, y_s)$ and (x_t, y_t) , respectively) for square cross section (S2) with respect to the E_1/E_2 ration. Comparison between BECAS and VABS.

BECAS			VABS	
E_1/E_2	x_s	y_s	x_s	y_s
1E+00	0.000E+00	0.000E+00	0.000E+00	0.000E+00
1E+01	2.045E-02	0.000E+00	2.045E-02	-2.306E-17
1E+02	2.450E-02	0.000E+00	2.450E-02	5.817E-17
1E+03	2.495E-02	0.000E+00	2.495E-02	-1.385E-16
1E+04	2.500E-02	0.000E+00	2.500E-02	8.010E-17
1E+05	2.500E-02	0.000E+00	2.500E-02	1.683E-16

E_1/E_2	x_t	y_t	x_t	y_t
1E+00	0.000E+00	0.000E+00	0.000E+00	0.000E+00
1E+01	2.045E-02	0.000E+00	0.000E+00	0.000E+00
1E+02	2.450E-02	0.000E+00	2.450E-02	-2.596E-19
1E+03	2.495E-02	0.000E+00	2.495E-02	1.266E-19
1E+04	2.500E-02	0.000E+00	2.500E-02	4.118E-19
1E+05	2.500E-02	0.000E+00	2.500E-02	9.174E-19

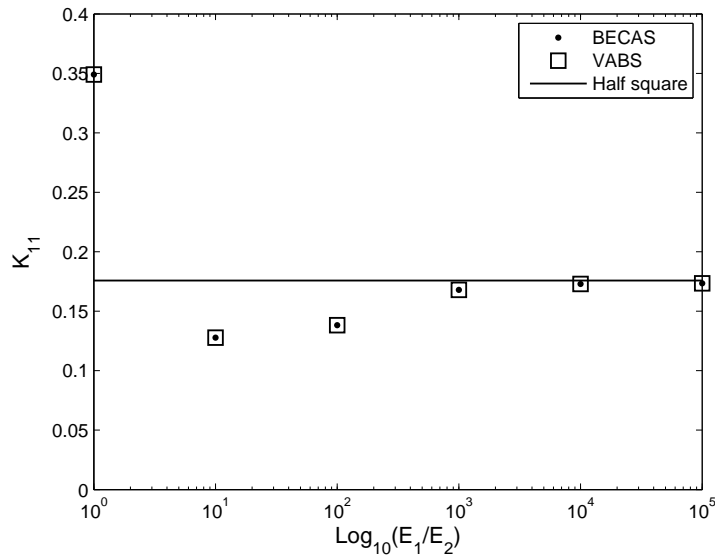


Figure 4.5: Variation of $K_{s,11}$ entry of the cross section stiffness matrix with respect to the ratio E_1/E_2 for the square cross section (S1). Results for BECAS and VABS compared with the solution for half the section.

section but consider only one extreme value of the stiffness ratio. To the authors' best knowledge there is no study reported in the literature where a similar study is performed.

Finally the cross section warping displacements are presented for different values of ψ in Figure 4.6 considering $E_1/E_2 = 1000$. As the stiffness of material #2

vanishes the extension-bending and shear-torsion coupling terms arise ($K_{s,26}$ and $K_{s,35}$ in Table 4.5). These coupling effects are visible in the warping displacements. For $\tau_x = 1$ the distortion induced by the shear strain is superimposed by a torsion type of deformation pattern. When $\tau_z = 1$ the tension strain induces a bending type of in-plane deformation visible in the arched form of the cross section.

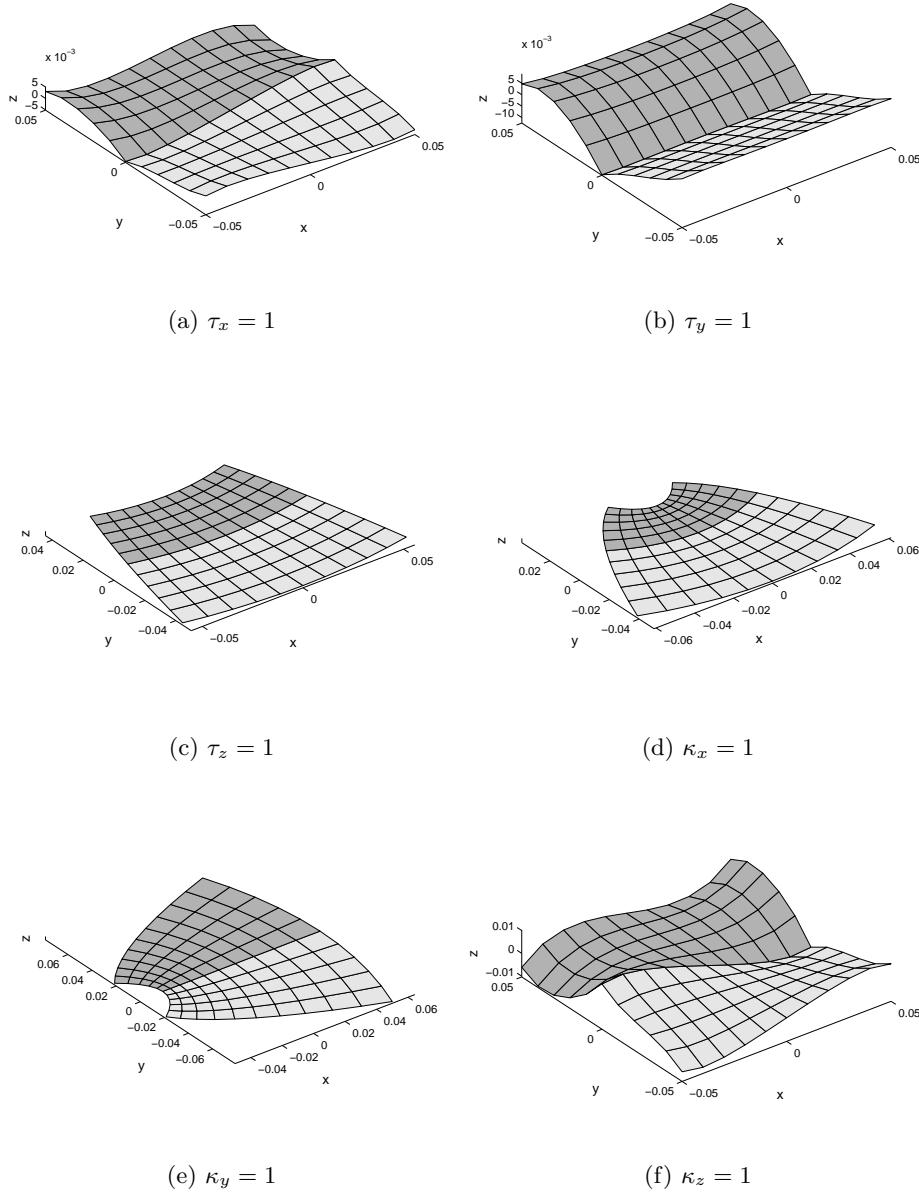


Figure 4.6: Cross section warping displacements for square cross section (S2) where $E_1/E_2 = 1000$ (displacements not to scale).

Square cross section of orthotropic material - S3

In the last example, it is considered that the solid square cross section is made of layered orthotropic material. The fiber plane lies parallel to the xz plane (cf. Figure 4.1) and rotate around the y axis. The variation of the magnitude of the non-zero entries in the cross section stiffness matrix with respect to the fiber orientation are presented in Table 4.7. As can be seen there is a very good agreement between the

Table 4.7: Non-zero entries of cross section stiffness matrix for square cross section (S3) with respect to fiber orientation (fiber plane parallel to xz plane). Comparison between BECAS and VABS.

	BECAS	VABS	Rel. Diff. (%)	BECAS	VABS	Diff. (%)
			0 °	22.5 °		
$K_{s,11}$	5.039E-01	5.039E-01	2.129E-10	7.598E-01	7.598E-01	1.627E-10
$K_{s,22}$	4.201E-01	4.201E-01	2.123E-10	4.129E-01	4.129E-01	1.632E-10
$K_{s,33}$	4.800E+00	4.800E+00	-2.035E-13	3.435E+00	3.435E+00	7.482E-11
$K_{s,44}$	4.001E-03	4.001E-03	6.634E-10	2.489E-03	2.489E-03	7.052E-10
$K_{s,55}$	4.001E-03	4.001E-03	6.686E-10	2.274E-03	2.274E-03	9.388E-10
$K_{s,66}$	7.737E-04	7.737E-04	9.584E-10	9.499E-04	9.499E-04	9.845E-10
$K_{s,13}$	0.000E+00	0.000E+00	0.000E+00	7.387E-01	7.387E-01	2.335E-10
$K_{s,46}$	0.000E+00	0.000E+00	0.000E+00	-4.613E-04	-4.613E-04	9.910E-10
			45 °	67.5 °		
$K_{s,11}$	8.421E-01	8.421E-01	3.985E-10	6.039E-01	6.039E-01	2.663E-10
$K_{s,22}$	4.473E-01	4.473E-01	1.616E-10	4.883E-01	4.883E-01	1.954E-10
$K_{s,33}$	1.713E+00	1.713E+00	1.057E-10	1.241E+00	1.241E+00	4.043E-12
$K_{s,44}$	1.326E-03	1.326E-03	6.825E-10	1.032E-03	1.032E-03	6.659E-10
$K_{s,55}$	1.274E-03	1.274E-03	9.726E-10	1.030E-03	1.030E-03	6.778E-10
$K_{s,66}$	1.018E-03	1.018E-03	9.663E-10	9.171E-04	9.171E-04	9.804E-10
$K_{s,13}$	4.017E-01	4.017E-01	6.091E-10	6.317E-02	6.317E-02	4.366E-10
$K_{s,46}$	-2.422E-04	-2.422E-04	1.042E-09	-4.786E-05	-4.786E-05	1.023E-09
			90 °			
$K_{s,11}$	5.0202E-01	5.0202E-01	1.9581E-10			
$K_{s,22}$	5.0406E-01	5.0406E-01	2.1603E-10			
$K_{s,33}$	1.2000E+00	1.2000E+00	0.0000E+00			
$K_{s,44}$	1.0004E-03	1.0004E-03	7.2271E-10			
$K_{s,55}$	1.0002E-03	1.0002E-03	6.6684E-10			
$K_{s,66}$	8.5081E-04	8.5081E-04	9.5579E-10			
$K_{s,13}$	0.0000E+00	0.0000E+00	0.0000E+00			
$K_{s,46}$	0.0000E+00	0.0000E+00	0.0000E+00			

results from BECAS and VABS. For laminate orientations other than 0° and 90° , the shear-extension and bending-torsion couplings become non-zero. These effects are typical of laminated composite beams. The influence of these couplings on the cross section warping displacements can be observed in Figures 4.7 and 4.8. Comparing with the isotropic case in Section 4.2.1, the bending deformation resulting from the curvature $\tau_z = 1$ is now accompanied of an out-of-plane distortion induced by the torsion coupling. Finally, the position of shear and tension center do not depend on the orientation of fibers in the laminate (i.e., $x_s = y_s = x_t = y_t = 0$). However, note that according to the definition of the shear center (see Section 2.5.2), in this case the position of the shear center is not a property of the cross section. Instead, because the bend-twist coupling $\mathbf{K}_{s,46} \neq 0$, the shear center position will depend linearly on the coordinate z .

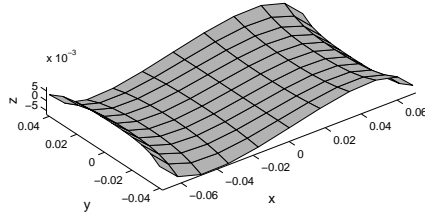
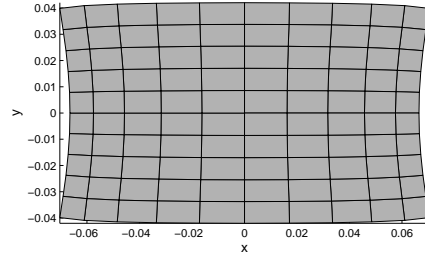
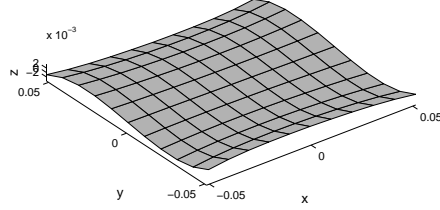
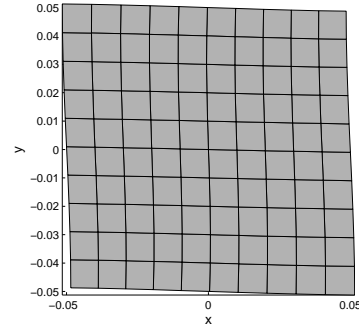
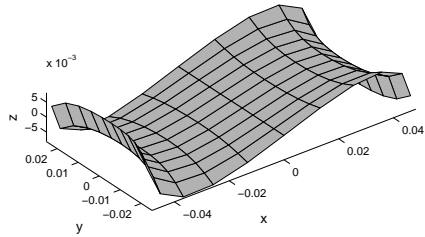
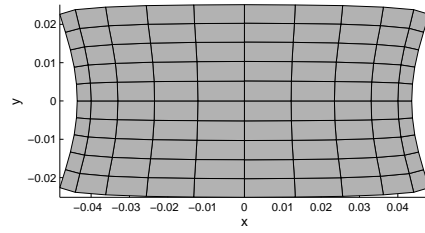
(a) $\tau_x = 1$ (b) $\tau_x = 1$ (c) $\tau_y = 1$ (d) $\tau_y = 1$ (e) $\tau_z = 1$ (f) $\tau_z = 1$

Figure 4.7: Cross section warping displacements for square cross section (S3) with fibers oriented at 45° . Out-of-plane (left) and in-plane (right) deformation (displacements not to scale).

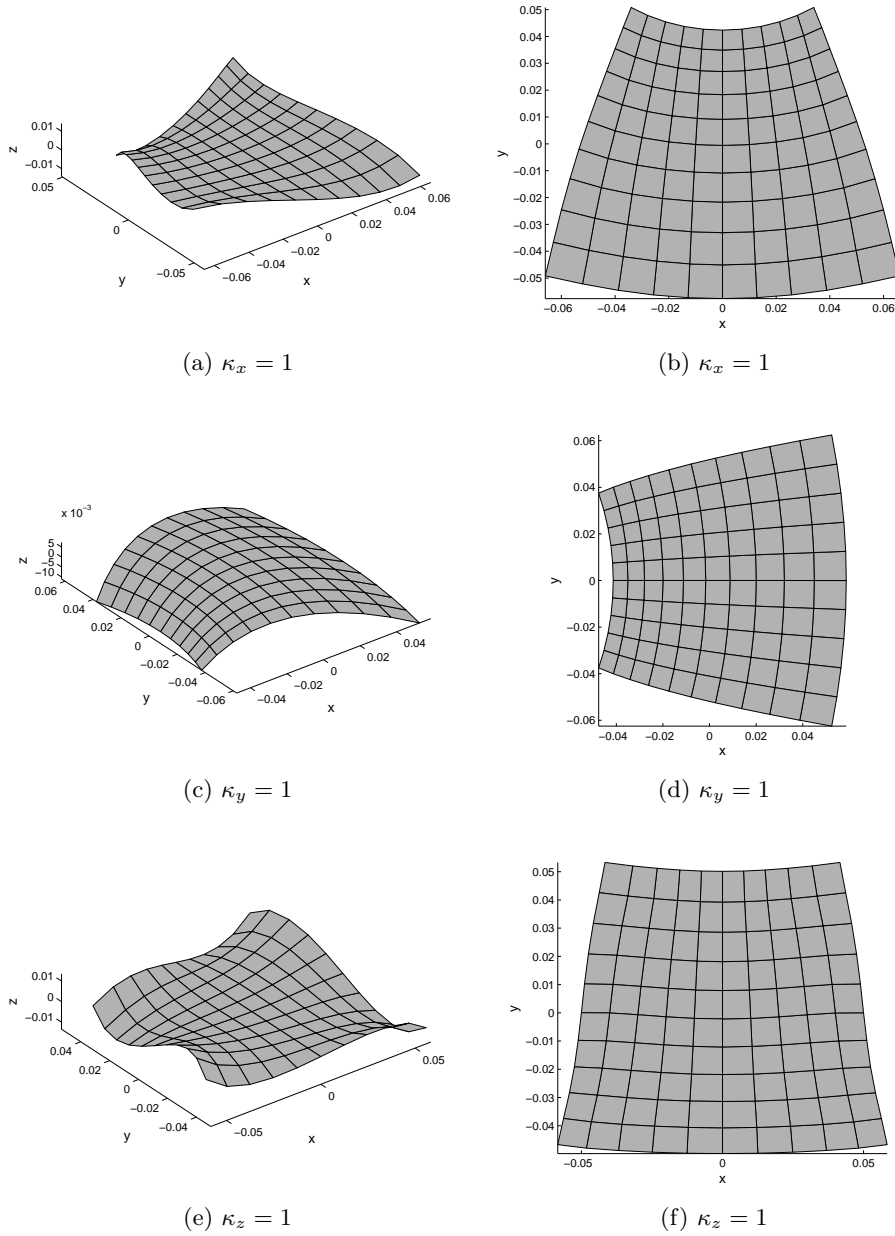


Figure 4.8: (continuation) Cross section warping displacements for square cross section (S3) with fibers oriented at 45° . Out-of-plane (left) and in-plane (right) deformation (displacements not to scale).

4.2.2 Cylinder

In this section results are presented based on the cylinder cross section. The geometrical dimensions of the cylindrical cross section are presented in Table 4.8 and the geometry and finite element mesh are presented in Figure 4.8.

Table 4.8: Geometrical dimensions of cylinder section.

Outer radius (R)	0.1 m
Thickness (t)	0.01 m

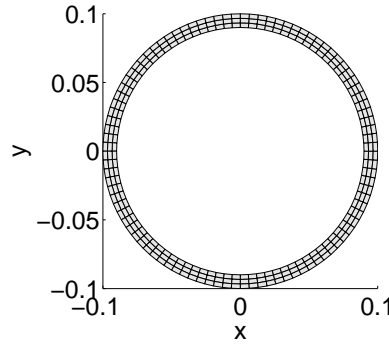


Figure 4.9: Geometry and finite element mesh of cylinder cross section with one material (C1).

Cylinder cross section of isotropic material – C1

In the first case it is assumed that the cylinder is made of isotropic material #1. The non-zero stiffness entries for both BECAS and VABS are presented in Table 4.9. As can be seen there is a very good agreement between the two approaches. The warping displacements are presented in Figure 4.10. As expected the shear strains are the only which induce out-of-plane deformation. Due to the axial symmetry the torsion strain will not induce any out-of-plane deformation. The same holds for the shear and elastic positions which coincide with the origin of the cross section coordinate system. Thus, according both BECAS and VABS $x_s = y_s = x_t = y_t = 0$.

Table 4.9: Non-zero entries of cross section stiffness matrix for cylinder cross section (C1). Comparison between BECAS and VABS.

	BECAS	VABS	Rel. Diff. (%)
$K_{s,11}$	1.249E-01	1.249E-01	7.200E-04
$K_{s,22}$	1.249E-01	1.249E-01	7.200E-04
$K_{s,33}$	5.965E-01	5.965E-01	1.675E-13
$K_{s,44}$	2.697E-03	2.697E-03	5.587E-09
$K_{s,55}$	2.697E-03	2.697E-03	5.587E-09
$K_{s,66}$	2.248E-03	2.248E-03	7.200E-04

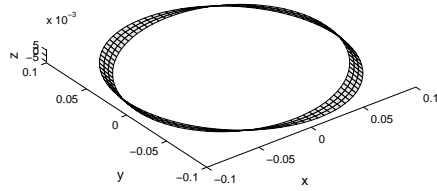
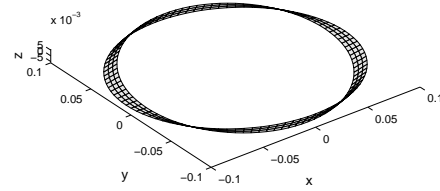
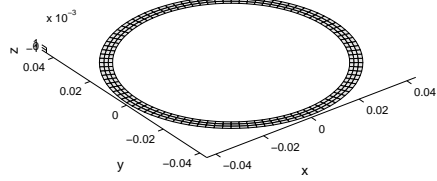
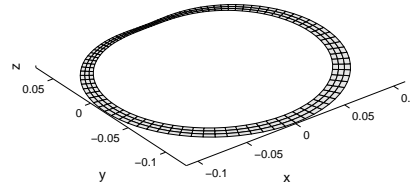
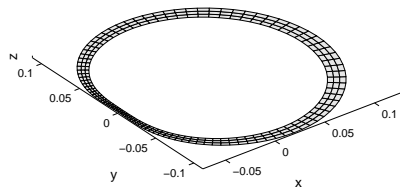
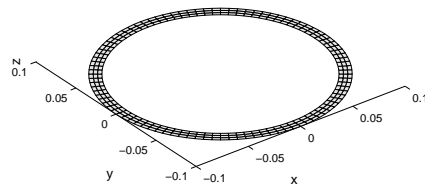
(a) $\tau_x = 1$ (b) $\tau_y = 1$ (c) $\tau_z = 1$ (d) $\kappa_x = 1$ (e) $\kappa_y = 1$ (f) $\kappa_z = 1$

Figure 4.10: Cross section warping displacements for cylinder cross section (C1) (displacements not to scale).

Half-cylinder cross section of isotropic material – C2

The cylinder cross section studied in the previous chapter is divided in two to generate the half cylinder cross section studied here. The geometry and finite element mesh are presented in Figure 4.11. This is an open cross section and the out-of-plane deformation is significant and should therefore be accounted for in the estimation of the stiffness properties. The value of the non-zero entries in the cross section stiff-

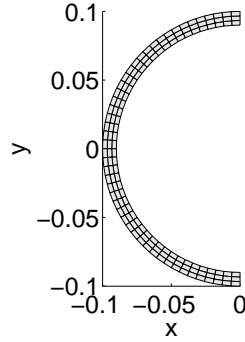


Figure 4.11: Geometry and finite element mesh of half-cylinder cross section (C2).

ness matrix as estimated by both BECAS and VABS are presented in Table 4.10. As can be seen there is a very good agreement between the two methods. The same is observed in the estimated positions of the elastic and shear center as presented in Table 4.11. Finally, the warping displacements for different values of the strain parameters ψ are presented in Figure 4.12. Note that the magnitude of the warping displacements for $\kappa_z = 1$, torsional curvature, are of the order of $O(10^7)$. Hence it is expected that the resulting strains and stresses will also be very large also. This result serves to illustrate the fact that open cross sections are weaker in torsion than closed cross sections.

Table 4.10: Non-zero entries of cross section stiffness matrix for half-cylinder cross section (C2). Comparison between BECAS and VABS.

	BECAS	VABS	Rel. Diff. (%)
$K_{s,11}$	4.964E-02	4.964E-02	7.195E-04
$K_{s,22}$	6.244E-02	6.244E-02	7.200E-04
$K_{s,33}$	2.982E-01	2.982E-01	0.000E+00
$K_{s,44}$	1.349E-03	1.349E-03	4.672E-09
$K_{s,55}$	1.349E-03	1.349E-03	4.637E-09
$K_{s,66}$	9.120E-04	9.120E-04	7.200E-04
$K_{s,35}$	1.805E-02	1.805E-02	8.862E-12
$K_{s,26}$	-7.529E-03	-7.529E-03	7.200E-04

Table 4.11: Shear and elastic center positions $((x_s, y_s)$ and (x_t, y_t) , respectively) for half-cylinder cross section (C2). Comparison between BECAS and VABS.

	BECAS	VABS	Diff. (%)
x_s	-1.206E-01	-1.206E-01	0
y_s	0.	0	0
x_t	-6.051E-02	-6.051E-02	0
y_t	0.	0	0

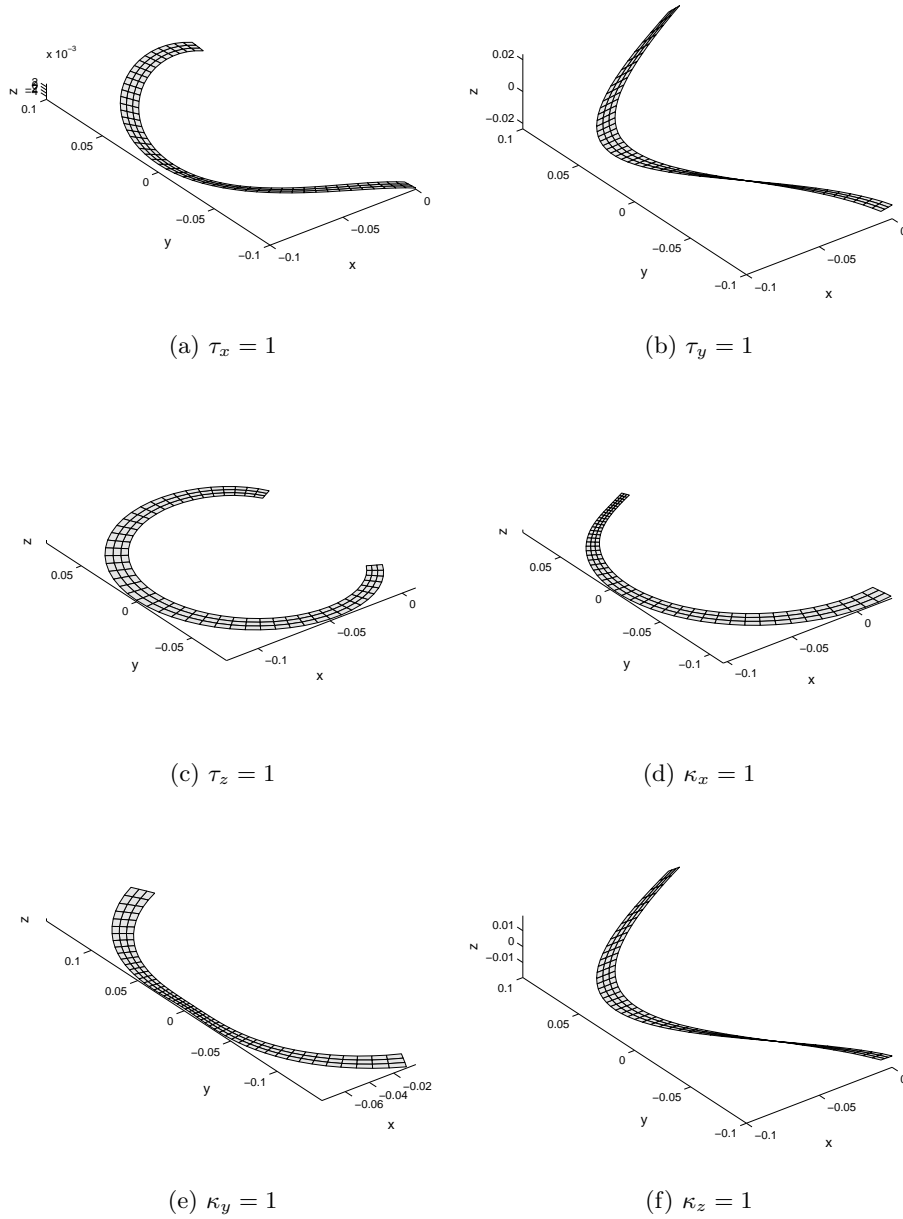


Figure 4.12: Cross section warping displacements for half-cylinder cross section (C2) (displacements not to scale).

Cylinder cross section of two isotropic material (half) – C3

The effect of extreme material inhomogeneity is investigated here following the approach described in Section 4.2.1 for the solid square cross section. The cylindrical cross section is divided in two. One half is made of the isotropic material #1 while the second half of the cylinder cross section is made of the isotropic material #2. The distribution of the two materials in the cross section can be seen in Figure 4.13. The resulting non-zero entries of the cross section stiffness matrix are given

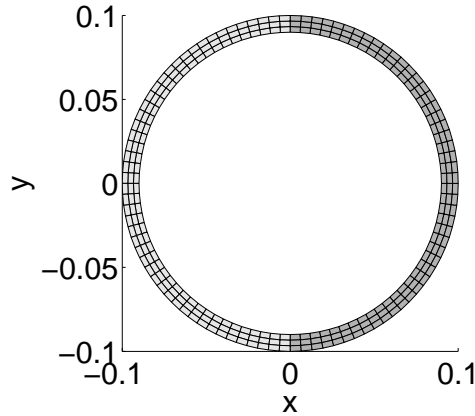


Figure 4.13: Geometry and finite element mesh of cylinder cross section with two materials (C3) – isotropic material #1 (light) and #2 (dark).

in Table 4.12 with respect to the ration E_1/E_2 . As can be seen there is a very good match between BECAS and VABS. As the stiffness of the isotropic material #2 vanishes the entries of the cross section stiffness matrix converge to those which were obtained when only half the cross section was considered (see Section 4.2.2). Note once again the behaviour of the $K_{s,11}$ entry with respect to the ration E_1/E_2 plotted in Figure 4.14. Just like in the case of the solid square cross section in Section 4.2.1, the shear stiffness seems to decrease past the half-cylinder values having a minima at $E_1/E_2 = 10$. Finally the variation of the positions of the shear and elastic centers with respect to the ration E_1/E_2 are presented in Table 4.13. There is a very good agreement between BECAS and VABS. Also, note that the positions of the shear and elastic center do not explain the behavior of the $K_{s,11}$ entry. The warping deformations for $E_1/E_2 = 1000$ are presented in Figure 4.15. The warping deformations in this case are also relatively large and in the same order of magnitude as the half-cylinder cross section.

Table 4.12: Non-zero entries of cross section stiffness matrix for cylinder cross section (C3) with respect to E_1/E_2 . Comparison between BECAS and VABS.

BECAS							
E_1/E_2	$K_{s,11}$	$K_{s,22}$	$K_{s,33}$	$K_{s,44} = K_{s,55}$	$K_{s,66}$	$K_{s,26}$	$K_{s,35}$
1E+00	1.25E-01	1.25E-01	5.96E-01	2.70E-03	2.25E-03	-1.90E-18	0.00E+00
1E+01	3.99E-02	6.87E-02	3.28E-01	1.48E-03	1.08E-03	-6.78E-03	1.62E-02
1E+02	3.75E-02	6.31E-02	3.01E-01	1.36E-03	9.29E-04	-7.45E-03	1.79E-02
1E+03	4.74E-02	6.25E-02	2.99E-01	1.35E-03	9.14E-04	-7.52E-03	1.80E-02
1E+04	4.94E-02	6.24E-02	2.98E-01	1.35E-03	9.12E-04	-7.53E-03	1.80E-02
1E+05	4.96E-02	6.24E-02	2.98E-01	1.35E-03	9.12E-04	-7.53E-03	1.80E-02
VABS							
E_1/E_2	$K_{s,11}$	$K_{s,22}$	$K_{s,33}$	$K_{s,44}$	$K_{s,55} = K_{s,55}$	$K_{s,34}$	$K_{s,16}$
1E+00	1.25E-01	1.25E-01	5.96E-01	2.70E-03	2.25E-03	-1.94E-18	0.00E+00
1E+01	3.99E-02	6.87E-02	3.28E-01	1.48E-03	1.08E-03	-6.78E-03	1.62E-02
1E+02	3.75E-02	6.31E-02	3.01E-01	1.36E-03	9.29E-04	-7.45E-03	1.79E-02
1E+03	4.74E-02	6.25E-02	2.99E-01	1.35E-03	9.14E-04	-7.52E-03	1.80E-02
1E+04	4.94E-02	6.24E-02	2.98E-01	1.35E-03	9.12E-04	-7.53E-03	1.80E-02
1E+05	4.96E-02	6.24E-02	2.98E-01	1.35E-03	9.12E-04	-7.53E-03	1.80E-02
Diff (%)							
E_1/E_2	$K_{s,11}$	$K_{s,22}$	$K_{s,33}$	$K_{s,44}$	$K_{s,55} = K_{s,55}$	$K_{s,34}$	$K_{s,16}$
1E+00	-7.20E-04	-7.20E-04	-1.68E-13	-5.59E-09	-7.20E-04	-2.17E+00	0.00E+00
1E+01	-7.20E-04	-7.20E-04	-3.05E-13	-5.33E-09	-7.20E-04	-7.20E-04	-2.15E-11
1E+02	-7.20E-04	-7.20E-04	-3.32E-13	-4.82E-09	-7.20E-04	-7.20E-04	-2.13E-11
1E+03	-7.20E-04	-7.20E-04	0.00E+00	-4.67E-09	-7.20E-04	-7.20E-04	-4.45E-12
1E+04	-7.19E-04	-7.20E-04	-7.05E-12	-4.66E-09	-7.20E-04	-7.20E-04	2.21E-12
1E+05	-7.19E-04	-7.20E-04	1.27E-11	-4.68E-09	-7.20E-04	-7.20E-04	-2.23E-12

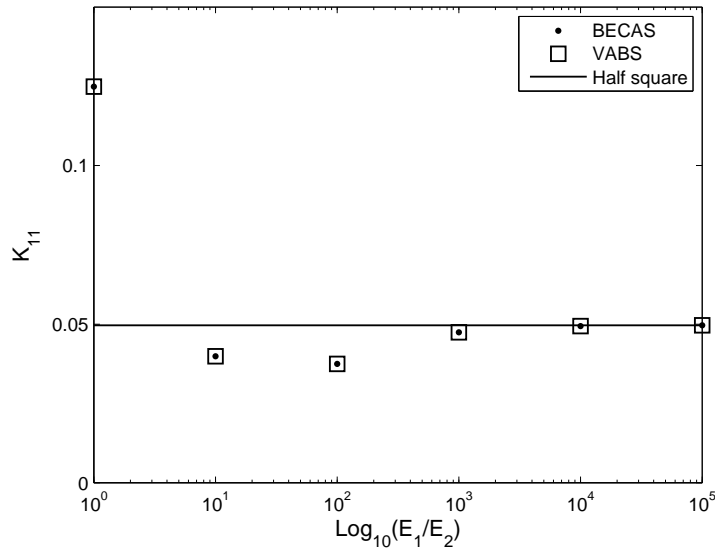
Figure 4.14: Variation of $K_{s,11}$ entry of the cross section stiffness matrix with respect to the ratio E_1/E_2 for the cylinder cross section (C3). Results for BECAS and VABS compared with the solution for half cylinder.

Table 4.13: Shear and elastic center positions $((x_s, y_s)$ and (x_t, y_t) , respectively) for cylinder cross section (C3) with respect to the ratio E_1/E_2 . Comparison between BECAS and VABS.

BECAS			VABS	
E_1/E_2	x_s	y_s	x_s	y_s
1E+00	0.000E+00	0.000E+00	0.000E+00	0.000E+00
1E+01	-9.866E-02	0.000E+00	-9.866E-02	-1.069E-15
1E+02	-1.182E-01	0.000E+00	-1.182E-01	-1.415E-15
1E+03	-1.203E-01	0.000E+00	-1.203E-01	-1.292E-15
1E+04	-1.206E-01	0.000E+00	-1.206E-01	3.740E-16
1E+05	-1.206E-01	0.000E+00	-1.206E-01	1.308E-15
E_1/E_2	x_t	y_t	x_t	y_t
1E+00	0.000E+00	0.000E+00	0.000E+00	0.000E+00
1E+01	-4.951E-02	0.000E+00	-4.951E-02	3.279E-17
1E+02	-5.931E-02	0.000E+00	-5.931E-02	1.920E-17
1E+03	-6.039E-02	0.000E+00	-6.039E-02	3.411E-18
1E+04	-6.050E-02	0.000E+00	-6.050E-02	4.960E-18
1E+05	-6.051E-02	0.000E+00	-6.051E-02	-1.255E-18

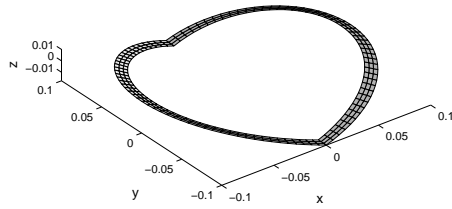
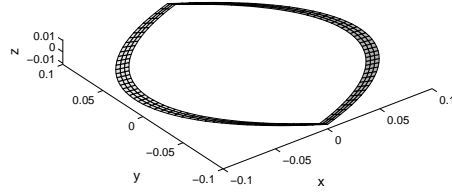
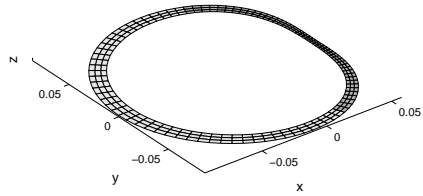
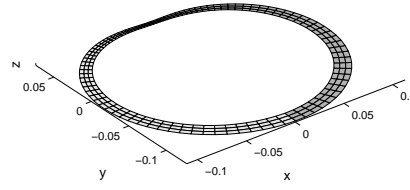
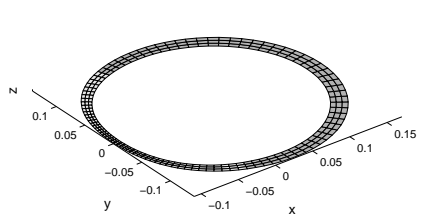
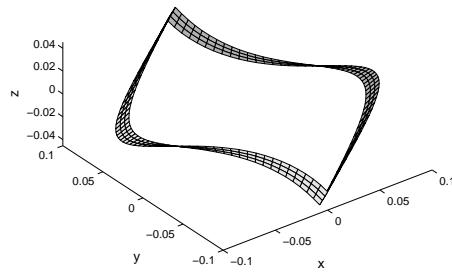
(a) $\tau_x = 1$ (b) $\tau_y = 1$ (c) $\tau_z = 1$ (d) $\kappa_x = 1$ (e) $\kappa_y = 1$ (f) $\kappa_z = 1$

Figure 4.15: Cross section warping displacements for cylinder cross section (C3) with $E_1/E_2 = 1000$ (displacements not to scale).

Cylinder cross section of two isotropic materials (layered) – C4

In the final numerical example using the cylinder cross section we assume a layered structure through the thickness. The material distribution, geometry and cross section finite element mesh are presented in Figure 4.16. It is assumed in this case that $E_1/E_2 = 1000$. The resulting non-zero entries of the cross section stiffness matrix as

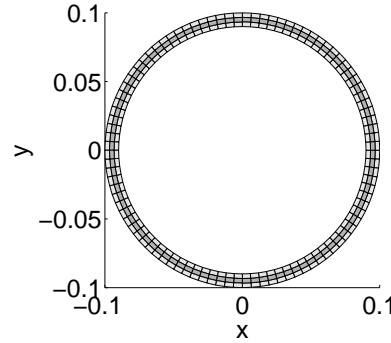


Figure 4.16: Geometry and finite element mesh of cylinder cross section with two isotropic materials (layered) (C4) – isotropic material #1 (light) and #2 (dark).

estimated by both BECAS and VABS are presented in Table 4.14. As can be seen there is a very good agreement between the two cross section analysis tools. The

Table 4.14: Non-zero entries of cross section stiffness matrix for cylinder cross section with two isotropic materials (layered) (C4). Comparison between BECAS and VABS.

	BECAS	VABS	Rel. Diff. (%)
$K_{s,11}$	8.3114E-02	8.3115E-02	7.1996E-04
$K_{s,22}$	8.3114E-02	8.3115E-02	7.1996E-04
$K_{s,33}$	3.9784E-01	3.9784E-01	0.00
$K_{s,44}$	1.8012E-03	1.8012E-03	0.00
$K_{s,55}$	1.8012E-03	1.8012E-03	0.00
$K_{s,66}$	1.5010E-03	1.5010E-03	7.1996E-04

warping displacements resulting from different cross section strains are presented in Figure 4.17. The deformation patterns are very similar to those obtained in the case where only the isotropic material #1 is used. The differences can be seen in the shear deformation which shows some local perturbations due to the lower stiffness of middle layer.

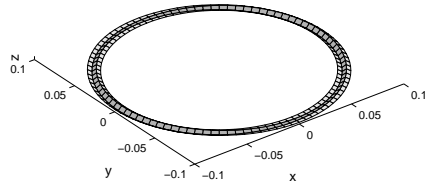
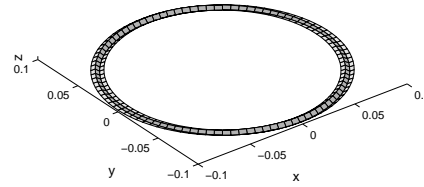
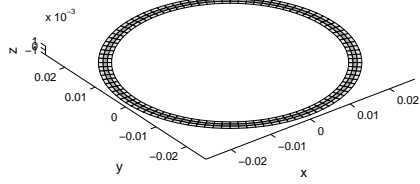
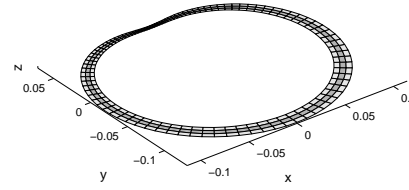
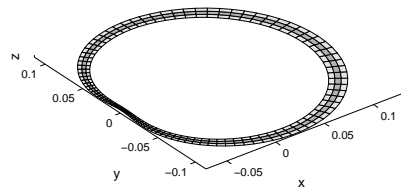
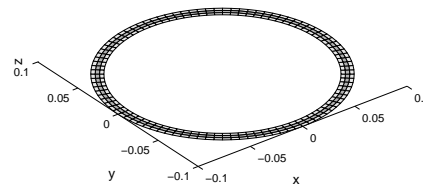
(a) $\tau_x = 1$ (b) $\tau_y = 1$ (c) $\tau_z = 1$ (d) $\kappa_x = 1$ (e) $\kappa_y = 1$ (f) $\kappa_z = 1$

Figure 4.17: Cross section warping displacements for cylinder cross section with two isotropic materials (layered) (C4) (displacements not to scale).

4.2.3 Three cells

In the final group of numerical examples a three cell sectional geometry is considered. The geometry, corresponding dimensions and finite element mesh for the three cell cross section are presented in Figure 4.18. Some cross section analysis theories rely on the integration of the shear flux over each of the closed cells. The aim of this example is to illustrate the ability of BECAS to correctly estimate the stiffness properties of cross sections regardless of the number of cells in the cross section.

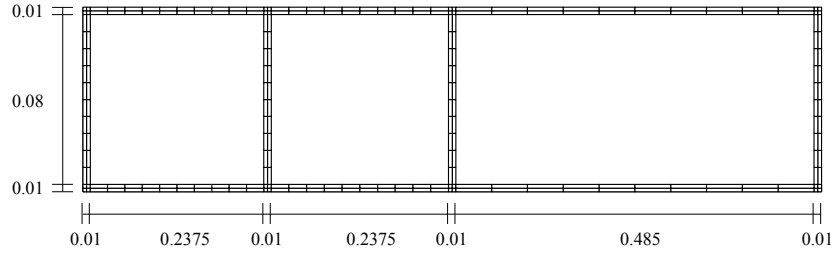


Figure 4.18: Geometry and finite element mesh of three cells cross section of one isotropic material (T1).

Three cells cross section of isotropic material – T1

In this example all faces of the three cell cross section are made of isotropic material #1. The resulting non-zero entries of the cross section stiffness matrix as determined by both BECAS and VABS, are presented in Table 4.15. The estimated positions

Table 4.15: Non-zero entries of cross section stiffness matrix for three cells cross section (T1). Comparison between BECAS and VABS.

	BECAS	VABS	Rel. Diff. (%)
$K_{s,11}$	7.61E-01	7.61E-01	7.20E-04
$K_{s,22}$	2.93E-01	2.93E-01	6.92E-04
$K_{s,33}$	2.92E+00	2.92E+00	3.35E-13
$K_{s,44}$	3.29E-02	3.29E-02	5.88E-08
$K_{s,55}$	2.94E-01	2.94E-01	1.63E-09
$K_{s,66}$	3.95E-02	3.95E-02	7.20E-04
$K_{s,26}$	-8.26E-03	-8.26E-03	6.91E-04
$K_{s,35}$	5.75E-02	5.75E-02	-1.55E-11

of the shear and elastic center are presented in Table 4.16. As can be seen there is a very good agreement between BECAS and VABS for all results. The warping displacements obtained for different values of the components of ψ are presented in Figure 4.19. As can be seen the shear-torsion coupling term $K_{s,26}$ and the extension-bending coupling $K_{s,35}$ are non-zero. The effect of these couplings on the warping deformations can be seen for $\tau_y = 1$ and $\tau_z = 1$, respectively. This is due to the shift in the shear and elastic center positions due to the asymmetric geometry.

Table 4.16: Shear and elastic center positions $((x_s, y_s)$ and (x_t, y_t) , respectively) for three cells cross section (T1). Comparison between BECAS and VABS.

	BECAS	VABS	Diff. (%)
x_s	-2.823E-02	-2.823E-02	0
y_s	0.	0	0
x_t	-1.969E-02	-1.969E-02	0
y_t	0.	0	0

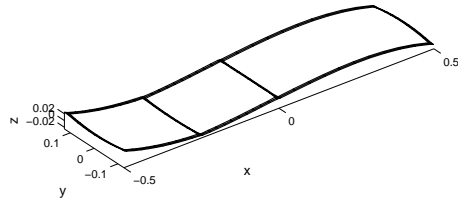
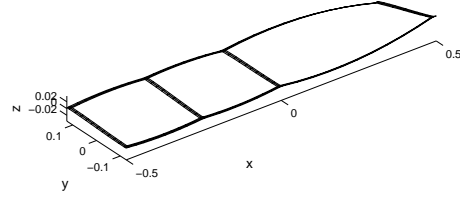
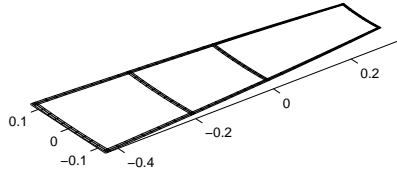
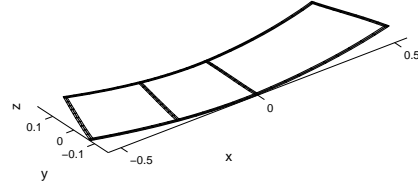
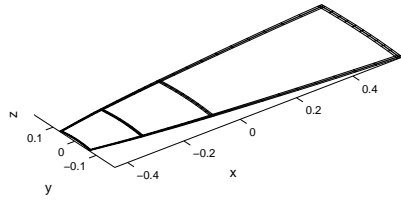
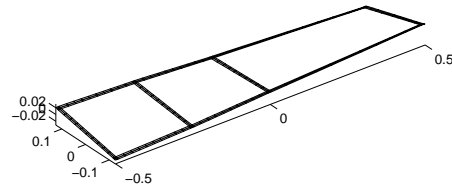
(a) $\tau_x = 1$ (b) $\tau_y = 1$ (c) $\tau_z = 1$ (d) $\kappa_x = 1$ (e) $\kappa_y = 1$ (f) $\kappa_z = 1$

Figure 4.19: Cross section warping displacements for three cells cross section (T1) (displacements not to scale).

Three cells cross section of orthotropic top faces and isotropic webs - T2

In the last numerical experiment the top faces of the three cells cross section are laminated using the orthotropic material oriented at 45° . The vertical faces are made of isotropic material. The material distribution is visible in Figure 4.20. The aim is

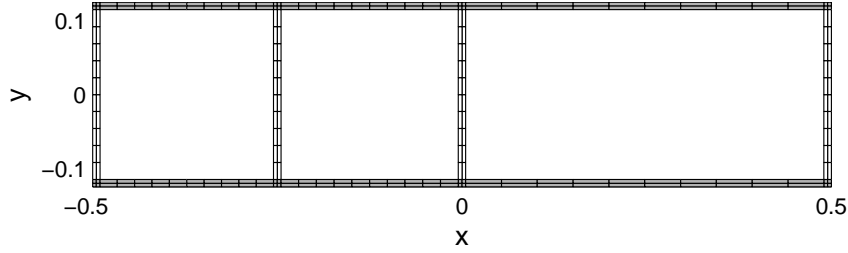


Figure 4.20: Geometry and finite element mesh of three cells cross section with orthotropic material at 45° in the top faces (dark) and isotropic material in the vertical shear webs (light) T2.

to combine in one experiment the effects of material anisotropy and inhomogeneity using a closed thin-walled multi-cell cross section. The non-zero entries of the cross section stiffness matrix as estimated by BECAS and VABS are presented in Table 4.17. As can be seen there is a very good agreement between both methods. The resulting positions of the shear and elastic center are presented in Table 4.18. Like before, both BECAS and VABS present a very good agreement in the estimation of the shear and elastic center.

Table 4.17: Non-zero entries of cross section stiffness matrix for three cells cross section with orthotropic material at 45° in the top faces and isotropic material in the vertical webs (T2).

	BECAS	VABS	Rel. Diff. (%)
$K_{s,11}$	1.79E+00	1.79E+00	1.36E-10
$K_{s,22}$	3.22E-01	3.22E-01	2.13E-09
$K_{s,33}$	4.37E+00	4.37E+00	2.98E-11
$K_{s,44}$	5.23E-02	5.23E-02	2.16E-10
$K_{s,55}$	3.81E-01	3.81E-01	1.21E-10
$K_{s,66}$	7.73E-02	7.73E-02	3.29E-10
$K_{s,31}$	-8.48E-01	-8.48E-01	1.13E-10
$K_{s,35}$	5.64E-02	5.64E-02	-3.88E-11
$K_{s,15}$	2.75E-03	2.75E-03	6.11E-09
$K_{s,26}$	-1.49E-02	-1.49E-02	2.42E-09
$K_{s,24}$	-3.13E-03	-3.13E-03	2.16E-09
$K_{s,64}$	1.83E-02	1.83E-02	5.79E-10

Table 4.18: Shear and elastic center positions $((x_s, y_s)$ and (x_t, y_t) , respectively) for three cells cross section T2. Comparison between BECAS and VABS.

	BECAS	VABS	Diff. (%)
x_s	-4.300E-02	-4.300E-02	0
y_s	0.	0	0
x_t	-1.456E-02	-1.456E-02	0
y_t	0.	0	0

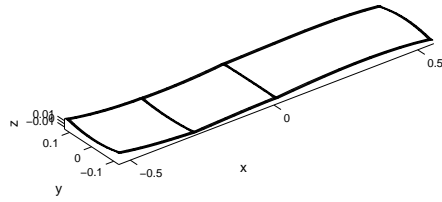
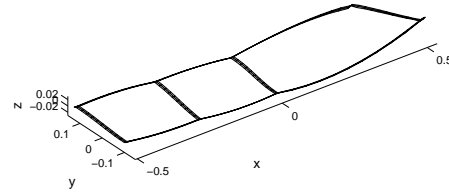
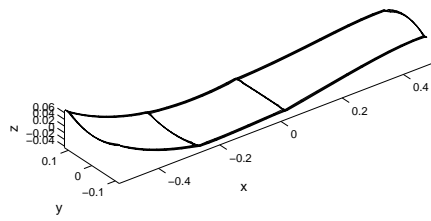
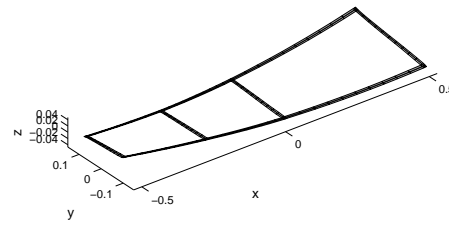
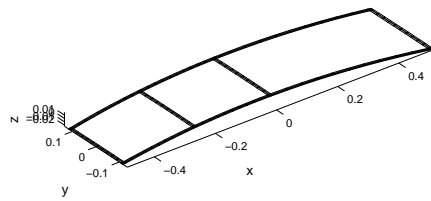
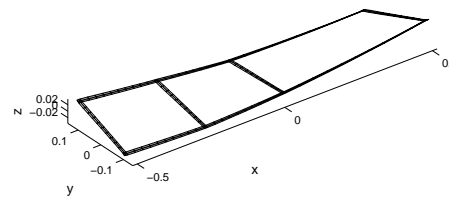
(a) $\tau_x = 1$ (b) $\tau_y = 1$ (c) $\tau_z = 1$ (d) $\kappa_x = 1$ (e) $\kappa_y = 1$ (f) $\kappa_z = 1$

Figure 4.21: Cross section warping displacements for three cells cross section with orthotropic material at 45° in the top faces and isotropic material in the vertical shear webs T2 (displacements not to scale).

Chapter 5

User's Manual

The usage of BECAS is described in this chapter. The aim is to go through the functionalities of BECAS and discuss its practical usage within a structural analysis environment. BECAS is implemented as a Matlab toolbox. The following functions are available

- **BECAS_Uutils** - Build arrays for BECAS calculations.
- **BECAS_Constitutive_Ks** - Calculation of the cross section stiffness matrix;
- **BECAS_Constitutive_Ms** - Calculation of the cross section mass matrix;
- **BECAS_CrossSectionProps** - Calculation of the cross section properties;
- **BECAS_RecoverStrains** - Calculation of the three-dimensional strains at each point in the cross section;
- **BECAS_RecoverStresses** - Calculation of the three-dimensional stresses at each point in the cross section;
- **BECAS_TransformationMat** - Rotate and translate the cross section constitutive matrices;
- **BECAS_Becas2Hawc2** - Generate output for latest version of Hawc2.
- **BECAS_3D_Uutils** - Build working arrays for BECAS calculations.
- **BECAS_3D_Constitutive_Ks** - Calculation of the cross section stiffness matrix based on solid finite element models of the cross section;
- **BECAS_3D_CrossSectionProps** - Calculation of the cross section properties;

The version of BECAS based on two-dimensional finite element discretizations of the cross section is presented first. The use of the BECAS_3D tool is discussed last in Section 5.3.

Note that the BECAS toolbox also includes a number of functions for visualization of the input and output. The description of this functions has been omitted as it falls beyond the scope of this manual.

Part of the MATLAB code in BECAS is generated through MAPLE. There are four MAPLE files which follow together with the BECAS code:

- **GenerateMatricesBECAS.mw** used to generate all the element stiffness matrices which are included in the MATLAB function **Quad4** used within the function **BECAS_Constitutive_Ks**.
- **LayerRotationBECAS.mw** used to generate the code for the function which rotates the material constitutive matrix **Q** in the MATLAB function **BECAS_Utils** when orienting the fibers in a layer.
- **FiberPlaneRotationBECAS.mw** used to generate the code for the function which rotates the material constitutive matrix **Q** when orienting the fiber plane in an element in the MATLAB function **BECAS_Utils**.

5.1 Input

In order to run BECAS the following input is necessary:

- **nl_2d** - ($n_n \times 3$) array with the list of nodal positions where each row is in the form (*node number, x coordinate, y coordinate*), where n_n is the total number of nodes. The node numbering need not be in any specific order.
- **el_2d** - ($n_e \times 8$) array with the element connectivity table where each row is in the form (*element number, node 1, node 2, node 3, node 4, node 5, node 6, node 7, node 8*), where n_e is the total number of elements. The element numbering need not be in any specific order. The value of *node 5* through *node 8* has to be zero for Quad4 element to be used. Otherwise, Quad8 is automatically chosen.
- **emat** - ($n_e \times 4$) array with element material properties assignment where each row is in the form (*element number, material number, fiber angle, fiber plane angle*), where n_e is the total number of elements. The element numbering need not be in any specific order. The *material number* corresponds to the materials assigned in the **matprops** array.
- **matprops** - ($nmat \times 10$) array with the material properties where each row is in the form ($E_{11}, E_{22}, E_{33}, G_{12}, G_{13}, G_{23}, \nu_{12}, \nu_{13}, \nu_{23}, \rho$), where $nmat$ is the total number of different materials considered. The material mechanical properties given with respect to the material coordinate system have been defined as
 - E_{11} the Young modulus of material the 1 direction.
 - E_{22} the Young modulus of material the 2 direction.
 - E_{33} the Young modulus of material the 3 direction.
 - G_{12} the shear modulus in the 12 plane.
 - G_{13} the shear modulus in the 13 plane.
 - G_{23} the shear modulus in the 23 plane.
 - ν_{12} the Poisson's ratio in the 12 plane.
 - ν_{13} the Poisson's ratio in the 13 plane.

- ν_{23} the Poisson's ratio in the 23 plane.
- ρ the material density.

The rotation of the material constitutive tensor is described in Section 3.2.

5.1.1 Example

All the files necessary to run all the examples presented for the Validation in Section 4 are distributed together with BECAS. These files can be used as a starting point for the development of new input for BECAS.

5.2 List of functions and output

The different functions included in the BECAS library and corresponding output are described in this chapter.

5.2.1 BECAS_Utils

The function `BECAS_Utils` is used to build working arrays. It is included inside all the other functions in the 2D version of BECAS. It is called using

```
[utils]=BECAS_Utils(nl_2d,el_2d,emat,matprops)
```

5.2.2 BECAS_Constitutive_Ks

The function `BECAS_Constitutive_Ks` is the BECAS central function and is used primarily for the evaluation of the cross section stiffness matrix \mathbf{K}_s . The function is called using

```
[Ks,dX,dY,X,Y]=BECAS_Constitutive_Ks(nl_2d,el_2d,emat,matprops);
```

The output is

- \mathbf{K}_s - (6×6) array storing the cross section stiffness matrix \mathbf{K}_s .
- \mathbf{dX} - $(n_d \times 6)$ array $\frac{\partial \mathbf{X}}{\partial z}$.
- \mathbf{dY} - (6×6) array $\frac{\partial \mathbf{Y}}{\partial z}$.
- \mathbf{X} - $(n_d \times 6)$ array \mathbf{X} .
- \mathbf{Y} - (6×6) array \mathbf{Y} .

where $n_d = n_n \times 3$ is the number of degrees of freedom in cross section finite element equations.

5.2.3 BECAS_Constitutive_Ms

The function `BECAS_Constitutive_Ms` is used for the evaluation of the cross section mass matrix \mathbf{M}_s . It is called as

```
[Ms]=BECAS_Constitutive_Ms(nl_2d,el_2d,emat,matprops);
```

The output is

- \mathbf{M}_s - (6×6) array storing the cross section mass matrix \mathbf{M}_s .

5.2.4 BECAS_CrossSectionProps

The function `BECAS_CrossSectionProps` is used to determine a series of relevant cross section properties. It presumes that the cross section stiffness \mathbf{K}_s has been previously determined. The function is called using

```
[ ShearX,ShearY,ElasticX,ElasticY,...
  MassX,MassY,MassPerUnitLength,...
  AlphaPrincipleAxis,AlphaPrincipleAxis_ElasticCenter,...
  AreaX,AreaY,AreaTotal,...
  Ixx,Iyy,Ixy,Axx,Ayy,Axy]=...
  BECAS_CrossSectionProps(Ks,nl_2d,el_2d,emat,matprops);
```

The output is

- `ShearX` - the x_s position of the cross section shear center.
- `ShearY` - the y_s position of the cross section shear center.
- `ElasticX` - the x_t position of the cross section elastic center.
- `ElasticY` - the y_t position of the cross section elastic center.
- `MassX` - the x_m position of the cross section mass center.
- `MassY` - the y_m position of the cross section mass center.
- `MassPerUnitLength` - the cross section mass per unit length.
- `AlphaPrincipleAxis` - the orientation of the cross section elastic axis determined at the reference point (in radians).
- `AlphaPrincipleAxis_ElasticCenter` - the orientation of the cross section elastic center determined at the elastic center (in radians).
- `AreaX` - the x coordinate of the area centroid.
- `AreaY` - the y coordinate of the area centroid.
- `AreaTotal` - total cross section area.
- `Ixx` - the mass moment of inertia with respect to the x axis.
- `Iyy` - the mass moment of inertia with respect to the y axis.
- `Ixy` - the mass product of inertia.
- `Axx` - the area moment of inertia with respect to the x axis.
- `Ayy` - the area moment of inertia with respect to the y axis.
- `Axy` - the area product of inertia.

5.2.5 BECAS_RecoverStrains

The function `BECAS_RecoverStresses` is used to determine the three-dimensional strains components at the center of each element and at each Gauss point in the cross section finite element mesh. The function is meant to be used after the one-dimensional beam finite element solution has been determined. The resulting strain values are given in the global coordinate systems. The function is called as

```
[ElementStrain_GlobalCS,NodalStrain_GlobalCS]=...
  BECAS_RecoverStrains(theta0,dX,dY,X,Y,nl_2d,el_2d,emat,matprops);
```

Part of the input is coming from the `BECAS_Constitutive_Ks` function. The extra input consists of

- `theta0` - (1×6) array holding the cross section generalized forces and moments (i.e., the variable $\boldsymbol{\theta} = [\mathbf{T}^T \mathbf{M}^T]^T$ defined in Section 2.2.1). The magnitude of the entries are generally determined based on the one-dimensional beam finite element solution.

The output is

- `ElementStrain_GlobalCS` - $(6 \times n_e)$ array holding the three-dimensional strain components evaluated at the center of each of the elements in the cross section finite element mesh.
- `NodalStrain_GlobalCS` - $((6 \times n_{gp}) \times n_e)$ array holding the three-dimensional strain components evaluated at the each of the Gauss points (n_{gp} Gauss points at each element) in the cross section finite element mesh.

Note: function is not yet validated.

5.2.6 BECAS_RecoverStresses

The function `BECAS_RecoverStress` is used to determine the three-dimensional stress components at each element or at each Gauss point in the cross section finite element mesh. The function is meant to be used after the one-dimensional beam finite element solution has been determined. The stresses are evaluated based on the strains determined using the `BECAS_RecoverStrains`. The resulting stress values are given in both the global and material coordinate systems. The function is called as

```
[ElementStress_GlobalCS,ElementStress_MaterialCS,...
  NodalStress_GlobalCS,NodalStress_MaterialCS] = ...
  BECAS_RecoverStress(ElementStrain_GlobalCS,...
  NodalStrain_GlobalCS,nl_2d,el_2d,emat,matprops);
```

The output is

- `ElementStress_GlobalCS` - $(6 \times n_e)$ array holding the three-dimensional stress components in the global coordinate system evaluated at the center of each of the elements in the cross section finite element mesh.

- **ElementStress_MaterialCS** - $(6 \times n_e)$ array holding the three-dimensional stress components in the local coordinate system evaluated at the center of each of the elements in the cross section finite element mesh.
- **NodalStress_GlobalCS** - $((6 \times n_{gp}) \times n_e)$ array holding the three-dimensional strain components in the global coordinate system evaluated at the each of the Gauss points (where n_{gp} are the number of Gauss points at each element) in the cross section finite element mesh.
- **NodalStress_MaterialCS** - $((6 \times n_{gp}) \times n_e)$ array holding the three-dimensional strain components in the material coordinate system evaluated at the each of the Gauss points (where n_{gp} are the number of Gauss points at each element) in the cross section finite element mesh..

Note: function is not yet validated.

5.2.7 BECAS_Becas2Hawc2

The function **BECAS_Becas2Hawc2** is used to generate input for RISØ's HAWC2 code for the aeroelastic analysis of wind turbines. It is presumed that the functions **BECAS_Constitutive_Ks**, **BECAS_Constitutive_Ms**, and **BECAS_CrossSectionProps** have been previously called. Extra input is required for this function, namely, the following have to be defined:

- **RadialPosition** - coordinate of the section along the span of the blade.
- **OutputFilename** - name of file to which the output is written (e.g., **OutputFilename** = 'BECAS2HAWC2.out').

The function is called as

```
BECAS_Becas2Hawc2(OutputFilename, RadialPosition, ...
  Ks, Ms, ...
  ShearX, ShearY, ...
  ElasticX, ElasticY, ...
  MassX, MassY, ...
  AlphaPrincipleAxis_ElasticCenter, ...
  AreaX, AreaY, AreaTotal, ...
  Axx, Ayy, Axy, ...
  nl_2d, el_2d, emat, matprops)
```

5.2.8 BECAS_TransformMat

The function **BECAS_TransformMat** is used to determine the translated and rotated values of the cross section constitutive stiffness or mass matrices. The function requires extra input, namely:

- **p** - column array specifying the coordinates of the new reference point (e.g., **p** = [ShearX ShearY] to translate the matrix to the shear center).

- **alpha** - angle of rotation around the z axis, in degrees, defined positive in the counter-clockwise direction (e.g., **alpha=AlphaPrincipleAxis** to align with the elastic axis).

The function is called as

```
[M]=BECAS_TransformationMat(M,p,alpha);
```

5.2.9 Examples

All the files required for the replication of the validation examples are distributed together with BECAS. The user should specify the name of the corresponding folder in the file `Inputdata4RunMe.m`. The file `RunMe.m` which calls BECAS should then be ran to obtain the results.

5.3 The BECAS 3D implementation

An alternative implementation of BECAS using solid finite elements is described here. The main advantage of this approach concerns the possibility of using layered solid finite elements. All BECAS functions associated with this implementation start by BECAS_3D.

5.3.1 Input

The input to the BECAS_3D group of functions is

- **k3d** - $n_d \times 3$ array with the sparse form of stiffness matrix of the cross section slice meshed with solid finite elements, where n_d is the number of degrees of freedom in the solid finite element model. Each row in the **k3d** array is in the form (*row number, column number, value*), where row and column number correspond to the row and column positions in the global stiffness matrix.
- **n1_3d** - $n_{n,3d} \times 3$ array with the list of nodal positions where each row is in the form (*node number, x coordinate, y coordinate, z coordinate*), where $n_{n,3d}$ is the total number of nodes in the solid finite element model. The node numbering needs to be in the same order as it is listed in the **k3d** matrix.

5.3.2 List of functions and output

The following functions are part of the BECAS_3D group of functions.

5.3.3 BECAS_3D_Uutils

The function BECAS_3D_Uutils is used to build working arrays. It is included inside all the other functions in the 3D version of BECAS. It is called using

```
[utils] = BECAS_3D_Uutils(k3d,n3d);
```

5.3.4 BECAS_3D_Constitutive_Ks

This is the main function of the `BECAS_3d` and is used to determine the cross section stiffness matrix \mathbf{K}_s . It is called using

```
[Ks,dX,dY,X,Y]=BECAS_3D_Constitutive_Ks(k3d,n3d);d
```

The output is

- \mathbf{Ks} - (6×6) array storing the cross section stiffness matrix \mathbf{K}_s .
- \mathbf{dX} - $(n_d \times 6)$ array $\frac{\partial \mathbf{X}}{\partial z}$.
- \mathbf{dY} - (6×6) array $\frac{\partial \mathbf{Y}}{\partial z}$.
- \mathbf{X} - $(n_d \times 6)$ array \mathbf{X} .
- \mathbf{Y} - (6×6) array \mathbf{Y} .

where $n_d = n_n \times 3$ is the number of degrees of freedom in cross section finite element equations.

5.3.5 BECAS_3D_CrossSectionProps

The function `BECAS_3D_CrossSectionProps` returns some relevant cross section properties. It presumes that the cross section stiffness matrix \mathbf{K}_s has been previously determined. The function is called through

```
[ShearX,ShearY,ElasticX,ElasticY,AlphaPrincipleAxis]=...  
BECAS_3D_CrossSectionProps(Ks);
```

The output is

- `ShearX` - the x_s position of the cross section shear center.
- `ShearY` - the y_s position of the cross section shear center.
- `ElasticX` - the x_t position of the cross section elastic center.
- `ElasticY` - the y_t position of the cross section elastic center.
- `MassX` - the x_m position of the cross section mass center.
- `MassY` - the y_m position of the cross section mass center.
- `MassPerUnitLength` - the cross section mass per unit length.
- `AlphaPrincipleAxis` - the orientation of the cross section elastic

Bibliography

- [1] Ganguli R., Chopra I., *Aeroelastic optimization of a helicopter rotor with composite coupling*, Journal of Aircraft, 32(6), 1326-1334, 1995
- [2] Li L., Volovoi V. V., Hodges D. H., *Cross-sectional design of composite rotor blades*, Journal of the American Helicopter Society, 53(3), 240-251, 2008
- [3] Blasques J. P., Stolpe M., *Maximum stiffness and minimum weight optimization of laminated composite beams using continuous fiber angles*, Structural and Multidisciplinary Optimization, DOI: 10.1007/s00158-010-0592-9, 2010
- [4] Hansen M. O. L., Sørensen J. N., Voutsinas S., Sørensen N., Madsen H. A., *State of the art in wind turbine aerodynamics and aeroelasticity*, Progress in Aerospace Sciences, (42), 285-330, 2006
- [5] Chaviaropoulos, P.K., et al., *Enhancing the damping of wind turbine rotor blades - the DAMPBLADE project*, Wind Energy, 9, 163-177, 2006.
- [6] Giavotto V., Borri M., Mantegazza P., Ghiringhelli G., Carmaschi V., Maffioli G.C., Mussi F., *Anisotropic beam theory and applications*, Composite Structures, (16)1-4, 403-413, 1983
- [7] Borri M., Merlini T., *A large displacement formulation for anisotropic beam analysis*, Meccanica, (21), 30-37, 1986
- [8] Borri M., Ghiringhelli G. L., Merlini T., *Linear analysis of naturally curved and twisted anisotropic beams*, Composites Engineering, (2)5-7, 433-456, 1992
- [9] Ghiringhelli G. L., Mantegazza P., *Linear, straight and untwisted anisotropic beam section properties from solid finite elements*, (4)12, 1225-1239, 1994
- [10] Ghiringhelli G. L., *On the thermal problem for composite beams using a finite element semi-discretization*, Composites Part B, (28B), 483-495, 1997
- [11] Ghiringhelli G. L., *On the linear three dimensional behaviour of composite beams*, Composites Part B, (28B), 613-626, 1997
- [12] Ghiringhelli G. L., Masarati P., Mantegazza P., *Characterisation of Anisotropic, Non-Homogeneous Beam Sections with Embedded Piezo-Electric Materials*, Journal of Intelligent Material Systems and Structures, (8)10, 842-858, 1997
- [13] Yu W., Hodges D. H., Volovoi V., Cesnik C. E. S., *On Timoshenko-like modelling of initially curved and twisted composite beams*, International Journal of Solids and Structures, (39), 5101-5121, 2002

- [14] Yu W., Volovoi, V. V., Hodges D. H., Hong X., *Validation of the Variational Asymptotic Beam Sectional Analysis (VABS)*, AIAA Journal, (40)10, 2105-2113, 2002
- [15] Chen H., Yu W., Capellaro M., *A critical assessment of computer tools for calculating composite wind turbine blade properties*, Wind Energy, (13)6, 497-516, 2010
- [16] Jung S. N., Nagaraj V. T., Chopra I., *Assessment of composite rotor blade modeling techniques*, Journal of the American Helicopter Society, (44)3, 188-205, 1999
- [17] Volovoi V. V., Hodges D. H., Cesnik C. E. S., Popescu B., *Assessment of beam modeling methods for rotor blade applications*, Mathematical and Computer Modeling, (33), 1099-1112, 2001
- [18] Horgan C. O., *On Saint-Venant's principle in plane anisotropic elasticity*, Journal of Elasticity, (2)3, 169-180, 1972
- [19] Choi I., Horgan C. O., *Saint-Venant's principle and end effects in anisotropic elasticity*, Transactions of the ASME, 424-430, 1977
- [20] Horgan C. O., Knowles J. K., *Recent developments concerning Saint-Venant's principle*, Advances in Applied Mechanics, (23), 180-262, 1983
- [21] Christensen O., *Differentialligninger af uendelige rødder*, ed. Institut for Matematik, Danmarks Tekniske Universitet, 30-32, 2009
- [22] Hogdes D. H., *Nonlinear composite beam theory*, Progress in Astronautics and Aeronautics, (213), 2006
- [23] Bendsøe, M.P., Sigmund, O., *Topology Optimization: Theory, Methods and Applications*, 2nd Edition, Springer-Verlag, Berlin, 2003
- [24] Reddy J. N., *Mechanics of laminated Composite plates and shells: theory and analysis*, 2nd Edition, CRC Press, 1997
- [25] Peters S. T., *Handbook of composites*, 2nd Edition, Chapman & Hall, London, 1998
- [26] Timoshenko S., Goodier J. N., *Theory of elasticity*, McGraw-Hill, 1951